IMPROVING THE ANTI-HIV POTENCY OF DIFFERENT COMPOUNDS THROUGH SYNERGY AND COVALENT LINKAGE: DIMERIZATION STUDIES OF CXCL8

A Dissertation

by

IOANNIS KAGIAMPAKIS

Submitted to the Office of Graduate Studies of
Texas A&M University
in partial fulfillment of the requirements for the degree of

DOCTOR OF PHILOSOPHY

August 2010

Major Subject: Biochemistry

IMPROVING THE ANTI-HIV POTENCY OF DIFFERENT COMPOUNDS THROUGH SYNERGY AND COVALENT LINKAGE: DIMERIZATION STUDIES OF CXCL8

A Dissertation

by

IOANNIS KAGIAMPAKIS

Submitted to the Office of Graduate Studies of
Texas A&M University
in partial fulfillment of the requirements for the degree of

DOCTOR OF PHILOSOPHY

Approved by:

Co-Chairs of Committee,	Patricia LiWang
	Martin J. Scholtz
Committee Members,	Vlad Panin
	Michael Polymenis
Head of Department,	Gregory D. Reinhart

August 2010

Major Subject: Biochemistry

ABSTRACT

Improving the Anti-HIV Potency of Different Compounds through Synergy and Covalent Linkage: Dimerization Studies of CXCL8.

(August 2010)

Ioannis Kagiampakis, B.S.; M.S., University of Crete, Greece

Co-Chairs of Advisory Committee: Dr. Patricia LiWang
Dr. Martin J. Scholtz

In the first part of my dissertation we focused on the development of covalently linking compounds that bind gp120 with those that bind gp41 in order to block HIV fusion. We used griffithsin or CD4M33, that both bind to gp120, covalently linked with C-peptide C37 of gp41. The results show the linked compound Griff37 is several-fold more potent than griffithsin alone in both fusion and viral assay, making Griff37 an attractive candidate for further development as a microbicide against HIV.

In the second part of my dissertation we investigate the effect of combining HIV fusion inhibitors having differing mechanisms of action. We used P2-RANTES and RANTES that both bind to the chemokine receptor CCR5 on the surface of the human cells along with C-peptides C37 and C34 that bind the viral envelop glycoprotein gp41. We found that the combination of RANTES with C37/C34 has an additive effect on fusion assay. In contrast P2-RANTES and C37/C34 shows synergy in inhibition of cell fusion. In viral assays using MAGI cells the synergy between P2-RANTES and C37/C34 is minimal.

In the third part of my dissertation we focused on characterization of two examples of evolutionarily conserved unfavorable sequence motifs that affect quaternary structure. In contrast to the straightforward action of favorable sequences, these unfavorable motifs produce interactions disfavoring one outcome to indirectly promote another one. To identify such motifs, we propose and developed a statistically validated computational method combining structure and phylogeny. This approach was applied in an analysis of the alternate forms of homodimerization exhibited in the chemokine family. We identified two evolutionarily conserved sequence motifs in the CC subfamilies: a drastic two-residue deletion (ΔRV) and a simple point mutation (V27R). Cloned into the CXCL8 background, these two motifs were experimentally proven to confer a monomeric state. NMR analyses indicate that these variants are structured in solution and retain the chemokine fold. Structurally, the motifs retain a chemokine tertiary fold while introducing unfavorable quaternary interactions that inhibit CXCL8 dimerization.

DEDICATION

To

My family and friends.

Their help was immeasurable.

ACKNOWLEDGEMENTS

I would like to thank my advisors Dr. Patricia LiWang and Dr. Jerry Tsai for the support and the opportunity to work in their labs. I thank Dr. Martin Scholtz for serving as co-chair of my committee. I thank Dr. Vlad Panin, and Dr. Michael Polymenis for serving as members of my committee. I thank Dr. Andy LiWang and Dr. Jerry Tsai who were former members of my committee. I thank the members of both Dr. Andy LiWang and Dr. Patricia LiWang group.

I thank Sinae Kim and Dr. Marina Vannucci for the statistical analysis of the alignments of chemokine family sequences. I thank Dr. Roger Smith for the FACs experiments of CCR5 receptors internalization. I thank Arbi Gharibi and Kristabelle Alatas, my undergrads, for all the help that they gave me on the experiments. I thank Marie K. Mankowski , Beth A. Snyder and Roger G. Ptak for the great work they did on viral assays. I thank Sarah Min for proofreading my dissertation.

TABLE OF CONTENTS

Page

CHAPTER Page

CHAPTER Page

LIST OF FIGURES

Page

LIST OF TABLES

CHAPTER I

INTRODUCTION AND BACKGROUND

AIDS Epidemics

According to the World Health organization (WHO) (http://www.who.int/hiv/pub/epidemiology/epidemic/en/index.html), in 2008 an estimated 33.4 million people worldwide were living with HIV. Of that number, 31.3 million were adults and 15.7 million were women. In that same year, 2.7 million were infected with HIV, the majority of them (2.3 million) adults. There were 2 million AIDS related deaths in 2008.

AIDS is a global epidemic concentrated in Sub-Saharan Africa. An estimated 22.4 million adults live with HIV in that area, and this represents 5.2% of the total population. The following list adopted by WHO gives details on current epidemiological statistics on HIV/AIDS (Figure I-1).

Although new incidences of HIV are on the decline and there are indications of success in HIV prevention, the battle against HIV is far from concluded. Currently there is no cure against HIV, with a single possible exception: there is one case where the transplantation of CCR5 Δ32/Δ32 stem cells into a patient with acute myeloid leukemia and an HIV-1 infection showed no detectable virus for more than 1.5 years post-transplantation (67).

This dissertation follows the style of *Journal of Virology*.

Regional HIV and AIDS statistics, 2001 and 2008

	Adults and children living with HIV	Adults and children newly infected with HIV	Adult prevalence (%)	Adult and child deaths due to AIDS
Sub-Saharan Africa				
2008	22.4 million [20.8 million–24.1 million]	1.9 million [1.6 million–2.2 million]	5.2 [4.9–5.4]	1.4 million [1.1 million–1.7 million]
2001	19.7 million [18.3 million–21.2 million]	2.3 million [2.0 million–2.5 million]	5.8 [5.5–6.0]	1.4 million [1.2 million–1.7 million]
Middle East and North Africa				
2008	310 000 [250 000–380 000]	35 000 [24 000–46 000]	0.2 [<0.2–0.3]	20 000 [15 000–25 000]
2001	200 000 [150 000–250 000]	30 000 [23 000–40 000]	0.2 [0.1–0.2]	11 000 [7800–14 000]
South and South-East Asia				
2008	3.8 million [3.4 million–4.3 million]	280 000 [240 000–320 000]	0.3 [0.2–0.3]	270 000 [220 000–310 000]
2001	4.0 million [3.5 million–4.5 million]	310 000 [270 000–350 000]	0.3 [<0.3–0.4]	260 000 [210 000–320 000]
East Asia				
2008	850 000 [700 000–1.0 million]	75 000 [58 000–88 000]	<0.1 [<0.1]	59 000 [46 000–71 000]
2001	560 000 [480 000–650 000]	99 000 [75 000–120 000]	<0.1 [<0.1]	22 000 [18 000–27 000]
Oceania				
2008	59 000 [51 000–68 000]	3900 [2900–5100]	0.3 [<0.3–0.4]	2000 [1100–3100]
2001	36 000 [29 000–45 000]	5900 [4800–7300]	0.2 [<0.2–0.3]	<1000 [<500–1200]
Latin America				
2008	2.0 million [1.8 million–2.2 million]	170 000 [150 000–200 000]	0.6 [0.5–0.6]	77 000 [66 000–89 000]
2001	1.6 million [1.5 million–1.8 million]	150 000 [140 000–170 000]	0.5 [<0.5–0.6]	66 000 [56 000–77 000]
Caribbean				
2008	240 000 [220 000–260 000]	20 000 [16 000–24 000]	1.0 [0.9–1.1]	12 000 [9300–14 000]
2001	220 000 [200 000–240 000]	21 000 [17 000–24 000]	1.1 [1.0–1.2]	20 000 [17 000–23 000]
Eastern Europe and Central Asia				
2008	1.5 million [1.4 million–1.7 million]	110 000 [100 000–130 000]	0.7 [0.6–0.8]	87 000 [72 000–110 000]
2001	900 000 [800 000–1.1 million]	280 000 [240 000–320 000]	0.5 [0.4–0.5]	26 000 [22 000–30 000]
Western and Central Europe				
2008	850 000 [710 000–970 000]	30 000 [23 000–35 000]	0.3 [0.2–0.3]	13 000 [10 000–15 000]
2001	660 000 [580 000–760 000]	40 000 [31 000–47 000]	0.2 [<0.2–0.3]	7900 [6500–9700]
North America				
2008	1.4 million [1.2 million–1.6 million]	55 000 [36 000–61 000]	0.6 [0.5–0.7]	25 000 [20 000–31 000]
2001	1.2 million [1.1 million–1.4 million]	52 000 [42 000–60 000]	0.6 [0.5–0.7]	19 000 [16 000–23 000]
TOTAL				
2008	33.4 million [31.1 million–35.8 million]	2.7 million [2.4 million–3.0 million]	0.8 [<0.8–0.8]	2.0 million [1.7 million–2.4 million]
2001	29.0 million [27.0 million–31.0 million]	3.2 million [2.9 million–3.6 million]	0.8 [<0.8–0.8]	1.9 million [1.6 million–2.2 million]

Figure I-1: Regional HIV and AIDS statistics, 2008.

Adopted by WHO
(http://www.who.int/hiv/pub/epidemiology/epidemic/en/index.html)

People who naturally have the CCR5 Δ32/Δ32 mutation do not express CCR5 on their cell surface and show resistance to HIV-1 infection since CCR5 plays a key role in the infection process, as I will describe later in this chapter. There are also no vaccines against HIV. Recently in Thailand, a clinical trial of the combination of two vaccines (RV144 trial), one of them immunizing against the viral envelope glycoprotein gp120, and the other against HIV replication, failed to give solid conclusions about the usefulness of this combination (94).

In clinical use today are antiretroviral drugs that can be categorized into the following four groups:

1) Reverse transcriptase inhibitors (RTIs) (This group is further divided into three subcategories: a) nucleoside inhibitors, b) nucleotide analogues inhibitors (NRTIs), c) nonnucleoside inhibitors (NNRTIs)). Their role is to inhibit the reverse transcription of the viral genome.

2) Protease inhibitors (PI) that block the maturation of viral proteins,

3) Integrase inhibitors that inhibit the integration of the viral genome into the host chromosome and

4) Fusion inhibitors that block the fusion of the virion to the target cell (9).

Combination treatment of HIV patients with antiretroviral drugs (usually a triple combination of two NRTIs together with one PI or one NNRTI) succeeds in most cases to drop the viral load to undetectable levels. In ~5% of cases, therapy fails and the virus rebounds. It is obvious that until the development of a successful vaccine emerges, a race between virus adaptation and new anti-HIV drug development will take place. Most of my dissertation is focusing on the development of new anti-HIV fusion inhibitors that can

be used as a vaginal microbicide. The importance of microbicide development can be appreciated by the results of epidemiological studies from WHO that recognize that heterosexual intercourse is the leading cause of virus spread. Transition probability per exposure event is 1 in 200 to 1 in 2000 for the female genital tract and 1 in 700 to 1 in 3000 for the male genital tract (65, 66). An effective HIV microbicide for the female genital tract will provide an extra "weapon" in HIV prevention, especially in third world countries where the use of condoms may not be a woman's choice.

HIV host invasion

One of the biggest challenges in developing an HIV microbicide is finding a compound that will inhibit the multiple ways the virus has adapted to penetrate the human epithelium and infected different target cells without the compound causing inflammation at the area of application. In other words, the microbicide needs to be at the proper "place" at the proper time in order to be effective and to not recruit inflammatory cells that are the targets of HIV. In the following paragraph I will describe current knowledge on virus invasion, focusing on the vaginal epithelium.

It has been shown that during heterosexual intercourse, women can acquire HIV through the non-keratinized squamous epithelium of the vagina and endocervix and the single-layer columnar epithelium of the endocervix. Men can be infected through the inner foreskin of the penis and the penile urethra (65, 66).

But how does HIV actually penetrate the mucosa during heterosexual intercourse in women? Five cells types (Epithelial cells, Langerhans cells, Dendritic cells, T-cells and Macrophages) that exist in the epithelium and stroma of the vagina and uterine ectocervix play key roles in HIV invasion (Figure I-2).

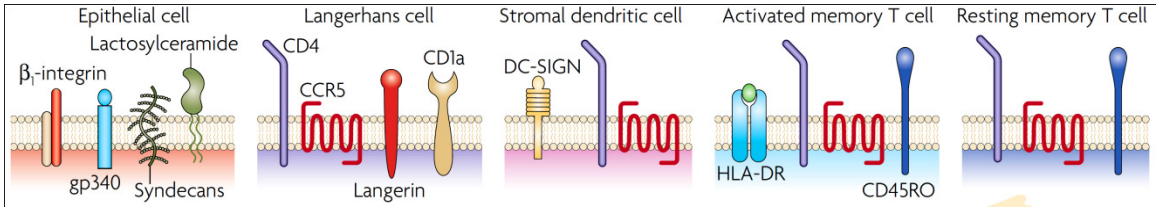

Figure I-2: Cells that exist in vaginal epithelium and stroma.

These cells play key roles in HIV host invasion through heterosexual intercourse. Figure adopted by (66).

There are many models that describe how HIV infects the genital mucosa in women. The most recent ones are:

1) Macro – abrasion of the epithelium allows free virus or infected donor cells to invade deep into the epithelium (stroma) where DCs, T-cells and macrophages are abundant. These 3 cells types can cause productive HIV infection and transfer the virion to the lymph nodes (65, 66).
2) Free HIV virions can be trapped in mucus and move inside the epithelium through gaps between epithelial cells. Langerhans cells are inside the epithelium and are the first cells the virion encounters. Inside these cells, the virion can be degraded in Birbeck granules or cause a productive infection. Infected Langerhans cells can migrate into the submucosa and through venous microvessels to lymph nodes. Inside the epithelial layer but deeper than Langerhans cells, can also be found resting memory T cells and dendritic cells. Virions can productively infect both these types of cells and migrate to lymph nodes (65, 66).

3) Free virions can move deeper into the epithelial layer via transcytosis through epithelial cells, especially near the basal level of the squamous epithelium (65, 66).

Infection of T-cells by the HIV-1 free virion

T-cells may not be the first cells that the virus encounters and can infect productively as it gets deeper in the vagina epithelium, but these are the cells that have been studied the most on a molecular basis and that I have used as a model system to test the new drug design. A detailed description of the HIV fusion process on a molecular level will follow.

The viral spike consists of two heavily glycosylated proteins named gp120 and gp41. Both of these proteins form trimers (Figure I-3) (154). Before human-virus interaction, gp120 structurally covers gp41 and gp41 has a transmembrane domain that anchors the spike on the viral membrane. The HIV-1 virion has, on average, 14 ± 7 spikes on its surface (197).

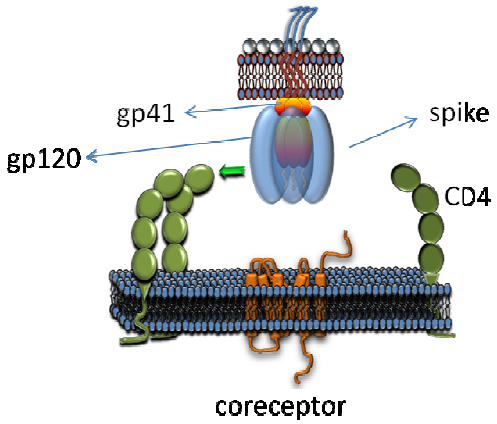

Figure I-3: HIV-1 spike consists of glycoproteins gp120 and gp41.
T-cell has CD4 (receptor) and CCR5 or CXCR4 (coreceptors) on its surface.

The first step of the fusion process is the interaction of viral glycoprotein gp120 with the T-cell surface receptor CD4 (Figure I-3). Gp120–CD4 interaction causes conformational changes to gp120, revealing cryptic epitopes that are located in the V3 domain and the bridging sheet of gp120 (27). These epitopes allow interaction between gp120 and the chemokine receptor CXCR4 or CCR5 (coreceptors). In this state, the viral spike is considered in the "open" form. After this initial interaction the number of HIV-1 receptors and coreceptors is increased in the vicinity (193) (Figure I-4).

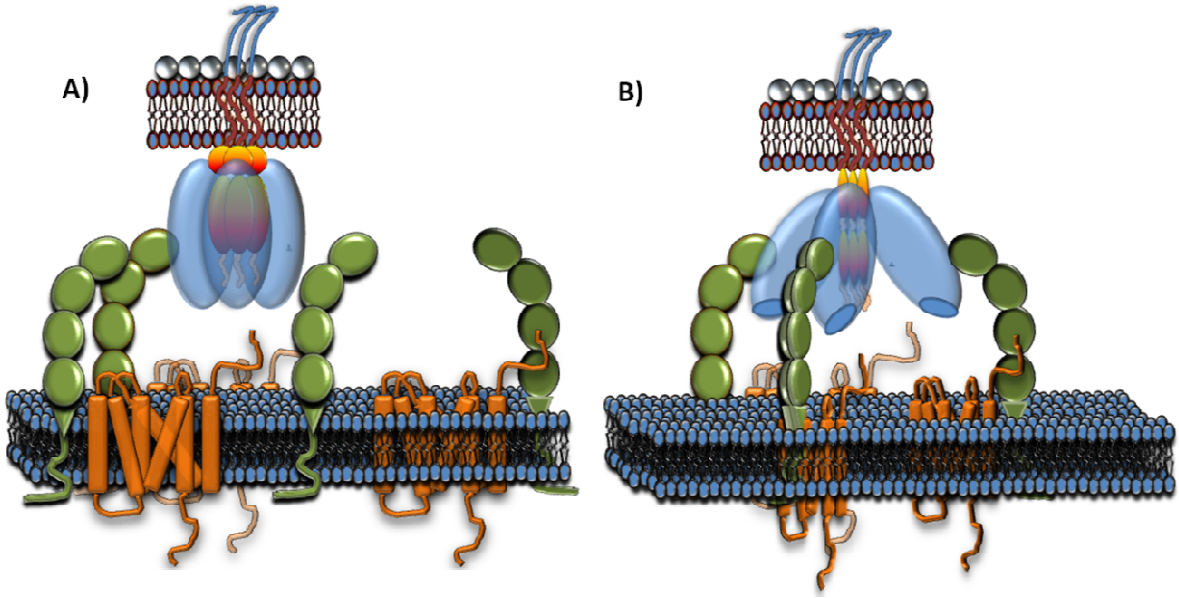

Figure I-4: HIV spike.

A) "Closed" form of the HIV-1 spike. Gp120 covers almost all of gp41. The initial interaction of gp120-CD4 results in the accumulation of receptors and coreceptors in the vicinity of the initial interaction. B) "Open" form of the viral spike. Gp41 is extended and accessible. Conformational changes in gp120 allow cryptic epitopes to be exposed. These epitopes will facilitate the interaction of gp120 with coreceptors (CCR5 or CXCR4).

Gp120–CD4 interaction does not only induce conformational changes to gp120 but also to gp41, allowing it to be in a more extended form. Gp41 consists of a cytoplasmic domain (CD), a transmembrane domain (TM), a C-terminal heptad repeat (CHR), an N-terminal heptad repeat (NHR) and a fusion peptide that is located on the N-terminal tip of the protein (Figure I-5). When the spike is in the "open" form, the NHR of gp41 is accessible for C-peptide fusion inhibitors (C-peptide fusion inhibitors bind to the NHR area of gp41) (13, 135). I will talk about them later in detail.

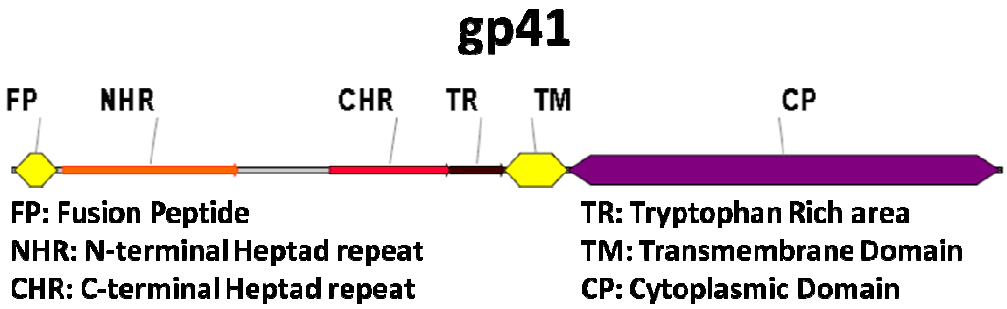

Figure I-5: gp41 domains

The next step in the fusion process is the interaction of gp120 with the coreceptors (Figure I-6). There is a long list of coreceptors that the HIV-1 virus can use to enter the cell (195), but the main coreceptors for T-cells are the chemokine receptors CCR5 and CXCR4. Both of them are G-protein coupled receptors. Which coreceptor a virus uses

to enter the cell dictates its tropism: R5-tropic or X4-tropic, respectively. If the virus uses both receptors then it is called R5/X4 tropic (135).

The gp120–CCR5/CXCR4 interaction results in the activation of the chemokine receptor and signaling. It has been shown that blocking intracellular Ca^{2+} release with protein kinase C inhibitors interferes with virion-targeted cell fusion (55). There is an accumulating body of evidence that viral-induced signaling is important for T-cell migration, adhesion and survival (192). It has also been suggested that this signaling affects post-fusion events like viral transcription (39, 97).

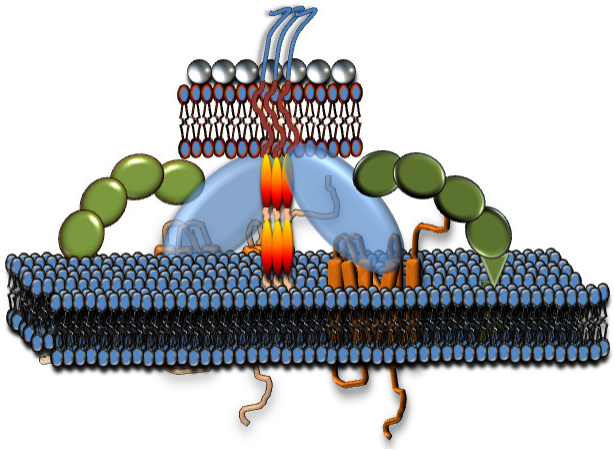

Figure I-6: Interaction of gp120 with the chemokine receptor CCR5 and CXCR4. The fusion peptide (FP) of gp41 has inserted into the target cell membrane.

Currently we do not know if all three gp120 subunits of one spike interact with three CD4 receptors or if they interact with three coreceptors, but there is evidence that more than one spike is needed for pore formation and HIV-1 fusion (164). The current hypothesis is that after gp120-coreceptor interaction, the fusion peptide (FP) of gp41 that is hydrophobic is inserted into the membrane of T-cells. At this point we do not have pore formation yet; only lipid mixing of the viral envelope and cell membrane is occurring (107) (Figure I-7).

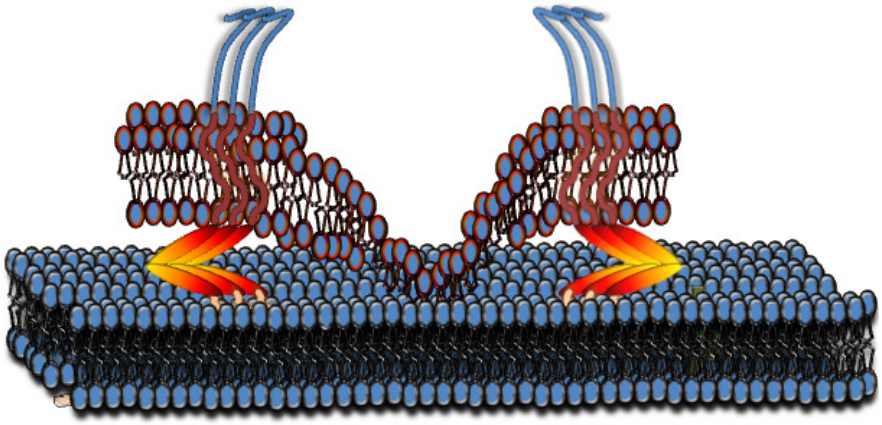

Figure I-7: Lipid mixing between viral and target cell membrane.
Red color indicates viral lipids. For simplicity, only gp41 is shown.

The HIV virion may enter the cell via endocytosis and fuse with endosomes in a dynamin-dependent matter. After the virion is inside the cell we observe pore formation

and the release of the capsid into the cell cytoplasm (113). A significant role in pore formation is played by the gp41 protein that forms a six-helix bundle when the C-terminal heptad repeat (CHR) interacts with the N-terminal heptad repeat (NHR)(114) (Figure I-8). C-peptides C37 and C34, which are considered fusion inhibitors, block the formation of this helix bundle. This formation is believed to stabilize the pore (107). The pore needs to be big enough and stable enough for the viral capsid to enter the target cell's cytoplasm.

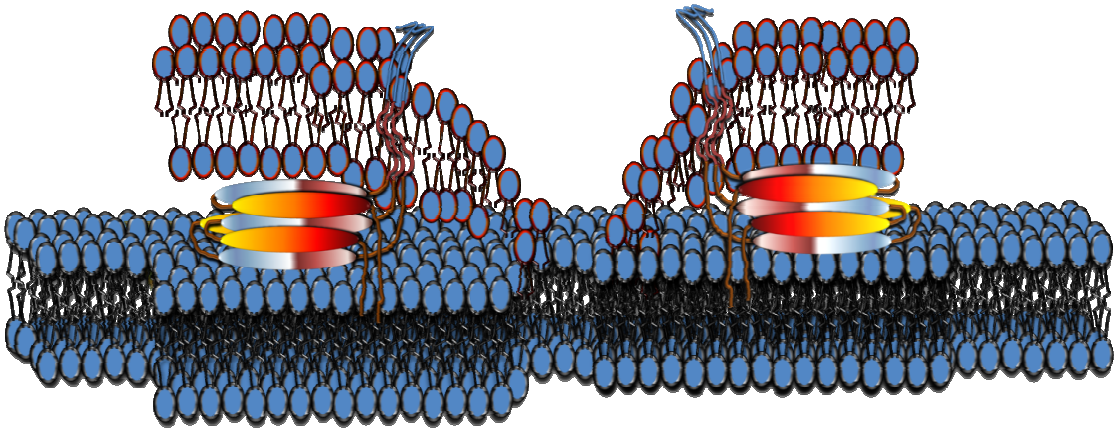

Figure I-8: Pore formation.

The six-helix bundle formation of gp41 is believed to stabilize the pore on the target cell membrane. When gp41 is in this stage, the fusion inhibitors that target N- and C-terminal heptad repeats are not able to bind to their targets.

New Anti-HIV-1 compounds

As it has been described earlier in this chapter**,** there is a constant need for new anti-HIV drugs. This problem has been approached in many ways, from testing libraries of chemical compounds for anti-HIV activity, to the rational design of new inhibitors for different steps of the viral life cycle. Part of my dissertation was to make new anti-HIV compounds using two approaches: 1) Linking two known anti-HIV compounds and 2) Testing for synergistic anti-HIV activity of known compounds.

Why would someone link two anti-HIV compounds? There are many reasons:

a) To increase the binding affinity of the chimeric compound to the target area. If both compounds bind to their target area at the same time, it is possible that the overall binding affinity of the linked compound will be higher than each compound separately. Higher binding affinity may correlate to higher anti-HIV activity (Figure I-9 A).

b) To deliver one of the compounds near its binding area. It is known that compounds, like C-terminal fusion inhibitor C37, bind unspecifically to the cell surface (73). It is possible that linking two compounds, one being more specific than the other, will lead to better delivery of the not-so-specific compound to its binding area. This delivery could lead to higher anti-HIV activity (Figure I-9 B).

c) It is easier for a virus to evade one anti-HIV compound through mutations than two linked compounds.

d) Properties of one anti-HIV compound could be beneficial for the other compound. For example, if one of the compounds can access its target area only when the viral spike is in an “open” form, it is logical to assume that linking this compound

with another compound that can induce this conformational change of the viral spike may lead to an improvement in anti-HIV potency of the chimeric compound (Figure I-9 A).

Another section of my dissertation investigates if particular anti-HIV compounds show synergy. Synergy is when different anti-HIV compounds cooperate with each other so that the final anti-HIV potency of the mix is better than the additive effects of the two compounds. Synergy is of particular interest for two main reasons: a) it can show the mechanism of action of the tested compounds and b) it can suggest medical protocols for drug administration in HIV patients.

The anti-HIV compounds that I used in my research were: Griffithsin, $CD4M33_{C1F23}$, C-peptides and P2-RANTES, a variant of chemokine RANTES (58). I linked Griffithsin with C37, $CD4M33_{C1F23}$ with C37, and Griffithsin with $CD4M33_{C1F23,}$ and I studied the possible synergy between P2 RANTES and C-peptide fusion inhibitor C37 and C34. In the following paragraphs I will describe each compound separately.

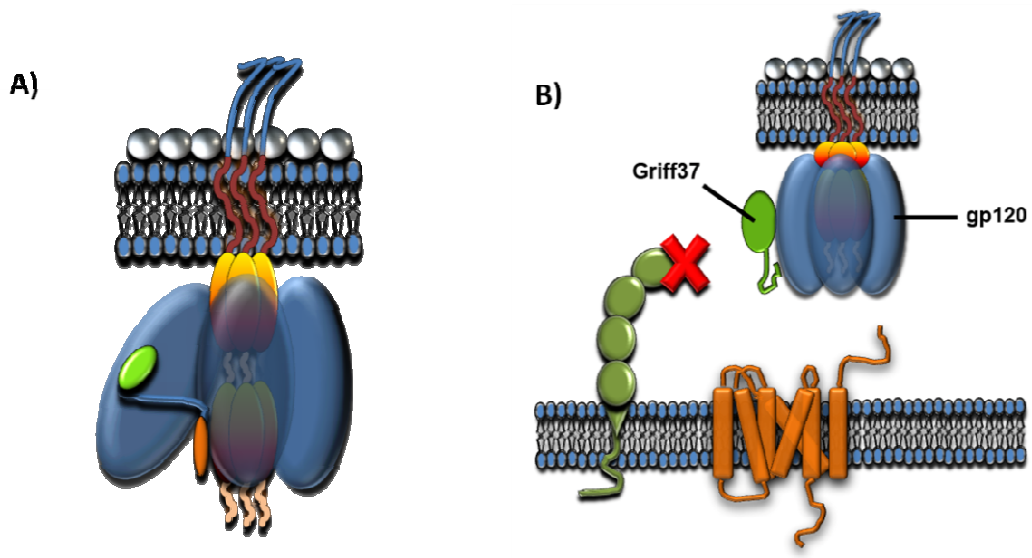

Figure I-9: Models of action of the chimeric proteins.

A) Two compounds are bound at the same time to their target areas. In this particular example CD4M33$_{C1F23}$ and C37 are bound to gp120 and gp41, respectively. CD4M33$_{C1F23}$ can induce conformational changes to gp120, allowing access of C37 to gp41. B) One compound is delivering the not-so-specific compound near its target area. In this case Griffithsin is linked with C37 (Griff37) and is delivering C37 to the top of the viral spike. C37's target is the N-terminal heptad repeat (NTR) of gp41 that is part of the viral spike.

Griffithsin

Griffithsin is a lectin originally isolated from the red algal *Griffithsia sp*. (118). It shows activity against multiple viruses like HIV, severe acute respiratory syndrome (SARS), Ebola and herpes simplex virus (194, 198). It crystallizes as a domain-swapped dimer (198, 199) (Figure I-10). The monomeric form has 121 amino acids and a molecular weight of 12,858 Da. As a lectin it can bind sugars like glucose, galactose,

mannose, maltose and fucose (118). The affinity of Griffithsin to mannose monosaccharide is 102.0 ± 13.0 μM and to 1→6*α*-mannobiose 83.3±17.5 μM, respectively, and these interactions are entropically driven (199).

Griffithsin shows anti-HIV activity in a broad spectrum of HIV strains with an IC_{50} in the pM range and is currently in pre-clinical trials as a microbicide (194). ELISA assays reveal that Griffithsin binds both envelope glycoproteins gp120 and gp41 probably by bindings to the complex mannose on the surface of these proteins, so it is proposed that Griffithsin is a fusion inhibitor interrupting the gp120 – CD4 interaction.

Co-crystallization of Griffithsin with mannose or 1→6*α*-mannobiose unveils that the Griffithsin dimer forms an almost equilateral triangle of surface areas which binds three molecules of mannose. The residues of Griffithsin that play an important role in the Griffithsin – mannose interaction according to the crystal structure are Tyr28, Asp30, Tyr68, Asp70, Tyr110 and Asp112 (198) (Figure I-11).

We linked Griffithsin with C-peptide fusion inhibitor C37. The original hypothesis was that Griffithsin will bring C37 on the viral spike near gp41 (Figure I-9 B). In this way, we could have inhibition by griffithsin as well as enhanced inhibition by C37 binding gp41.

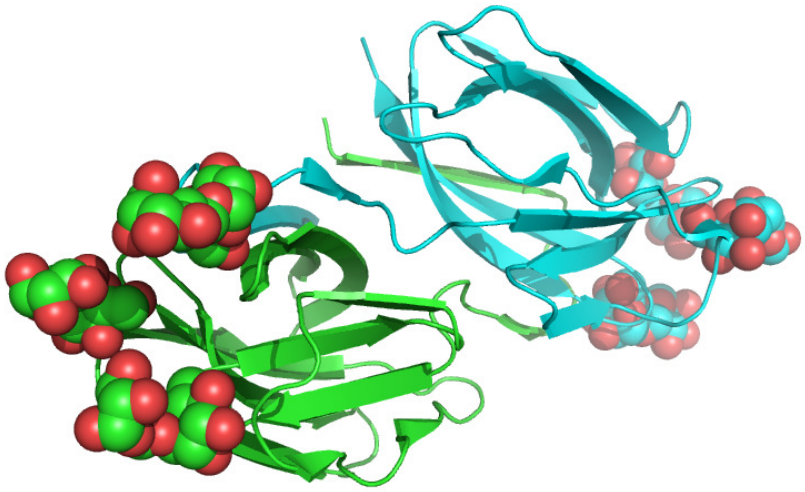

Figure I-10: Domain-swapped dimer of Griffithsin.

1→6*α*-mannobiose shown as balls

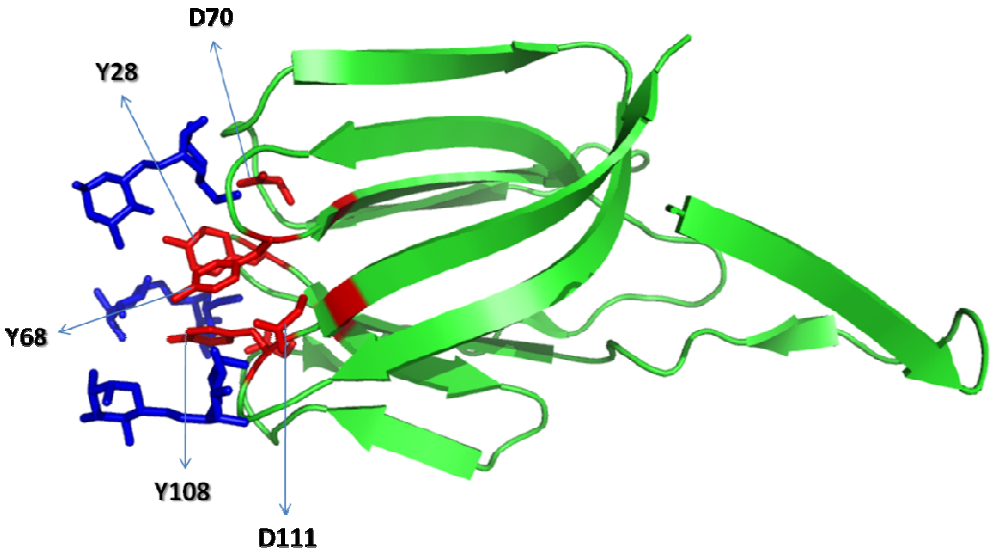

Figure I-11: Griffithsin structure with 1→6*α*-mannobiose.

For simplicity only one molecule from the dimer is shown. Red color indicates important residues for the interaction with 1→6*α*-mannobiose. Blue: 1→6*α*-mannobiose (PDB ID: 2HYQ)

CD4M33$_{C1F23}$

In 1998, Kwong et al. published the structure of the HIV gp120 envelope glycoprotein in complex with soluble CD4 (sCD4) and Fab 17b (84). By dissecting this structure it became obvious that at the sCD4 – gp120 interaction, 22 CD4 residues and 26 gp120 residues made direct inter-atomic contacts. At the sCD4 site all these contacts are concentrated in the span of 25 to 64. The most important residues of this group are Phe 43 and Arg 59. Phe 43 by itself accounts for 23% of the total contacts between sCD4 and gp120.

In 1999, Vita et al. used the scorpion scyllatoxin, a 31 aa peptide that is structurally similar to the CDR2-like loop of sCD4, and inserted mutations that made it similar to sCD4. This produced the CD4M9 peptide that showed moderate anti-HIV activity (176). Further development of this peptide produced the peptide CD4M33 with significantly better anti-HIV activity (109). This peptide replaces the Phe at position 23 with a biphenylalamine (Bip) residue and instead of Cysteine at position 1 there is a thiopropionic acid (Figure I-12). CD4M33, like sCD4, can induce conformational changes to gp120, making gp41 accessible for C-peptides that block the formation of the six-helix bundle (109).

The initial hypothesis was that if we linked C37 with CD4M33, the CD4M33 would open the viral spike and deliver C37 to gp41 (Figure I-9 A). In this way we hoped to have simultaneous binding of CD4M33 and C37 to their target areas. As a small alteration, since CD4M33 has unnatural amino acids, we chose to make a chimera between CD4M33 and CD4M9 that we named CD4M33$_{C1F23}$. We expressed C37 linker

$CD4M33_{C1F23}$ in *E.coli*, since every applicable drug needs to be easily produced. Sequences for the various peptides I discussed above are the following:

scyllatoxin AFCNL RM CQLSCRSLGLLGKCIGD K CECVKH

CD4M9 Ac -CNL AR CQLRCKSLGLLGKCAGS F CACGP

CD4M33 Tpa - NL HF CQLRCKSLGLLGKCAGS Bip CACV

$CD4M33_{C1F23}$ CNL HF CQLRCKSLGLLGKCAGS F CACV

Red colored items in the CD4M9 sequence are the mutations that are the same in the sCD4 sequence.

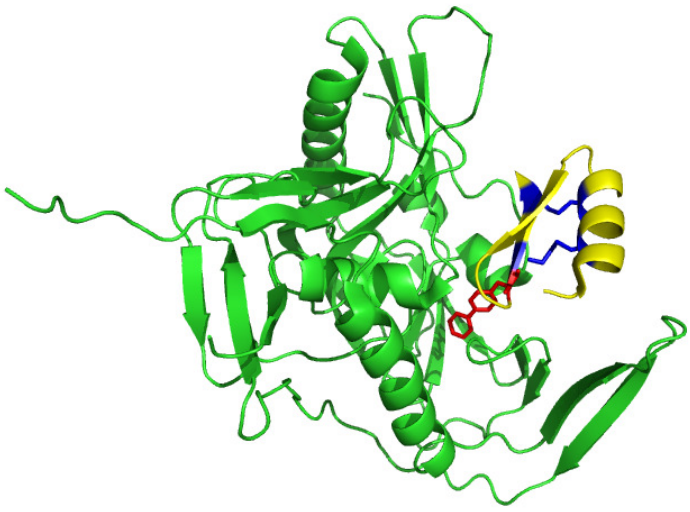

Figure I-12: CD4M33 (yellow) - gp120 (green) interactions.

Disulfide bonds are shown in blue, and red corresponds to the biphenylalamine (Bip) residue of CD4M33.

C-peptide fusion inhibitor C37 and C34

C37 and C34 are two overlapping peptides that come from the C-terminal heptad repeat sequence of gp41. C37 is 3 aa longer than C34 at the N-terminus. Both of these peptides show anti-HIV activity in the nM range and they are unstructured when in solution (14). After the addition of N36, a peptide from the N-terminal heptad repeat of gp41, to a C34 solution in 1:1 ratio, the formation of antiparallel interacting helical structures is observed (95). It is believed that the mechanism of action of these two peptides is by blocking the formation of the six-helix bundle of gp41, destabilizing the fusion pore on the target cell membrane and stopping the insertion of the viral capsid into the target cell cytoplasm. The most famous C-peptide is T20 (enfuvirtide), which is currently in clinical use as one of the last lines of defense against HIV when other drugs fail. In Figure I-13, the amino acid sequences of T20 and C37 are shown.

```
T20                          YTSLIHSLIEESQNQQEKNEQELLELDKWASLWNWF
C37     HTTWMEWDREINNYTSLIHSLIEESQNQQEKNEQELL
```

Figure I-13: T20 and C37 amino acid sequences.

The overlapping amino acids are shown with red color.

P2-RANTES

RANTES is a chemokine that binds to G-protein coupled receptors CCR1, CCR3, CCR4 and CCR5, and mediates activation and chemotaxis in a series of cells like T cells, macrophages, eosinophils and basophils (48). RANTES has been found to block HIV through competition with envelope glycoprotein gp120 for binding with CCR5 coreceptors (Figure I-6) (48).

Hartley et al. used a phage display library of randomly mutated and extended N-terminal RANTES and screened for improved anti-HIV activity. Using this method they discovered FSPLSSQSS-RANTES, named P2-RANTES, which shows a nM range of anti-HIV activity in various assays (57). P2-RANTES acts against HIV in two different ways: 1) it competes with viral glycoprotein gp120 for binding with CCR5 and b) internalizes CCR5. Low CCR5 density negatively affects virus infectivity and increases the potency of T20 in blocking HIV (62, 147). We hypothesized that since P2-RANTES causes internalization of CCR5, it may cause an increase in the anti-HIV potency of C-peptide fusion inhibitors C37 and C34. In Figure I-14 you can see the crystal structure of P2-RANTES that has been solve by our lab (73).

Figure I-14: P2-RANTES structure.

Red color indicates amino acids FSPLSSQSS that have been added onto the RANTES amino acid sequence. (PDB ID: 2VXW)

CXCL8 (Interleukin-8)

The second chapter of this dissertation is focused on CXCL8 studies and is independent of HIV fusion inhibitors. CXCL8 is a CXC chemokine that plays an important role in recruiting leukocytes to the sites of injury and bacterial infections (chemotaxis) (120). It is also a contributor in many types of cancer and metastasis since increased expression of CXCL8 or CXCL8 receptors have been found in cancer cells and tumor-associated macrophages (179).

CXCL8 binds and activates two G-protein coupled receptors (CXCR1 and CXCR2) (140). Its monomeric form is the high affinity receptor ligand and the CXCL8 N-loop is shown to be important for receptor binding (145).

All chemokines have similar structures even if they share less than 20% of aa sequence similarity. They can also dimerize in different ways. CXCL8 forms a tight dimer using the β1 strand; on the other hand, CCL4 (MIP-1β) dimerizes using the N-terminal area of the protein, in particular Pro8, Phe13 and the 40's loop. We suggest that evolutionary pressures kept chemokine structure very similar between different members of the family, while at the same time allowing changes in the ways its members dimerized. Using a local sequence alignment of CCL4 related chemokines, we designed mutations to break the CXCL8 dimer, as described in detail in the Chapter IV.

CHAPTER II

A POTENT STRATEGY TO INHIBIT HIV-1 BY BINDING BOTH gp120 AND gp41

Introduction

About 2.7 million people are infected with HIV each year, and women comprise 50% of the 33 million people living with AIDS (40). In the developing world, effective prevention strategies are lacking, often because women have limited freedom in choosing sexual situations or in insisting on condom use. Therefore, the development of an anti-HIV microbicide is extremely important. Properties that are desirable in a microbicide include the ability to effectively inhibit HIV infection at low concentrations, the ability to be applied topically on a regular basis without causing inflammation, stability to fluctuating temperatures, and inexpensive production.

The early events in an HIV-1 infection in T-cells can be described as follows. The HIV-1 envelope protein gp120 first makes contact with the human cell surface protein CD4, which causes conformational changes in gp120. The gp120-CD4 interaction facilitates the formation and exposure of the binding site on gp120 for its co-receptor on the human cell, the chemokine receptor CCR5 (or CXCR4 in some strains) (41-44). These HIV-cell interactions lead to the exposure of HIV-1 protein gp41, which mediates cell fusion. Gp41 exists as a trimer having three major segments: The N-terminal fusion peptide (FP) which inserts into the cell, the so-called N-terminal heptad repeat, and the C-terminal heptad repeat. After the fusion peptide has inserted into the

cell membrane, the N-terminal segment and C-terminal segment come together to form a 6 helix bundle, a trimer of hairpins (reviewed in (45,46)). This action has the effect of pulling the viral membrane surface close to the cellular surface, facilitating the formation or stabilization of a viral pore. It has recently been reported that these events may in part occur in the endosome: early binding events in cell fusion may occur at the cell surface, after which the entire complex is internalized into an endosome for the final fusion process (19).

There are several strategies that have been shown to be successful in the inhibition of early events in HIV infection (entry inhibition). Blocking the gp120-CD4 binding interaction has been shown to be useful (47-49), and this is likely the interaction that is targeted by the alga-derived protein griffithsin (23). Griffithsin is a leading candidate for a microbicide, having been shown to potently inhibit HIV infection (23,50), to be stable to warm temperatures and in the low pH environment of cervical fluid (50), and having recently been shown to be able to be produced in gram quantities from overexpression in plants (51). The mechanism of action of griffithsin is likely based on its ability to bind the saccharides (particularly mannose) that cover the surface of both HIV gp120 and gp41. In this regard, griffithsin has been shown to inhibit binding by gp120 to CD4 (23). As evidence that the mechanism of this inhibition involves griffithsin binding to the glycosylated surface of gp120/gp41, exogenous addition of several types of individual saccharides has been shown to block the ability of griffithsin to inhibit HIV (23). Also, griffithsin crystallizes in the presence of mannose (25), glucose and N-acetyl glucosamine (52), in each case revealing three saccharide binding sites per monomer. A smaller molecule that is targeted to the gp120-CD4 interaction is

the designed peptide CD4M33. This 27 amino acid peptide has been shown to bind gp120 tightly, although micromolar concentrations are required to inhibit in cell-cell fusion assays using vaccinia technology (29).

Another very effective anti-HIV strategy has been to inhibit the "trimer of hairpins" formation of gp41. This has been effectively accomplished by peptides that bind to the helical regions of gp41, disallowing the full 6-helix bundle formation (45). The molecule T-20 is such a peptide that is derived from the C-terminal heptad repeat of gp41 (a "C-peptide"), thereby effectively binding the N-terminal region of the protein (31,53,54). T-20 is currently in clinical use, and further work has also focused on the similar C-peptides C34 and C37, which are nearly identical to each other (differing by three extra amino acids at the N-terminus for C37) and that also bind to the N-terminal region of gp41 and prevent the 6 helix bundle formation that is critical for viral fusion (45,55-57).

We hypothesized that a single compound with the capability of interrupting both the gp120-CD4 interaction as well as the formation of the gp41 6-helix-bundle could have advantages for several reasons. From a structural standpoint, the physical distance between target binding areas for linked compounds are not large since both gp120 and

gp41 are part of the same complex in the viral spike. Functionally, a linked compound may improve binding affinity and/or specificity compared to its individual counterparts. Such a compound may have advantages in terms of the ability to target the virus under conditions of blood flow or in the milieu of a physiological environment. Finally, an inhibitor comprising two separate strategies may provide comprehensive protection against multiple clades of virus even in the event of viral mutation.

In the present study, we tested several linked compounds that encompass the strategy of binding both gp120 and gp41. It was found that one compound, griffithsin-linker-C37 (Griff37) is effective at lower concentrations than griffithsin alone or in combination with C37 (1:1) in cell-cell fusion assays and in viral assays, and that this inhibitor exhibits a great deal of specificity under conditions of wash-out and competition. Overall, this and the other HIV inhibitors reported here may be useful as general anti-HIV therapeutics or, more specifically, as anti-HIV microbicides.

Experimental Procedures

Protein production and purification

Peptide fusion inhibitors N-acetylated, C-term amidated C37 and N-acetylated, C-term amidated C37(Q652L) were obtained from Genescript (Piscataway, NJ). The genes for GriffC37 and C37CD4M33$_{C1F23}$ DNA were synthesized by Genscript. All the constructs were placed into pET-15b (Novagen, Madison, WI). The amino acid sequence of CD4M33$_{C1F23}$ is: CNLHF CQLRC KSLGL LGKCA GSFCA CV. The amino acid sequence of the linker used for Griff37 as well as C37CD4M33$_{C1F23}$ is: SSSGG GGSGG GSSSG S with minor variations between the different constructs due to cloning procedures. The gene for griffithsin and Griff37 includes a 6 histidine affinity tag as well as a thrombin cleavage site, similar to that previously described (58). The sequence for Griff37 (Griffithsin-linker-C37) is: MGGSS HHHHH HSSGL VPRGS LTHRK FGGSG GSPFS GLSSI AVRSG SYLDA IIIDG VHHGG SGGNL SPTFT FGSGE YISNM TIRSG DYIDN ISFET NMGRR FGPYG GSGGS ANTLS NVKVI QINGS AGDYL DSLDI YYEQY SSSGG GGSGG GSSSG SHTTW MEWDR EINNY TSLIH SLIEE SQNQQ EKNEQ ELL.

The sequence for C37CD4M33$_{C1F23}$ is: MHHHH HHIEG RHTTW MEWDR EINNY TSLIH SLIEE SQNQQ EKNEQ ELLSS SGGGG SGGGG SSSSC NLHFC QLRCK SLGLL GKCAG SFCAC V.

Griffithsin was expressed in BL21(DE3) (Novagen) *E. coli* cells in LB broth. Protein production was induced upon addition of IPTG to a final concentration of 1 mM, followed by incubation for 4 h at 37°C. Pellets from these cells were resuspended in a 30

mL solution (500 mM NaCl, 20 mM Tris (pH 8), 10 mM benzamidine), then French pressed twice at 16,000 psi. After centrifugation for 1h at 17,000 g, the supernatant was loaded onto a Ni chelating column (Amersham Pharmacia Biotech) equilibrated with 50 mM Tris (pH 8.0), 500 mM NaCl, and eluted with a gradient using 500 mM imidazole, 50 mM Tris (pH 8.0), 500 mM NaCl. The fractions containing purified protein were dialyzed in a buffer (20 mM Tris (pH 8.0)) at 4°C overnight. The concentrated protein was further purified on a C4 reversed phase chromatography column (Vydac, Hesperia, CA), then lyophilized in a Labconco freeze dry system (Labconco Corporation). For NMR and some functional studies, protein was produced in minimal media with $^{15}NH_4Cl$ as the sole nitrogen source, using the same purification procedure after production. In early preparations, cleavage of the N-terminal Histidine tag at the thrombin site was attempted by incubation at room temperature in the presence of thrombin. This cleavage was unsuccessful, so experiments proceeded in the presence of the His tag for griffithsin, Griff37, Griff37(Q652L), and GriffCD4M33$_{C1F23}$,. Others have shown that the presence of an N-terminal His tag does not affect the activity of griffithsin (23,58).

Griff37 (which is griffithsin-linker-C37), Griff37(Q652L), GriffCD4M33$_{C1F23}$ and C37CD4M33 $_{C1F23}$ were expressed in BL21(DE3) either in LB media or minimal media as indicated above, although these proteins were found in the inclusion body. Therefore, after induction for 4 hours upon addition of 1mM IPTG at 37^{o}C, the cells were resuspended in 30 mL 5 M guanidinium chloride, 500 mM NaCl, 20 mM Tris (pH 8.0), then French pressed at 16,000 psi. After centrifugation for 1 hour at 17,000 g to remove undissolved material, the supernatant was loaded onto a Ni chelating column (Amersham Pharmacia Biotech) equilibrated with 5M Guanidinium, 50 mM Tris (pH 8.0), 500 mM

NaCl). Elution was carried out with 5M Guanidium, 500 mM imidazole, 50 mM Tris (pH 8.0), 500 mM NaCl. Fractions containing purified protein were combined and □-mercaptoethanol was added to a final concentration of 10mM and incubated for 2h with slow stirring. The protein was then dialyzed in 20 mM Tris (pH 8.0) at 4°C overnight and it was further purified as described above, with C4 reversed phase chromatography followed by lyophilization. For C37CD4M33 $_{C1F23}$, a further step of proteolytic cleavage of the His-tag by Factor Xa was added (reaction buffer: 50mM Tris-HCl, pH 7.5, 150mM NaCl, 1mM $CaCl_2$). Cleaved protein was finally purified with C4 reversed phase chromatography, and then lyophilized in a Labconco freeze dry system.

The proteins were analyzed by mass spectrometry on an Agilent 1100 HPLC and Thermo Fisher LCQ ion trap mass spectrometer (Stanford University). Expected values based on amino acid sequence are shown in parentheses after each experimental value. Griffithsin: 14552 (14554, assuming N-terminal Met cleavage); Griff37: broad peak at 20544 (20519); Griff37(Q652L): 20259 (20504); C37CD4M33$_{C1F23}$: 8696 (8709).

Cell culture

Seven cell lines were used:

1) HeLa-ADA cells that stably expressed HIV-1 Env from the CCR5-tropic strain ADA were maintained in DMEM supplemented with 10 % FBS plus 2 μM methotrexate (Sigma) as a selective reagent. This cell line was a kind gift from Dr. M. Alizon and Dr. Anne Brelot (Cochin Institute, Paris, France) (59).
2) HeLa-P5L cells that stably expressed human receptors CD4 and CCR5 were maintained in RPMI-1640 supplemented with 10 % FBS plus 0.5 mg/ml zeocin

(Invitrogen) for selection of CCR5 expression. They were a kind gift from Dr. M. Alizon and Dr. Anne Brelot (Cochin Institute, Paris, France) (59).

3) HeLa-TZM-bl cells that stably expressed human receptors CD4, CCR5 and CXCR4 were maintained in DMEM supplemented with 10 % FBS. This cell line was obtained through the NIH AIDS Research and Reference Reagent Program, Division of AIDS, NIAID, NIH and was a gift to that program from Dr. John C. Kappes, Dr. Xiaoyun Wu and Tranzyme Inc (60-63).
4) HL2/3 cells that stably expressed HIV-1 Env and Tat from the CXCR4-tropic strain HXB2 were obtained through the NIH AIDS Research and Reference Reagent Program, Division of AIDS, NIAID, NIH and were a gift to that program from Dr. Barbara K. Felber and Dr. George N. Pavlakis (64). The cells were maintained in DMEM supplemented with 10 % FBS and 500 μg/mL G418.
5) MAGI-CCR5 cells that stably expressed human CD4 and CCR5, naturally expressed CXCR4, and contain an HIV-1 LTR-β-galactosidase reporter gene construct were maintained in DMEM supplemented with 10% fetal bovine serum, 100 U/mL penicillin, 100 μg/mL streptomycin, 300 μg/mL L-glutamine, 0.2 mg/mL G418, 0.1 mg/mL hygromycin B and 1 μg/mL puromycin. These cells were obtained through the NIH AIDS Research and Reference Reagent Program, Division of AIDS, NIAID, NIH and were a gift to that program from Dr. Julie Overbaugh (65).
6) 293FT cells were maintained in DMEM supplemented with 10 % FBS and were a kind gift from Dr. Jennifer Manilay, originally obtained from Invitrogen (Carlsbad, CA).

7) Mouse 3T3 cells (a kind gift from Jean Phillipe Pellois, originally obtained from the American Tissue Type Collection (ATCC), were maintained in DMEM supplemented with 10 % FBS.

In addition, fresh human PBMCs were isolated and used in antiviral assays as previously described (66,67).

Virus isolates

HIV-1 isolates were obtained from the NIH AIDS Research and Reference Reagent Program, Division of AIDS, NIAID, NIH as follows: HIV-1 Ba-L from Dr. Suzanne Gartner, Dr. Mikulas Popovic and Dr. Robert Gallo (68,69); HIV-1 Ada-M (referred to as HIV-1 ADA) from Dr. Howard Gendelman (70-73); HIV-1 92HT599 from Dr. Neal Halsey and the DAIDS, NIAID; HIV-1 IIIB from Dr. Robert C. Gallo (74-76); HIV-1 91US005 from Dr. Beatrice Hahn and the DAIDS, NIAID and pNL3-4 from Dr. Malcolm Martin(77). HIV-1 Ba-L, 92HT599, NL4-3 and 91US005 were used for PBMC assays, while HIV-1 Ba-L, ADA, and IIIB were used for MAGI antiviral assays.

Cell-cell fusion assay

HIV-1 Envelope-mediated cell-cell fusion assays have already been described (59). Briefly, for the CCR5-tropic fusion assay, 10^4 HeLa-P5L cells (target) per well were seeded in a 96 well plate. After ~12 hours, media was replaced with 50 μL RPMI-1640. Serial dilutions of inhibitor were added to the wells of the plate: 20 μL of protein or peptide was added to the first well and mixed, then 20 μL was removed and added to the next well and so on. 10^4 HeLa-ADA cells (effector) in 50 μL RPMI-1640 were then added to each well (100 μL media per well total). The cells were allowed to fuse for 24 hours at 37^{o}C. Cells were then lysed by adding 0.5% NP-40 (US Biological) in PBS for

30min, then assayed for β-galactosidase activity after addition of 8 mM substrate CPRG (chlorphenol red-β-D-galactopyranoside, Calbiochem) in PBS with 20 mM KCl and 10 mM β-mercaptoethanol (Sigma). The absorbance at 570 nm (signal) divided by 630nm (background) was measured. The percentage of cell-cell fusion was calculated as [100 x (mean absorbance of treated well - mean absorbance of HeLa-P5L-only well)] / (mean absorbance of untreated well – mean absorbance of HeLa-P5L-only well). The "treated" wells contained inhibitor while "untreated" wells contained effector cells plus target cells in the absence of inhibitor. Kaleidagraph (Synergy Software, Reading PA) was used to fit the data into a four-parameter logistic equation. P-values were obtained using an unpaired, 2-tailed student's t-Test in Microsoft Excel. Supplemental Tables show more comparisons by this method.

In the CXCR4-tropic fusion assay, HeLa-TZM-bl cells were used as target cells and HL2/3 cells were used as effector cells. The rest of the procedure was identical to the CCR5-tropic fusion assay.

In the competition CCR5-tropic fusion assay, $5x10^3$ HeLa-P5L cells were seeded together with $5x10^3$ 3T3 cells per well. The rest of the procedure was identical to the normal CCR5-tropic fusion assay.

In the low temperature CCR5-tropic fusion assay, the addition of effector cells to target cells was immediately followed by 2 hours of incubation at 16^oC. The plate was returned afterwards to the 37^oC cell incubator for 24 hours.

In the wash-out assay, HeLa-ADA or HeLa-P5L cells were seeded in a 96 well plate the day before the assay. After the formation of the inhibitor gradient by serial dilution, as described above, the cells remained at room temperature for 30 min.

Afterwards, the media containing inhibitor was removed and every well was washed with PBS twice. New media without inhibitor was added and the complementary cell (HeLa-P5L cells or HeLa-ADA cells) were seeded in the plate.

Single round infection assay

HIV virions deleted in *vpr* and *env* were used to make single round infectious particles as follows. Plasmid pNL-luc3-R^-E^- containing the firefly luciferase gene, pSV-ADA(R5) and pSV-JRFL(R5) were kind gifts from Dr. Nathaniel Landau (78). For virus production, 293FT cells were doubly transfected with pNL-luc3-R^-E^- and either pSV-ADA or pSV-JRFL plasmids according to the product manual (ProFection Mammalian Transfection System (Promega)). 48 hours post-transfection, the supernatant was harvested, centrifuged at low speed, and filtered with a 0.45 um syringe filter. This viral stock was stored at -80 ^oC. For the assay, 10^4 TZM-bl cells per well were seeded in a 96 well plate. The next day, the media was removed and replaced with 50 μL of new media. Serial dilutions of inhibitor were carried out in the wells of the plate: 20 μL of protein or peptide was added to the first well and mixed, then 20 μL was removed and added to the next well and so on. Virus was added in an amount to obtain a luciferase signal between 60,000-80,000 arbitrary units for the ADA-env pseudo virus (while the control of non-infected cells gave ~600 arbitrary units) and 40,000-60,000 arbitrary units for the JR-FL-env pseudo virus. The total volume of media per well after pseudo virus addition was 100 μL. After 24 hours, old media was removed and replaced with new media. A further 24 hours later, the media was removed and the cells were lysed using Glo lysis Buffer (Promega) according to the manual. Luciferase substrate was then added (Luciferase Assay System (Promega)) and the plate was read using an Orion II microplate

luminometer (Berthold Techniques, Germany). The percentage of viral infection was calculated as [100 x (mean absorbance of treated well– mean absorbance of TZM-only well)] / (mean absorbance of viral infection in the absence of inhibitor – mean absorbance of TZM-only well). The results were plotted using Microsoft Excel, and the IC_{50} and IC_{90} were calculated using a linear equation fitted between two experimental points surrounding the IC_{50} or IC_{90}.

MAGI antiviral assays

The CCR5- and CXCR4-tropic MAGI antiviral assays were both performed using MAGI-CCR5 cells in a manner identical to the CCR5-tropic HIV-1 entry assay described previously (67), with the exception that the virus and test compounds were left in the culture for the entire 48 hour incubation period, compared to washing out of virus and test compound 3 hours post-infection for the HIV-1 entry assay.

HIV-1 strains Ba-L and ADA were used for the CCR5-tropic assays, and HIV-1 strain IIIB was used for the CXCR4-tropic assays. Co-receptor dependence for each of the viruses used to infect MAGI-CCR5 cells, which express both CCR5 and CXCR4, was verified through the use of AMD3100 (CXCR4 inhibitor; positive control inhibitor for IIIB, and negative control inhibitor for Ba-L and ADA) and TAK779 (CCR5 inhibitor; positive control inhibitor for Ba-L and ADA, and negative control inhibitor for IIIB) as control compounds (data not shown). Data processing was performed in a similar manner as described above for the single round infection assay.

NMR spectroscopy

Samples that were isotopically labeled with ^{15}N were prepared by growing BL21(DE3) containing the expression vector pET-15b in the presence of minimal medium containing $^{15}NH_4Cl$ as the sole nitrogen source as described above. Samples were dissolved in 20 mM sodium phosphate buffer pH 7.0 with 5% D_2O and a small amount of DSS (2,2-dimethyl-2-silapentane-5-sulfonate) for spectral referencing (79). The samples were placed in Shigemi tubes (Allison Park, PA). Spectra were measured at 25 °C on a four-channel 600 MHz Bruker Avance III spectrometer equipped with a GRASP II gradient accessory and a TCI cryoprobe, which has an actively-shielded Z-gradient coil and cooled preamplifiers for ^{13}C, ^{1}H, and ^{2}H. ^{1}H-^{15}N correlation spectra were measured with 760* points in the ^{1}H dimension and 64* points in the ^{15}N dimension, were processed using the program nmrPipe, and visualized using nmrDraw (80).

Results

Strategically linked compounds are potent in R5-tropic cell-cell fusion assays

We hypothesized that linking a gp120 binding protein with a gp41-binding protein could lead to an even more potent compound because potentially both gp120 and gp41 could be blocked from mediating the viral entry process. As a test of this hypothesis, the potent HIV entry inhibitor, griffithsin, was covalently linked via a 16 amino acid peptide linker with the gp41 binding peptide C37 to form "Griff37". Cell-cell fusion assays represent a common method of determining the antiviral potency of many compounds. In this technique, HeLa cells presenting human proteins CD4, CCR5 and/or CXCR4 on their surface (target cells) are combined with HeLa cells presenting HIV-1 Env proteins gp120 and gp41 on their surface and HIV-1 Tat in their cytoplasm (effector cells). The cells fuse by interaction of their respective surface proteins in an event that generally mimics the HIV entry process. The extent of cell-cell fusion can be measured using a reporter assay, because β-lactamase in the target cells is expressed under the control of the HIV-1 LTR promoter, which is activated by Tat from the effector cell upon fusion (59).

The results of CCR5-tropic cell-cell fusion assays are shown in Figure II-1 and Table II-1. Griffithsin alone performs well, with an IC_{50} of 1.31 nM ± 0.87, and the C-peptide C37 has an IC_{50} of 18.2 ± 7.5 nM in this assay. The two proteins in combination without being linked inhibit quite well, exhibiting an IC_{50} of 0.46 nM (for each protein, for a total concentration of 0.91 nM at 50% inhibition). However, when the griffithsin and C37 are covalently joined by a 16 amino acid linker to form Grft-linker-

C37 (hereafter referred to as Griff37), the effectiveness of the compound in the fusion assay increases dramatically, giving an IC_{50} of 0.15 ± 0.05 nM (Figure II-1A, 1B, Table II-1), which 8.7-fold greater than griffithsin alone. It has been reported that the activity of C-peptides can be enhanced by making the point mutation Q652L (81), so this point mutation was made in the linked compound. Griff37Q652L was produced and purified, but in the CCR5-tropic fusion assay this compound has approximately the same effectiveness as Griff37 (Table II-1).

As a further test of the overall strategy to link gp120 binding molecules with gp41 binding molecules, the peptide C37 was linked with a 16 amino acid linker to a modified version of the peptide CD4M33, an HIV inhibitor that was designed to bind gp120 in a manner similar to the protein CD4 (82). While the published peptide contains unnatural amino acids in positions 1 and 23, we replaced these with natural amino acids Cys and Phe respectively in order to allow expression in *E. coli*. We will refer to this peptide as $CD4M33_{C1F23}$.

In CCR5-tropic fusion assays, C37-linker-CD4M33$_{C1F23}$ (C37CD4M33$_{C1F23}$) exhibited an IC_{50} of 6.84 ± 2.9 nM (Figure II-1 and Table II-1). This value is significantly lower than that for either component alone in cell-cell fusion assays, since C37 has an IC_{50} of 18.2 nM, and His-tag-containing CD4M33$_{C1F23}$ was not an effective inhibitor even at our highest tested amount of 1.4 μM. Published reports of CD4M33 also describe that micromolar amounts of the peptide are required to inhibit CCR5-tropic fusion in a cell-cell fusion assay using vaccinia technology (82). We also produced the compound Griffithsin–linker-CD4M33$_{C1F23}$ (GriffCD4M33$_{C1F23}$), which could provide two molecules that bind to gp120. This compound performed reasonably well in CCR5-tropic cell-cell fusion assays, with an IC_{50} of 3.47 ± 0.97 nM, but did not appear to have enhanced activity compared to the individual components of the molecule.

These results suggest the possibility that combining a gp120 binding protein (such as Griffithsin *or* CD4M33) with a gp41 binding protein (such as C37) is a potent strategy for inhibition of CCR5-tropic HIV.

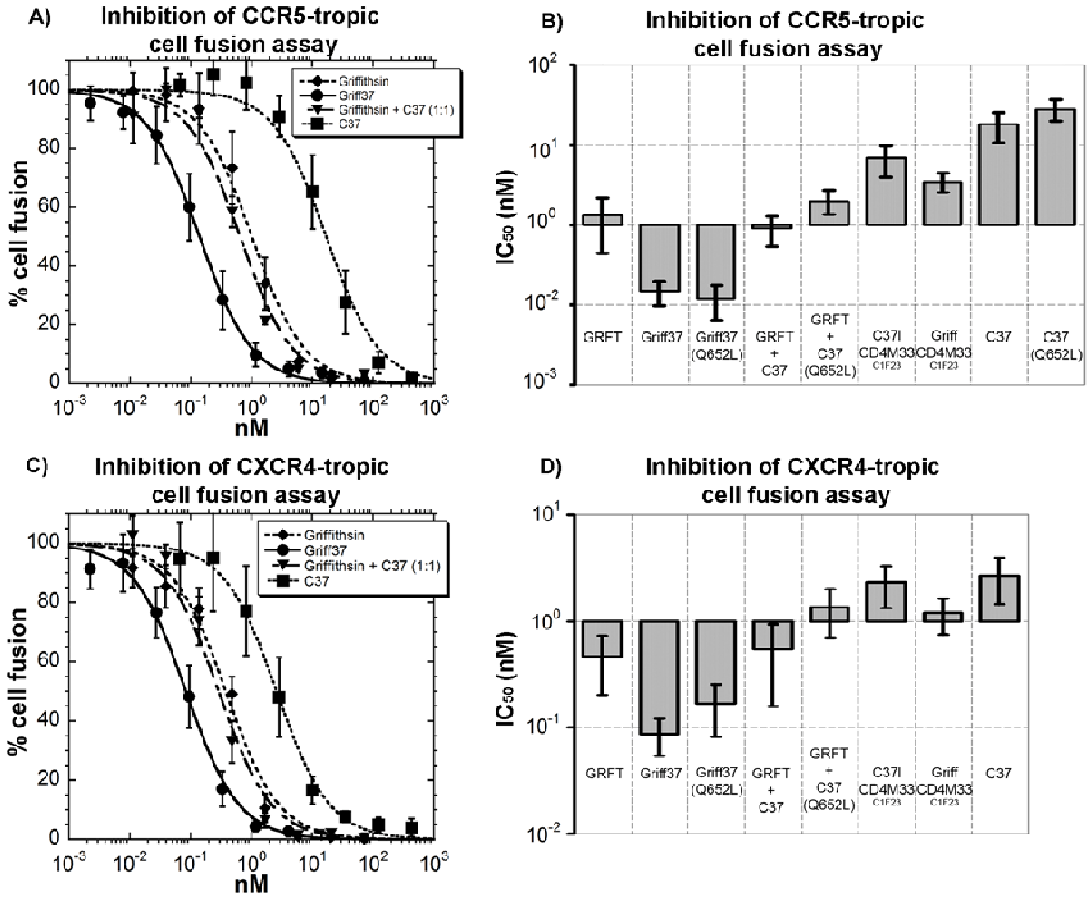

Figure II-1: Cell-cell fusion assays.

A. Sample CCR5-tropic fusion assay using HeLa-ADA effector cells and HeLa-P5L CCR5-bearing target cells.

B. Histogram showing the IC_{50} of several HIV inhibitors in CCR5-tropic fusion assays: 1. Griffithsin (GRFT); 2.Griff37; 3. Griff37(Q652L); 4.Griffithsin + C37 (1:1); 5. Griffithsin + C37 (Q652L) (1:1); 6. C37CD4M33$_{C1F2}$; 7. GriffCD4M33$_{C1F23}$; 8. C37; 9. C37Q652L. Each experiment was done at least 3 times in triplicate, and the results are presented as the average plus/minus the standard deviation.

C. Sample CXCR4-tropic fusion assay using HL2/3 effector cells and TZM-bl CXCR4-bearing target cells.

D. Histogram showing the IC50 of several HIV inhibitors in CXCR4-tropic fusion assays. 1. Griffithsin; 2.Griff37; 3. Griff37(Q652L); 4.Griffithsin + C37 (1:1); 5. Griffithsin + C37 (Q652L) (1:1); 6. C37CD4M33$_{C1F2}$; 7. GriffCD4M33$_{C1F23}$; 8. C37. Each experiment was done at least 3 times in triplicate, and the results are presented as the average plus/minus the standard deviation.

Table II-1: Inhibition of HIV env-mediated cell-cell fusion.

IC_{50} values for cell-cell fusion assays under various conditions. All combinations are reported as total protein concentration. Each experiment was done in triplicate and repeated at least 3 times except where noted. Numbers in parentheses indicate the p-value resulting from a t-Test of that compound in comparison to griffithsin + C37. N.D.: Not determined. The peptide C37 is a product of chemical synthesis and is capped at both ends, with N-terminal acetylation and C-terminal amidation

Compound	CCR5-tropic fusion assay	CXCR4-tropic fusion assay	CCR5-tropic fusion assay with competition	CCR5-tropic fusion assay with wash-out on HeLa-P5L cells	CCR5-tropic fusion assay with wash-out on HeLa-ADA cells
	IC_{50} (nM)	IC_{50} (nM)	IC_{50} (nM)	IC_{50} (nM)	IC_{50} (nM)
Griffithsin	1.31 ± 0.87	0.468 ± 0.265	1.73 ± 0.60	7.34 ± 3.58	4.28 ± 1.50
Griff37	0.148 ± 0.052 ($2.98*10^{-5}$)	0.088 ± 0.033 (0.046)	0.369 ± 0.034 (0.000067)	1.41 ± 0.75 (0.0292)	3.39 ± 0.56 (0.0588)
Griffithsin + C37 (1:1)	0.911 ± 0.367	0.542 ± 0.385	1.04 ± 0.23	13.3 ± 7.3	6.23 ± 1.73
Griff37 (Q652L)	0.121 ± 0.056 ($7.70*10^{-6}$)	0.167 ± 0.085 (0.0633)	N.D.	N.D.	N.D.
Griffithsin + C37(Q652L) (1:1)	2.01 ± 0.66	1.35 ± 0.65	N.D.	N.D.	N.D.
$C37CD4M33_{C1F23}$[1]	6.84 ± 2.85	2.30 ± 0.98	7.78 ± 1.56	561 ± 318	77.8 ± 1.2
$GriffCD4M33_{C1F23}$[1]	3.47 ± 0.97	1.19 ± 0.44	12.6 ± 1.4[2]	50.7 ± 9.0	N.D.
C37	18.2 ± 7.5	2.70 ± 1.27	61.4 ± 7.9	No inhibition	No inhibition
C37(Q652L)	28.2 ± 8.3	N.D.	N.D.	N.D.	N.D.

[1]. $CD4M33_{C1F23}$ is a recombinantly produced protein based upon the synthetically produced peptide CD4M33 designed by Martin et al (29).

[2]. This experiment was done in triplicate repeated two times.

Strategically linked compounds are potent in CXCR4-tropic cell-cell fusion assays

The linked combination of griffithsin and C37 was also quite potent in CXCR4-tropic cell-cell fusion assays. As shown in Figure II-1 and Table II-1, while griffithsin alone exhibited an IC_{50} of 0.47 ± 0.27 nM, the linked Griff37 was 5.3-fold more potent, similar to the point mutant of the linked compound, Griff37Q652L (Table II-1). When unlinked, the combination of griffithsin and C37 were only slightly more potent than each separately (Figure II-1C, 1D and Table II-1).

When C37 was linked with the gp120-binding peptide $CD4M33_{C1F23}$, the resulting $C37CD4M33_{C1F23}$ gave an IC_{50} of 2.30 ± 0.98 nM. Since this is close to the value of C37 alone, and CD4M33 has been shown to inhibit in a CXCR4-tropic fusion assay in the micromolar range (IC_{50} of 0.8 ± 0.09 μM) (29), it appears that linking the two inhibitors in this case does not improve inhibition. Interestingly, these results differ from the CCR5-tropic cell-cell fusion assay, where the $C37CD4M33_{C1F23}$ compound gave an IC_{50} that was significantly better than either compound alone (Figure II-1 and Table II-1).

Strategically linked compounds perform well in viral and pseudoviral assays

To confirm that the strategy of linking a gp120-binding protein with a gp41-binding peptide is successful in inhibiting HIV replication, a series of assays were performed using several types of target cells and viral strains. In replication competent HIV assays, the linked compound Griff37 consistently performs better than griffithsin alone. For example, when the CCR5-tropic HIV-1 strain Ba-L is used to infect MAGI cells, griffithsin alone exhibits an IC_{50} of 0.04 ± 0.01 nM, while Griff37 is 2.7-fold better, with an IC_{50} of 0.015 ± 0.005 nM (Table II-2, Figure II-2) and the unlinked combination

of griffithsin and C37 has an IC_{50} of 0.05 nM in each protein. Similarly, when the CCR5-tropic HIV-1 strain ADA infects MAGI cells, Griff37 is 2-fold better than griffithsin alone and 6.3-fold better than the unlinked combination of griffithsin and C37 (total protein concentration) (Table II-2). The effect in most cases is even more dramatic when comparing concentration at 90% inhibition (IC_{90}) for these compounds against viral strains: For Ba-L, Griff37 is 6.4-fold more potent than Griffithsin and 9.4-fold more effective than the unlinked combination (Table II-2); similar results are observed for inhibition of strain ADA.

As described for fusion assays, these compounds are also highly effective against CXCR4-tropic HIV strains. When MAGI cells are infected by the CXCR4-tropic strain HIV-1 IIIB, Griff37 again shows several-fold higher potency than its components (Table II-2).

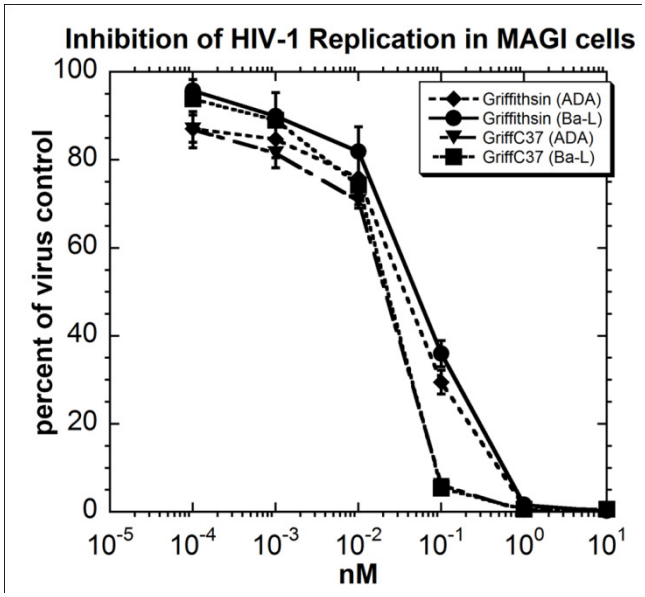

Figure II-2: HIV viral assays.

ADA and Ba-L virus strains were used to infect MAGI cells. Griff37 (both lines nearly overlapping) performs better than griffithsin in both cases.

Table II-2: Inhibition of HIV-1 replication in MAGI cells.

IC_{50} and IC_{90} values for viral replication assays. All combinations are reported as total protein concentration. Numbers in parentheses indicate the p-value resulting from a t-Test of that compound in comparison to Griffithsin + C37. Each experiment was done in triplicate and repeated 2 times.

Compound	Ba-L (CCR5-tropic)		ADA (CCR5-tropic)		IIIB (CXCR4-tropic)	
	IC_{50} nM	IC_{90} nM	IC_{50} nM	IC_{90} nM	IC_{50} nM	IC_{90} nM
Griffithsin	0.040 ± 0.010	0.515 ± 0.055	0.030 ± 0.010	0.450 ± 0.040	0.145 ± 0.065	0.890 ± 0.110
C37[1]	7.56 ± 1.07	79.7 ± 2.5	6.15 ± 1.40	68.9 ± 4.2	10.3 ± 1.9	> 100
Griffithsin + C37 (1:1)	0.100 ± 0.030	0.750 ± 0.020	0.095 ± 0.015	0.705 ± 0.005	0.230 ± 0.020	2.21 ± 0.57
Griff37	0.015 ± 0.005 (0.1077)	0.080 ± 0.010 (0.0011)	0.015 ± 0.005 (0.037)	0.085 ± 0.005 (0.00013)	0.035 ± 0.005 (0.011)	0.325 ± 0.065 (0.081)

Similar results are observed when human PBMCs are infected with HIV-1 Ba-L. In this case, griffithsin alone has an IC_{50} of 0.28 ± 0.17 nM, while Griff37 is 4.7-fold better, with an IC_{50} of 0.059 ± 0.0004 nM, and the unlinked components griffithsin plus C37 are less than two-fold better than griffithsin alone (Table II-3). When the CCR5-tropic HIV-1 clinical isolate 91US005 is used to infect PBMCs, the result is about a two-fold improvement for Griff37 over griffithsin alone (Table II-3). GriffC37 also shows a 3.8-fold increase in anti-HIV potency compared to Griffithsin alone in CXCR4-tropic strains NL4-3 and 92HT599 (primary strain; Table II-3). Since the griffithsin-containing compounds were clearly more potent than the $CD4M33_{C1F23}$ -containing compounds, the $CD4M33_{C1F23}$ compounds were not tested in replication competent viral assays.

Table II-3: Inhibition of HIV-1 replication in PBMCs.

IC_{50} and IC_{90} values for viral replication assays. All combinations are reported as total protein concentration. Numbers in parentheses indicate the p-value resulting from a t-Test of that compound in comparison to Griffithsin + C37. Each experiment was done in triplicate and repeated 2 times.

Compound	Ba-L (CCR5-tropic)		91US005 (CCR5-tropic)		NL4-3 (CXCR4-tropic)		92HT599 (CXCR4-tropic)	
	IC_{50} nM	IC_{90} nM	IC_{50} nM	IC_{90} nM	IC_{50} nM	IC_{90} nM	IC_{50} nM	IC_{90} nM
Griffithsin	0.280 ± 0.170	0.760 ± 0.150	0.280 ± 0.170	0.760 ± 0.150	0.170 ± 0.040	0.725 ± 0.125	0.74 ± 0.37	1.86 ± 0.89
C37[1]	2.39 ± 0.635	7.40 ± 1.20	2.39 ± 0.635	7.40 ± 1.20	2.89 ± 0.39	8.33 ± 0.25	14.5 ± 1.4	27.2 ± 0.6
Griffithsin + C37 (1:1)	0.33 ± 0.05	0.97 ± 0.33	0.33 ± 0.05	0.97 ± 0.33	0.220 ± 0.040	0.58 ± 0.02	0.76 ± 0.24	1.77 ± 0.03
Griff37	0.059 ± 0.0004 (0.044)	0.155 ± 0.065 (0.204)	0.059 ± 0.0004 (0.077)	0.155 ± 0.065 (0.155)	0.045 ± 0.005 (0.049)	0.205 ± 0.035 (0.011)	0.195 ± 0.025 (0.144)	0.630 ± 0.070 (0.004)

In single-round infection assays griffithsin and its analogs all perform quite well. HIV virions pseudotyped with Env from the CCR5-tropic HIV-1 strains JR-FL or ADA were both used in inhibition assays. While Griff37 performed better than griffithsin alone with strain JR-FL, it did not perform better using strain ADA (Table II-4). Indeed, using strain ADA in a single round infection assay was the only instance we identified in which Griff37 was not superior to griffithsin (Table II-1, Table II-2,

Table II-3, Table II-4). In addition, the combination of gp41 binding peptide C37 with gp120-binding $CD4M33_{C1F23}$, $C37CD4M33_{C1F23}$, also appears to perform moderately better than the components CD4M33 (~2 fold) or C37 alone (~13 fold) in

CCR5-tropic pseudoviral assays, although our CCR5 strains were not the same as those used by Martin (Table II-4 and (29)). Again this indicates that the combination of a gp120-binding molecule with a gp41-binding molecule can be a potent HIV inhibition strategy, particularly since the CD4M33 component of our C37CD4M33$_{C1F23}$ was not optimized for amino acid usage or foldedness during preparation.

Table II-4: Inhibition of HIV single round pseudovirus in TZM-bl cells.

IC_{50} and IC_{90} values for single round pseudovirus assays. Numbers in parentheses indicate the p-value resulting from a t-Test of that compound in comparison to griffithsin + C37. Each experiment was done in triplicate and repeated at least 3 times. N.D. : Not Determined

Compound	ADA (CCR5-tropic)		JR-FL (CCR5-tropic)	
	IC_{50} (nM)	IC_{90} (nM)	IC_{50} (nM)	IC_{90} (nM)
Griffithsin	0.008 ± 0.016	0.164 ± 0.069	0.035 ± 0.008	1.25 ± 0.19
Griff37	0.020 ± 0.016 (0.96)	0.172 ± 0.061 (0.12)	0.025 ± 0.022 (0.63)	0.260 ± 0.101 (0.0003)
Griffithsin + C37 (1:1)	0.021 ± 0.018	0.277 ± 0.184	0.032 ± 0.017	1.38 ± 0.39
Griff37(Q652L)	0.023 ± 0.006 (0.702)	0.274 ± 0.066 (0.52)	N.D.	N.D.
Griffithsin + C37(Q652L) (1:1)	0.021 ± 0.006	0.374 ± 0.192	N.D.	N.D.
C37CD4M33$_{C1F23}$	2.33 ± 2.83	17.3 ± 17.4	2.25 ± 1.39	24.3 ± 19.6
GriffCD4M33$_{C1F23}$	0.222 ± 0.017	2.69 ± 0.23	0.270 ± 0.147	2.89 ± 0.25
C37	27.2 ± 17.2	637 ± 290	15.2 ± 4.2	462 ± 357
C37(Q652L)	114 ± 5	N.D.	N.D.	N.D.

Strategically linked compounds maintain effectiveness in competition assays and in washing assays

For a potential therapeutic to be beneficial in an organism, it needs to be able to effectively find its target in the milieu of other cell types and potential binding partners. As a test of this ability, the CCR5-tropic cell-cell fusion assay was modified with the addition of fibroblast mouse 3T3 cells which are the most common cells at connective tissues. These cells are not able to be infected by HIV and do not have human coreceptors on their surface, but they present a myriad of proteins and carbohydrates that could potentially bind an anti-HIV therapeutic and confound its ability to inhibit in the assay.

As we previously reported, in a CCR5-tropic fusion assay in the presence of unrelated competitor cells, the peptide C37 performs significantly worse than in the absence of such cells, with an IC_{50} of 61.4 ± 7.9 nM ((83) and Table II-1). This leads to the possibility that Griff37 also performs worse in the presence of unrelated cells due to the presence of C37. However, the linked compounds perform quite well under these conditions. The presence of competitor cells does not greatly affect griffithsin-containing compounds, as griffithsin alone still performs well. But Griff37 again performs significantly better than griffithsin alone (Table II-1). When C37 is linked to gp120-binding peptide CD4M33 to make $C37CD4M33_{C1F23}$, the resulting IC_{50} is 7.78 ± 1.6, which is close to the value in the absence of competition. Similar results were also observed for Griff37 in single round infection assays using virus pseudotyped with Env from the CCR5-tropic HIV-1 strain JR-FL in the presence of competitor cells. In these experiments, all griffithsin-containing assays performed well, but Griff37 performed better than griffithsin alone (data not shown).

To determine whether the linked inhibitors maintain some of their activity under conditions of washing out, modified R5 fusion assays were carried out. In these assays, either the target cells or effector cells were placed in a well in the presence of inhibitor. The supernatant was then removed, cells were washed twice with PBS, and inhibitor-free media added, followed by the addition of the other cell type to allow fusion to proceed. Therefore, inhibition would only be observed for inhibitors that can maintain their presence rather than be washed away. In these assays, an IC_{50} for C37 could not be determined because it was apparently fully washed out. However, both griffithsin and Griff37 maintained nanomolar effectiveness when first bound to the ADA "HIV effector cells" before the washing step. When the inhibitors were incubated with the target cell before the washing step, both inhibitors still performed well, but Griff37 was 5.2-fold more effective than griffithsin alone (Table II-1). The fact that both griffithsin inhibitors retained some activity was somewhat unexpected since griffithsin should bind specifically to the HIV spike, which is not present on the target cells. Indeed, griffithsin does demonstrate specificity by failing to block infection with HIV virions pseudotyped with SVA-MuLV (IC_{50} >100 (μg/ml) (51). Possibly the washing conditions were too mild, as more vigorous washing does remove griffithsin inhibition (data not shown). Overall these experiments indicate that under physiological conditions where many different cell types and fluids may be present, these inhibitors maintain very high effectiveness, in contrast to C37 alone.

NMR experiments on the anti-HIV compounds

Nuclear magnetic resonance (NMR) is a very effective technique for determining structural details of proteins, including their extent of foldedness and the possibilities for their oligomeric state (84-86). Figure II-3A shows the ^{15}N-^{1}H correlation spectrum (^{15}N HSQC) of griffithsin alone, which is a 121 amino acid protein that crystallizes as a dimer (25). This type of spectrum shows one peak for every N-H pair in the protein, and therefore provides a fingerprint that is unique for each protein. The spectrum of griffithsin shows good peak dispersion in the ^{1}H dimension with well-resolved peaks, strongly suggesting a nicely folded protein, as would be expected for a stable, wild-type, relatively low molecular weight protein.

Figure II-3B shows the spectrum of the linked compound Griff37. Despite this protein exhibiting potent anti-HIV activity in numerous assays, the spectrum shows strong signal around 8.2 ppm in the ^{1}H dimension, indicative of unfolded or random coil protein in the sample. There are also peaks (of lower intensity) in the "folded" region of the spectrum (particularly above 9 ppm), and an overlay of this spectrum with griffithsin alone indicates that these peaks arise from folded griffithsin (overlay not shown). There are several likely explanations for the poor quality of this spectrum despite the protein being quite active. First, the 16 amino acid linker between griffithsin and C37 was designed to be structurally flexible, so the signal from this region is expected to resonate in the "unfolded" region of the spectrum. Second, the peptide C37 is likely unfolded in the absence of a binding partner (87), which would lead to peaks in the unfolded region of the spectrum due to this peptide, even if the peptide would be fully active when presented with a binding partner in an assay. Finally, if the Griff37 protein forms

oligomers or loose aggregates, line broadening would occur, which would have the effect of decreasing the intensity of all the peaks, particularly those from residues that are not free to move quickly in solution. Therefore, a globular protein like griffithsin would be expected to lose a great deal of signal intensity upon oligomerization. Overall, the spectrum of Griff37 suggests a sample that is at least partially folded (due to the clear presence of peaks that overlap with those in the griffithsin sample) but that may have a percentage of the sample unfolded and/or a portion of the sample in an oligomerized state.

NMR experiments were also carried out on the C37CD4M33$_{C1F23}$ peptide combination. Since this compound is a fusion of two peptides (albeit functionally active peptides), the unfolded peaks that are observed in the 8.2 ppm region of Figure II-3C were expected. However, there were also peaks indicative of folded protein (several circled in Figure II-3C). Since C34 (nearly identical to C37) has been shown to be unfolded in the absence of its gp41 binding partner (55), it is likely that the peaks in this region of the spectrum result from folded CD4M33$_{C1F23}$. The parent compound, CD4M33, was designed by Martin *et al.* to be a folded peptide containing unnatural amino acids and was produced for their work by chemical synthesis (29). Therefore, it is notable that although we made multiple changes to CD4M33, including the use of "natural" amino acids to replace the designed unnatural amino acids, the use of recombinant expression rather than synthesis, and linkage with another peptide, the resulting protein still is an active anti-HIV compound that is at least partly folded.

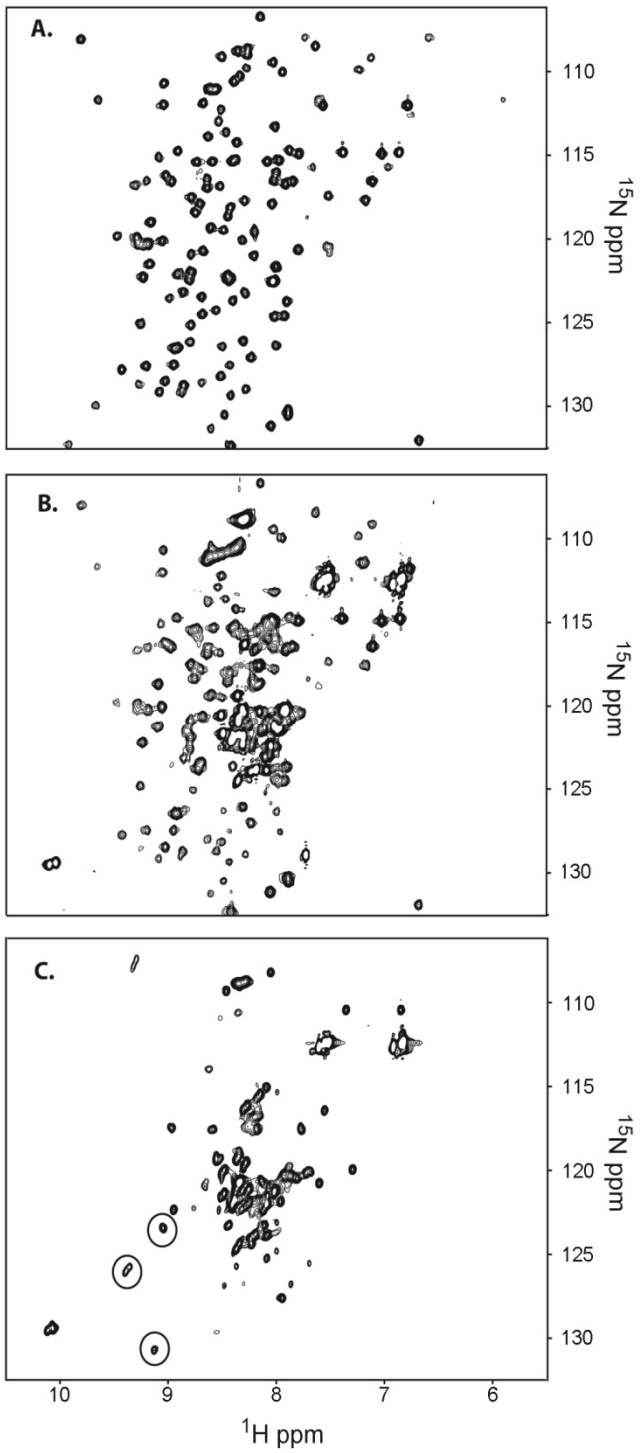

Figure II-3: ^{15}N-^{1}H correlation spectra of some of the HIV inhibitors used in this study.

A. Wild-type griffithsin. B. Griff37. C. C37CD4M33 $_{C1F23}$. Circled peaks on this spectrum indicate resonances that are consistent with folded protein.

Discussion

Many binding targets, both on the HIV-1 virion and on the human cell, have been established as effective sites for HIV inhibition. But an underexplored area for HIV inhibition is to elucidate an overall strategy, possibly combining multiple inhibitors, that optimizes the effectiveness of inhibition under a number of different conditions and viral strains. The present work examines the possible benefits of combining in a single compound both a gp120-binding and a gp41-binding moiety. It was found that such a strategy consistently performs well both in cell-cell fusion assays and in viral assays, using both CCR5- and CXCR4-tropic strains, as well as under conditions of competition and washing out. In most cases, the linked compounds performed better than their parent compounds, most strikingly in the case of improvement of the already highly potent protein griffithsin.

Griffithsin has shown a great deal of promise in tests of its anti-HIV microbicidal characteristics. In addition to remarkably high potency, it is stable upon incubation at 37 °C, which is a necessary property if it must remain active in the human body for hours or be stored without refrigeration (50). It also retains its activity in cervical/vaginal lavage fluid (50), is non-inflammatory in human cervical explants, is non irritating in a rabbit vaginal model and is active against multiple clades of HIV, indicating likely usefulness in many or all of the areas hardest hit by this disease (51).

The most effective inhibitor in our experiments was Griff37, or possibly its slight variant Griff37Q652L, both compounds that covalently link griffithsin with the C-peptide C37. This linked inhibitor performed at sub-nanomolar levels in both CCR5- and CXCR4-tropic fusion assays, and at mid-picomolar levels in viral assays. These values

are in almost every case better than for griffithsin alone and better than an unlinked combination of griffithsin and C37 (Table II-1, Table II-2, Table II-3, Table II-4). This indicates that the linked combination of inhibitors is indeed more potent that the individual components and worthy of strong consideration as a microbicide or therapeutic. These effects are not likely due to synergistic action of the two inhibitors, because an examination of the combination index (an indicator of synergy; (88)) showed at best moderate synergy in fusion assays, while showing no synergy or even antagonism in viral assays (data not shown).

In the replication competent viral assays, the improvement in the IC_{90} for the linked compound Griff37 was more statistically significant than the IC_{50} which is a positive indicator since 90% inhibition is perhaps more critical for truly stopping infection. Statistical significance is judged by a comparison of the p-values derived from the student's t-Test as described in Methods. The Table II-5 also contains p-values for a comparison of the linked compounds with their unlinked controls for many types of assay presented here. The greater effectiveness of Griff37 at the higher concentrations needed for 90% inhibition in the viral assay could be partly explained by the increasing importance of the C37 component at these concentrations because C37 inhibits at nanomolar levels. As the concentration of the inhibitor rises from picomolar levels (where griffithsin binds to gp120), to nanomolar levels, the C-peptide may contribute more to the overall inhibition. As a further test of the strategy of covalently linking a gp120-binding compound with a gp41-binding compound, the linked peptide $C37CD4M33_{C1F23}$ was produced. Again, this compound consistently showed more

potent inhibition than either component separately in the CCR5-tropic cell-cell fusion assay (Table II-1 and Table II-4).

Table II-5: t-Test P values for cell-cell fusion assay.

a) Griffithsin vs Griff37

CCR5 tropic	0.00020
CXCR4 tropic	0.005143
CCR5-tropic wash-out on HeLa-ADA cells	0.3933
CCR5-tropic fusion assay with wash-out on HeLa-P5L cells	0.0094
CCR5-tropic fusion assay with competition	0.000187

b) Griffithsin + C37 vs Griff37

CCR5 tropic	2.98E-05
CXCR4 tropic	0.046448
CCR5-tropic fusion assay with wash-out on HeLa-ADA cells	0.0558
CCR5-tropic fusion assay with wash-out on HeLa-P5L cells	0.0292
CCR5-tropic fusion assay with competition	0.000067

c) Griffithsin vs Griff37(Q652L)

CCR5 tropic	0.00053
CXCR4 tropic	0.074787

d) Griffithsin + C37(Q652L) vs Griff37(Q652L)

CCR5 tropic	7.70E-06
CXCR4 tropic	0.063342

e) GriffCD4M33C1F23 vs C37

CCR5 tropic	0.00265
CXCR4 tropic	0.570381

In deriving a set of possible models for the explanation of the effectiveness of Griff37, each model must account for the fact that this linked molecule is a significantly better inhibitor than the unlinked combination of the two components. In keeping with this observation, there are at least three plausible models for the mechanism of action of Griff37. The first model is that the griffithsin moiety binds to gp120 with high affinity, and the role of the linked C37 is simply to provide a more sizeable protein on gp120 (Figure II-4A), making a more effective blockade against binding to CD4 or CCR5. However, arguing against this simple steric mechanism is the evidence that griffithsin linked to the peptide CD4M33 (Griff CD4M33$_{C1F23}$) also would be expected to be able to provide a similar binding blockade, and yet this molecule does not show enhanced inhibition compared to griffithsin alone. A second model is one in which the griffithsin component binds to gp120, thereby delivering C37 close to its binding site on gp41. By being in physical proximity to gp41, C37 is able to bind gp41 and inhibit fusion if and when gp41 is exposed, possibly dislodging the linked griffithsin at that time. In this scenario, it is assumed that only one component of the linked pair is binding to its site at any given time, although they may both be in an on-off equilibrium with their respective binding sites (Figure II-4B).

In the third model of action for Griff37, both components (i.e. griffithsin and C37) are bound to their respective targets simultaneously. The 16 amino acid linker used in Griff37 was designed to be flexible and to allow simultaneous binding of the two components even if the binding sites were fairly distant. For example, an 8 amino acid extended chain in griffithsin spans about 24 Å, so a 16 amino acid linker could potentially allow binding at sites several tens of angstroms apart. In the structure and

structural model provided by Chen *et al*. in their work on unliganded SIV gp120 (89), much of the surface of gp120 is close enough to gp41 to allow simultaneous binding of griffithsin and C37. However, it has been shown that structural changes in gp120 to allow exposure of gp41 does not occur unless CD4 is bound, and the presence of griffithsin is very likely to stop the binding of gp120 to CD4 (23). Therefore, a "simultaneous binding" model of Griff37 action could possibly include two scenarios. In one scenario, griffithsin is bound to carbohydrates on gp120, but not in a correct position to abrogate CD4 binding, which allows gp120 to contact CD4 and expose gp41. The linked C37 moiety of Griff37 can bind gp41 and in this case provides "rescue" for the ineffective inhibition of griffithsin (Figure II-4C). Alternatively, the griffithsin of Griff37 may inhibit CD4 binding on the monomer of gp120 to which it is bound, but a neighboring gp120 of the trimer may contact CD4 and alter its conformation enough to expose the gp41 trimer (Figure II-4D). In this case, both griffithsin and C37 in the linked molecule can effectively bind to their target sites.

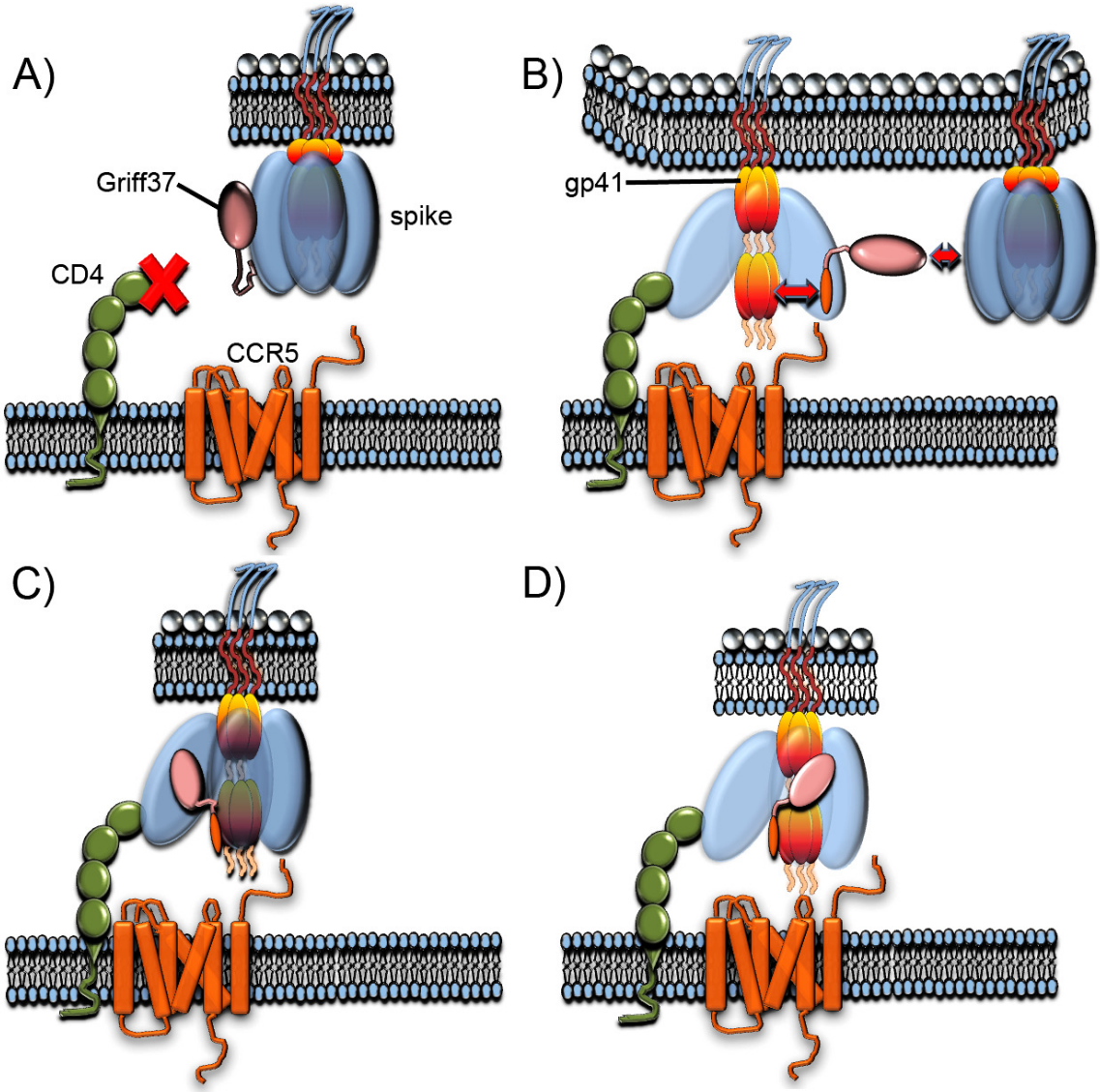

Figure II-4: Possible models of action of linked compound Griff37.

A) The inhibitory action of the molecule is due to griffithsin binding to gp120, but extra steric blocking is provided by C37. B) Inhibition is provided by either griffithsin or C37, but only one is properly bound to its target at any given time. C) Griffithsin binds to the "wrong" area of gp120, allowing CD4-gp120 interaction. This leads to exposure of gp41, so the C37 portion of Griff37 interacts with gp41, leading to inhibition. D) A CD4-gp120 interaction on one of the gp120 monomers allows partial opening of the spike so that griffithsin (bound to another gp120 monomer on the same trimer) can deliver C37 to gp41.

Similarly to the results with Griff37, experiments reported here with linked peptides also indicates the beneficial effects of binding both gp120 and gp41, although *E. coli* production without optimization leads to the possibility that the effect could be stronger after improved refolding conditions are determined. The compound C37CD4M33$_{C1F23}$ inhibits in CCR5-tropic fusion assays much better than either component alone, indicating the effectiveness of binding both targets of these compounds, possibly at the same time. Small differences in IC_{50} values between C37 and linked compound C37CD4M33 $_{C1F23}$ in the CXCR4-tropic cell-cell fusion assay may be explained by a lower affinity of CD4M33 $_{C1F23}$ for HXB2 Env. The lack of a proper control in this case (CD4M33 $_{C1F23}$ alone) is critical. It should be noted that the values for our version of CD4M33$_{C1F23}$ are expected to be significantly worse than the reported values for the CD4M33 peptide, since ours is fully recombinant without the benefit of selectively designed unnatural components. Another important point is the high number of cysteines (6 total) that C37CD4M33 $_{C1F23}$ has that could allow for potentially different combinations of S-S bonds leading to unfolded protein. Even if C37CD4M33 $_{C1F23}$ shows several folded peaks in the NMR spectrum, it is not clear that any or all of the proper disulfide bonds are formed. Therefore, it is possible that CD4M33 $_{C1F23}$ does not have the proper folding to bind as tightly to gp120 as the chemically synthesized CD4M33. Even with these drawbacks, it is fairly easy and economical to produce C37CD4M33$_{C1F23}$, and its relatively small size makes it an attractive candidate for further improvement.

It is possible that there are additional benefits to the linked compounds aside from improved potency. The C-peptide T-20 is clinically approved but suffers from the need

for frequent dosing due to a short lifetime of only hours *in vivo* (90). It has been shown that linking the similar peptide C34 with albumin (a larger protein) allows for high detectable plasma concentrations of the linked compound in rats for days, suggesting that linking a C-peptide with a larger protein may delay renal clearance and/or susceptibility to protease degradation (90). Our experiments involve the protein C37, which, like T-20, is derived from the sequence of gp41 and which is identical to C34 but has an additional 3 amino acids on the N-terminus. It is possible that Griff37 has an *in vivo* lifetime of several days due to its larger size, similar to albumin linked C34 (90). In addition, a benefit of a drug with two different sites of action is the difficulty of viral escape, since viral mutations to escape from one of the linked inhibitors would be expected to have little or no effect on the other inhibitor.

Other groups have also investigated the strategy of linking HIV inhibitors in order to increase effectiveness. One very effective linked compound is a CD4 antibody having each heavy chain extended with a gp-41-binding C-peptide. This chimeric protein showed HIV inhibition with an IC_{50} as low as 14 pM (91,92). This group also produced another excellent compound by linking a CCR5 antibody with a C-peptide (93). In both cases, the antibody was expressed having one C-peptide at the C-terminus of each heavy chain of the antibody, resulting in a ratio of 2:1 C-peptide: antibody. While both of these chimeric compounds would likely be highly effective microbicides, they have the disadvantage of being produced in a mammalian cell system (HEK cells), which would make it difficult to produce gram-quantities of the inhibitor. In our system, Griff37 was produced from *E. coli* in shaker flasks and could likely be produced in large quantities by fermentation or in a plant based expression system, both of which were recently shown to

be useful in making large quantities of functional griffithsin (51,58). Another effective HIV inhibitor was produced by linking two domains from CD4 with a single chain variable region from the antibody 17b, which is known to interact with gp120 on a site near its CCR5-binding region. This inhibitor was shown to be effective at nanomolar levels and was expressed by recombinant vaccinia virus (94). A recent study of a gp120 antibody in various monomeric/dimeric covalent configurations and a gp41 antibody in these configurations also showed the importance of multivalency in HIV inhibition (95).

Structurally, many questions remain unanswered about the compounds in the present study. Griffithsin consistently crystallizes as a dimer (25,26,52), which could imply that a linked compound may include two molecules of griffithsin and two molecules of C-peptide. However, the concentrations used in the functional assays are orders of magnitude lower than those for structural studies, so it has not yet been determined if the griffithsin dimer is a consideration in the function of the compounds reported here.

The ^{1}H, ^{15}N correlation spectrum of griffithsin alone shows a nicely dispersed set of peaks indicative of a fully folded protein (Figure II-3A). To our knowledge, this is the first NMR spectrum reported for griffithsin, although several high quality X-ray structures have been determined (25,26,52). The benefit of NMR spectra is that comparisons can quickly and easily be made between variants of a protein without the need for a full structural determination if sequence assignments have been completed. Such work for griffithsin is ongoing.

NMR spectra of the strategically linked compounds show some resonances to indicate that both Griff37 and C37CD4M33$_{C1F23}$ are folded, although it is not clear what

percentage of each sample is folded. The strong resonances in the unfolded region could simply be due to the presence of disordered C37 peptide and linker, or could in addition have a significant component from unfolded (and presumably non-functional) protein. In the latter case, small improvements to the refolding procedure may lead to significantly more potent inhibitors.

The strategically linked compounds reported here show picomolar levels of activity in many assays, but may still be able to be improved. For example, the C-peptide component may be able to be improved by capping the charged ends that occur naturally when a protein is expressed rather than synthesized (81). In our hands, N-acetylated, C-amidated C37 inhibits in the CCR5-tropic fusion assay with an IC_{50} of 18.2 nM, as reported above. However, C37 without the terminal modifications inhibits with an IC_{50} of >100 nM. Therefore, it is possible that capping the C-terminal end of Griff37 and $C37CD4M33_{C1F23}$ could increase the potency of these compounds. In addition, others have reported further improvements in C-peptides that increase their potency (96), which may be able to be incorporated into the strategy presented here.

This paper presents evidence that the strategy of linking a gp120 binding molecule with a gp41 binding molecule can lead to a compound that has greater anti-HIV activity than its individual components alone or in combination. It was demonstrated that the highly potent microbicidal candidate griffithsin could be made even more potent using this strategy.

In the next chapter, I will described the synergistic effect on HIV inhibition between P2-RANTES and C-peptides C34 and C37.

CHAPTER III

SYNERGY BETWEEN P2-RANTES AND gp41 BINDING PEPTIDES IN CELL-CELL FUSION ASSAYS

Introduction

In addition to the more established anti-HIV-1 strategies such as inhibition of protease or reverse transcriptase, viral entry inhibition has great potential in the fight against AIDS. Entry inhibition entails stopping HIV-1 before it breaches the cell, either as a strategy to prevent infection altogether or to curtail infection of new cells in an HIV-positive individual. Several strategies have proven effective at HIV-1 entry inhibition either *in vitro* or *in vivo*: binding to viral surface proteins gp120 and gp41, binding to human cell surface receptor CD4, and binding to human cell surface co-receptors CCR5 and CXCR4 (97-99). In particular, the synthesized peptide T-20 is believed to act by binding to gp41 (100,101) and is currently in clinical use. But several recent studies revealed that T-20 does not block the six-helix bundle pre-hairpin formation (31,97). Another peptide, C37, derived from C-terminus of gp41 (and nearly identical to the widely reported C-peptide C34 (10,31,56)) is also reported to have strong anti-HIV entry activity due to tightly binding to the gp41 N-terminal helices (56,102).

The potential for synergy between two entry inhibitors is important for two reasons. First, the therapeutic dose of the drugs will be lowered. Second, the ability of the virus to develop resistance to two agents at the same time is much less likely than for a single agent. Several studies have established that synergy can occasionally be

observed when two fusion inhibitors are combined in a viral assay or *in vitro* fusion assay (103-109). For example, some synergy is observed in the combination of CCR5 antibodies with T-20 (103,105), the combination of small molecular antagonists of coreceptors with T-20 (108,109), the combination of small molecular antagonists of CCR5 with CCR5 antibodies (103,105,107), and the combination small molecular antagonists of CCR5 with chemokines (105,108). A potent synergy was observed between PRO 542 (a fusion of CD4 and immunoglobulin containing multiple CD4 units) and T-20, in which the IC_{50} of each component was 0.84 nM and 1.3 nM, respectively, but in combination the IC_{50} was reduced to 0.039 nM and 0.35 nM, respectively in cell-cell fusion assays (106).

In this paper we report that synergy can also be observed when some CCR5 ligands are combined with gp41 binding peptides C37 and/or C34. In particular, a combination of the RANTES mutant P2-RANTES (33) and C37 in a 1:1 ratio yields an IC_{50} of 2.12 nM in an R5 tropic cell-cell fusion assay, which represents a dose reduction for both components and could lead to more effective HIV inhibition at lower doses. We also observe moderate synergy at 90% inhibition in various viral assays.

Experimental Procedures

Reagents

All cell culture media and supplements and fetal bovine sera were purchased from Invitrogen (Carlsbad, CA). The following were obtained through the NIH AIDS Research and Reference Reagent Program, Division of AIDS, NIAID, NIH: fusion inhibitor (N-acetylated derivative), the gene for HXB2-env (catalog number: 1069) from Dr. Kathleen Page and Dr. Dan Littman (110); the HeLa HL2/3 (64) cell line (containing genes from X4 strain HXB2) from Dr. Barbara K. Felber and Dr. George N. Pavlakis; the HeLa-TZM-bl cell line from Dr. John C. Kappes, Dr. Xiaoyun Wu and Tranzyme Inc. (60,62,63); the mouse monoclonal antibody to human CCR5; mouse anti human CCR5 monoclonal antibody from R&D Systems (catalog number: FABSP1, clone: 45502). The HeLa cell line stably expressing HIV-1 ADA (R5) env (referred to as HeLa-ADA) was a kind gift from Dr. M. Alizon (Cochin Institute, Paris, France) (59). A HeLa cell line stably expressing human receptor CD4 and CCR5 (referred to as HeLa-P5L) was a kind gift from Dr. M. Alizon and Dr. Anne Brelot (Cochin Institute, Paris, France) (59). The FITC (fluorescein isothiocyanate) labeled $F(ab')_2$ fragment of polyclonal goat anti-mouse IgG secondary antibody was purchased from Sigma (catalog number: F 2653). For C-peptides, although they were successfully expressed and purified from *E. coli*, it was found that acetylation at the C-terminus and amidation at the N-terminus (such as can be obtained from commercial synthesis) resulted in higher activity. Therefore, the peptides C37 and C34 (56) were obtained from Genescript company, and each was modified with acetylation at the C-terminus and amidation at the N-terminus. These commercial

produced peptides were used in all assays except the FACS assays, which used *E. coli*-produced C37.

Protein production and purification

For wild type chemokines RANTES protein expression and purification followed a standard chemokine refolding and purification method published previously (111-114).

The gene for the RANTES mutant, P2-RANTES, was amplified through standard thermocycling using the wild type RANTES as template (33), also adding the sequence for a Factor Xa cutting site upstream. This was inserted into pET32-Xa (Novagen) at the NcoI - BamHI sites, and the DNA sequence of this mutant was confirmed through DNA sequencing. Upon expression, the protein has a 6 histidine tag and a thioredoxin fusion protein on the N-terminus to facilitate the purification. When the fusion tag is removed (see below) the N-terminus of the P2-RANTES is exactly as published (33).

For production of the protein P2-RANTES, a slight variation on the standard chemokine refolding procedure was used. Protein production was induced by addition of IPTG to 1 mM in a culture of BL21(DE3) (Novagen) bearing the constructed plasmids, with shaking for 7 hours at 37ºC, and the cells were harvested by centrifugation at 6,000 x g for 30 minutes. The cells were resuspended in 30 mL of 500 mM NaCl, 20 mM Tris (pH 8), and 10 mM benzamidine and French pressed twice at 16,000 psi. After centrifugation for 30 minutes at 17,000 x g, the pellet was resuspended in 20 mL of 5 M guanidinium chloride, 50 mM Tris (pH 8), 500 mM NaCl. The solution was stirred overnight and then centrifuged for 30 minutes at 17,000 x g to remove remaining insoluble pellet. The soluble denatured proteins were loaded onto a 5 mL chelating column (Amersham Pharmacia Biotech) equilibrated with the same buffer (5 M

guanidinium chloride, 50 mM Tris (pH 8), 500 mM NaCl). The denatured proteins were purified through the chelating column using a gradient from 10% to 100% of 500 mM imidazole in 5 M guanidinium chloride, 50 mM Tris (pH 8), 500 mM NaCl. The fractions containing purified denatured protein were pooled together and slowly shaken (50 rpm) for 2 hours at room temperature after adding β-mercaptoethanol to 10 mM. The purified denatured proteins were dialyzed against 20 mM Tris-HCl, pH 8.0 overnight at 4ºC. After dialysis, precipitated matter was removed by centrifugation for 30 minutes at 15,000 x g and the protein was purified on a C4 reversed phase chromatography column (Vydac, Hesperia, CA), and lyophilized by the Labconco freeze dry system (Labconco Corporation). To remove the fusion tag, the protein powder was solubilized into ~1mL of 20 mM sodium phosphate (pH 2.5) and the volume was increased to ~ 40 mL in 20 mM Tris (pH 8), 50mM NaCl, and 2 mM $CaCl_2$. Factor Xa (Novagen) was used for the proteolytic cleavage, which typically took 2 weeks at room temperature. SDS-PAGE was used to monitor the cutting reaction. Finally, the cut proteins were purified over a C4 reversed phase chromatography column and lyophilized into powder.

For FACS assays, *E. coli*-produced C37 was used. Since C37 does not interact with cell surface receptor CCR5, it is not expected that this peptide will provide different results than if commercially produced peptides were used. For the C37 peptide, its corresponding gene (56) was amplified through standard thermocycling using the gene of HIV (HXB2) env as template, adding the sequence of a Factor Xa protease site upstream. The PCR product was placed into pET15b (Novagen, Madison, WI) at the Nde I-BamH I sites, and the DNA sequence of this mutant was confirmed through DNA sequencing. When it is expressed, the protein has a 6 histidine tag on the N-terminus that is

subsequently cleaved. The purification of this peptide is the same as described for P2-RANTES above.

Cell culture

The HeLa cell line stably expressing HIV-1 ADA (R5) env (referred to as HeLa-ADA) (59) was cultured in DMEM supplemented with 10 % FBS, and 100 units of penicillin and 0.1 mg/ml of streptomycin and the ADA (R5) env was selectively expressed by adding 2 μM methotrexate (Sigma) as previously published (33,59,115). A HeLa cell line stably expressing human receptor CD4 and CCR5 (referred to as HeLa-P5L) (59) was cultured in RPMI-1640 (Invitrogen) supplemented with 10 % FBS, and 100 units of penicillin and 0.1 mg/ml streptomycin. The expression of CCR5 was selectively expressed by adding zeocin (Invitrogen) 0.5 mg/ml. The HeLa-TZM cell line was cultured in DMEM supplemented with 10% FBS, 100 units of penicillin and 0.1 mg/ml of streptomycin as mentioned in the instructions provided by the NIH-ARRR.

Cell-cell fusion assay

Envelope-mediated cell fusion assays were carried out as described (33,59,115,116) with HeLa-P5L and HeLa-ADA cell lines (33,59,115,116), with minor modification. Briefly, 10^4 HeLa-P5L cells were seeded in a 96-well culture plate in 50 μl RPMI-1640 medium per well for 12 hours. The individual chemokine or the combinations of chemokines with C37 or C34 were added into the cell medium with serial dilution. Protein concentration was quantified by measuring the absorbance of the concentrated stock solution at 280 nm using the extinction coefficient method published by Pace (117), followed by serial dilution, done on the day of the assay. After the addition of the inhibitor, 50 μl HeLa-ADA (10^4 cells per well) in RPMI-1640 medium

were overlaid into the 96-well culture plate. After a further 24 hours of incubation at 37ºC for complete fusion, cells in the 96-well culture plate lysed by adding 0.5% NP-40 (US Biological) in PBS for 30 min at room temperature and assayed for β-galactosidase activity by the addition of 8 mM substrate CRPG (chlorphenol red-β-D-galactopyranoside, Calbiochem) in PBS with 20mM KCl and 10mM β-mercaptoethanol (Sigma) for 2 hours in the dark at room temperature. The absorbance at 570 nm (signal) divided by 630nm (background) was measured. The percentage of cell-cell fusion was calculated as [100 x (mean absorbance of treated well - mean absorbance of HeLa-P5L-only well)] / (mean absorbance of untreated well – mean absorbance of HeLa-P5L-only well). The "treated" wells contained inhibitor while "untreated" wells contained effector cells plus target cells in the absence of inhibitor. Essentially the same procedure was used for X4 fusion assays using the HL2/3 cell line. Experiments were performed in triplicate, repeated at least two times. Dose dependent inhibition curves were fitted with a four-parameter logistic equation (118) using KaleidaGraph (version 3.6, Synergy Software). No cell toxicity was observed for any dose of the proteins used in the assay.

MAGI antiviral assays

The CCR5- and CXCR4-tropic MAGI antiviral assays were both performed using MAGI-CCR5 cells in a manner identical to the CCR5-tropic HIV-1 entry assay described previously (67), with the exception that the virus and test compounds were left in the culture for the entire 48 hour incubation period, compared to washing out of virus and test compound 3 hours post-infection for the HIV-1 entry assay.

HIV-1 strains Ba-L and ADA were used for the CCR5-tropic assays, and HIV-1 strain IIIB was used for the CXCR4-tropic assays. Co-receptor dependence for each of

the viruses used to infect MAGI-CCR5 cells, which express both CCR5 and CXCR4, was verified through the use of AMD3100 (CXCR4 inhibitor; positive control inhibitor for IIIB, and negative control inhibitor for Ba-L and ADA) and TAK779 (CCR5 inhibitor; positive control inhibitor for Ba-L and ADA, and negative control inhibitor for IIIB) as control compounds (data not shown). Data processing was performed in a similar manner as described above for the single round infection assay.

Evaluation of synergy

Analysis of synergy, additivity or antagonism between chemokines and C37/C34 was performed using fixed ratios of drug combinations in antiviral assays according to the median effect principle of Chou and Talalay (88). Chemokines and C37/C34 were tested individually and in a fixed molar ratio combination over a range of serial dilutions. The Combination Index (CI), and the Dose Reduction Index (DRI) were calculated based on the published protocol from Chou (88) using Microsoft Excel. Based on this analysis, the CI value reflects the nature of the interaction between the drugs. $CI < 1$ indicates synergy; $CI = 1$ indicates additivity; and $CI > 1$ indicates antagonism. The DRI is a measure of how much the dose of each drug in a synergistic combination is reduced at a given effect level compared with the dose for each drug alone.

Statistical analysis

The 50% inhibitory concentration for each individual molecule and combination in case of the fusion assay was determined using KaleidaGraph (version 3.6, Synergy Software) from a standard four-parameter logistic regression (118). In the case of viral assay, the results were plotted using Microsoft Excel, and the IC_{50} and IC_{90} were calculated using a linear equation fitted between two experimental points surrounding the

IC_{50} or IC_{90}. Each experiment was done in duplicate or triplicate. Multiple IC_{50} or IC_{90} values obtained in this way from several repeats were then averaged together to obtain the data in Table III-1, Table II-2 and Table III-3. The error shown is the standard deviation of the averaged data. The Student t-Test (using the program Microsoft Excel) was applied for P value estimations that compared the statistical significance of the inhibitory concentration of a given molecule alone versus in combination.

FACS analysis

HeLa-TZM cells (10^5) were incubated for 30 min at 37°C in culture medium containing various concentration of (0-100 nM) of drugs in 10x75mm culture tubes (Fisher Scientific). After washing 4 times with 10 mL cold PBS, cells were incubated in 300 µl of 500 µg/ml mouse anti-human CCR5 monoclonal antibody in PBS-0.5% BSA (Sigma), and kept on ice for 45 min. The cells were then washed 3 times with cold PBS-0.5% BSA and incubated in 300 µl of 50 µg/ml FITC labeled polyclonal goat anti-mouse antibody in PBS-0.5% BSA, and kept on ice for 30 min. 1 aliquot of untreated cells were incubated with PBS-BSA for 30 minutes followed by 3 washes and incubation with the FITC-labeled goat anti-mouse IgG as control. Then the cells were washed 3 times with cold PBS-0.5% BSA and kept in PBS-0.5% BSA, and analyzed with a FACSCalibur (BD Biosciences, San Jose, CA) flow cytometer using CellQuest (BD Biosciences) acquisition software. Cell viability was determined by staining with propidium iodide (PI) at 1µg/ml final concentration 1 minute prior to analysis. FITC fluorescence was collected through a 530/30 bandpass filter, and PI fluorescence through a 650LP filter. List mode data were acquired on a minimum of 10,000 viable cells defined by a light scatter and lack of PI staining. Data were analyzed using FlowJo (Tree Star, Inc., Ashland, OR). First, a

region to define cells was set using a forward and side light scatter plot, and then viable (PI-negative) cells were determined by a plot of forward light scatter and PI fluorescence. Results are presented as histograms of FITC fluorescence.

For FACS analysis of surface CD4 on PBMC, IL-2-PHA stimulated PBM cells (1 mL at 10^6 cells/mL) were incubated for 60 min at 37°C in culture medium containing two concentrations of drugs in 10 x 75mm culture tubes (BD Biosciences). High dose tubes contained 25 nM C37, 10 nM P2-RANTES, and 6 nM mixtures of P2-RANTES-C37 at 1:1 and 10:1; low dose tubes contained 3 nM, 1.25 nM, 1 nM and 1 nM, respectively. After washing 2 times with 3 mL PBS, and 1 time with 4°C staining buffer (1% FBS in PBS), the cells were incubated in 150 µl of staining buffer-10 µL FITC-labeled mouse anti-human CD4 monoclonal antibody (BD Cat. No. 555346), and kept on ice for 30 min in the dark. Control cells were similarly treated using an irrelevant FITC-labeled mouse antibody (BD Cat. No. 554679). The cells were then washed 3 times with cold staining buffer and fixed with 500 mL of paraformaldehyde fixing solution (1% paraformaldehyde in PBS). The cells were analyzed with a LSR11 Special Order System (BD Biosciences, San Jose, CA) flow cytometer using FACSDiva (BD Biosciences) acquisition software. Cell viability was determined by trypan-blue exclusion staining before drug treatment. List mode data were acquired on a minimum of 10,000 viable cells defined by light scatter. F Gating was done on a population of untreated and unstained PBMC using a forward and side light scatter plot.

Results

Cell-cell fusion assays

The CC chemokines RANTES, MIP-1α and MIP-1β have been shown to inhibit infection by HIV-1, and this ability to block entry helped lead to the discovery of CCR5 as the HIV-1 coreceptor (119-122). In later years, however, it became clear that wild type chemokines were not as effective as some modified chemokines in HIV-1 inhibition (22). As shown in Table III-1 RANTES is a weak fusion inhibitor in a standard *in vitro* fusion assay, with an IC_{50} of 940 nM. Not surprisingly, RANTES and other CCR5 ligands are not notably effective in viral assays ((22) and unpublished). Upon combination of RANTES with gp41-binding peptide C37 (1:1 ratio), better inhibition of fusion is observed, with an IC_{50} of 51 nM total protein concentration Table III-1. Similarly, the combination of RANTES and fusion inhibitor peptide C34 (1:1 ratio) also shows better inhibition than RANTES alone, although the effect is not large, with an IC_{50} of 60 nM total protein concentration. This modest but repeatable effect was assessed using the combination index formula described by Chou and Talalay (88). The combination index (CI) of a two drug combination can be used to study the interactions of two drugs, where a value of 1 indicates no synergy between the two drugs (that is, their effects are merely additive), and values lower than 1 indicate synergy, with values closer to zero indicating more synergy. The combination of RANTES and C37 showed no synergy, with a CI value of 1.47, indicating that the two compounds were at best working additively (Table III-1). Similarly, RANTES in combination with C34 showed no synergy, giving a CI value of 1.09.

Table III-1: RANTES and P2-RANTES in combination with C37 and/or C34 inhibits HIV-1 (ADA) env mediated cell–cell fusion.

Inhibition of R5-tropic cell-cell fusion (10^4 HeLa-P5L cells and 10^4 HeLa-ADA cells per well) of individual fusion inhibitors and their combinations. Results are reported as the average IC_{50} ± standard deviation. Each experiment was done in triplicate, repeated at least three times. IC_{50} values of combinations are reported as total protein concentration. All R5-tropic fusion assays used 10^4 HeLa-P5L cells and 10^4 HeLa-ADA cells per well. P values are reported using the student's t-Test. All protein combinations were equimolar. CI is combination index, explained in Methods.

Drugs	Inhibitor one IC_{50}, nM	Inhibitor two IC_{50}, nM	Combination of First Inhibitor and Second Inhibitor, IC_{50}, nM	P-value Inhib1 compared to combo, Inhib2 compare to combo	Combination Index at 50% inhibition
P2-RANTES/C37	2.46±0.90	18.2±7.5	2.13±0.65	$1.9*10^{-4}$, $2.35*10^{-8}$	0.52
P2-RANTES/C34	2.46±0.90	29.1±7.3	2.41±0.88	$2.3 * 10^{-8}$, 0.0004	0.55
RANTES/C37	943±145	18.2±7.5	51.2±22.3	$3.74*10^{-6}$, 0.0007	1.47
RANTES/C34	943±145	29.1±7.3	59.9±14.6	0.001; 0.014	1.09

The RANTES variant "P2-RANTES" was discovered by Hartley *et al.,* who used phage selection of randomly N-terminally mutated RANTES to discover this analog that tightly binds CCR5 and internalizes the receptor with high efficiency (33). P2-RANTES performs quite well in fusion assays, having an IC_{50} of 2.4 nM in our hands (Figure III-1, Figure III-2) and 0.6-0.9 nM as reported by Hartley (33). However, in a 1:1 combination of P2-RANTES with C37, the IC_{50} of inhibition is 2.1 nM, which is 1.06 nM in each

component, giving a CI value of 0.52 and a dose reduction of 2.3 for P2-RANTES and a dose reduction of 19 for C37 (Figure III-2 and Table III-1). This value indicates moderate synergy with good potential for dose reduction. Similarly, the combination of P2-RANTES and C34 also resulted in good synergy and effectiveness, with a CI value of 0.56, a dose reduction in P2-RANTES of 2, and a dose reduction in C34 of 24 (Figure III-2 and Table III-1). As a control, fusion assays were carried out using HeLa HL2/3 cells, bearing gp160 from HXB2 (an X4 strain). In these experiments, C37 was effective at nanomolar concentrations (as expected for an inhibitor that binds gp41), P2-RANTES alone had no effect on fusion (as expected for a protein that binds CCR5), and the combination of C37 and P2-RANTES was no more effective than C37 alone (data not shown).

To determine which ratio of P2-RANTES and C37 best inhibits HIV-1 fusion, ratios of 1:4, 1:9, and 9:1were also tested. As shown in Figure III-2 and Table III-2, the ratio of P2-RANTES:C34 9:1 has an IC_{50} of 2.0 nM (combined protein concentration). The reduction in dose for these inhibitors is quite good: while the amount of P2-RANTES required for 50% inhibition in the combination is only about 1.3-fold less than when alone, the dose reduction for C34 is 146-fold less in combination compared to C34 alone. Each combination of P2-RANTES plus C-peptide resulted in a dose reduction in C-peptide, and usually a dose reduction in P2-RANTES as well (Table III-2).

HIV-1 infection assays

The combination of P2-RANTES and C37 in a ratio of 1:1 was tested for inhibitory capacity against different strains of HIV-1 in both MAGI and PBMC cells. As shown in Figure III-3 and Table II-2, P2-RANTES and C37 were each effective inhibitors, as reported previously (31,33,123). The combination of P2-RANTES and C37 (1:1 ratio) gives an IC_{50} of 1.67 nM (total protein concentration), and results in a CI of 0.4 (Table III-2) for the Ba-L HIV strain in PBMCs cells. P2-RANTES inhibits the replication of the HIV Ba-L strain in MAGI cells with an IC_{50} of 0.27 nM and IC_{90} of 5.7 nM. C37 inhibits HIV replication in the same strain at 6 nM and 85 nM respectively. These two drugs combined give an IC_{50} of 0.53 nM and an IC_{90} of 0.7 nM. The combination of P2 RANTES and C37 shows moderate synergy with 90% inhibition and a CI of 0.70. At 50% inhibition these two drugs act additively. HIV-1 ADA strains in MAGI cells show very similar results compared to the Ba-L strain in the same cells (Table III-3).

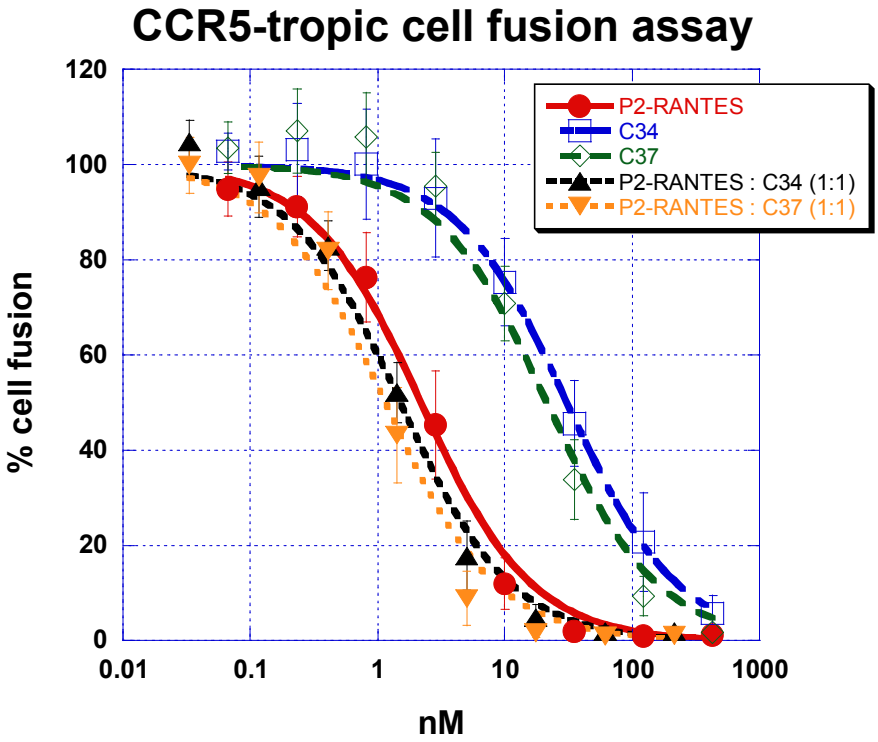

Figure III-1: CCR5-tropic cell fusion assay.

The error bars represent the standard deviation of more than 3 independent experiments. To underline the synergy effect the P2-RANTES:C37 and P2-RANTES:C34 assays have been plotted using the only concentration of P2-RANTES (not the combine compounds concentration) so the inhibition curves of the combined proteins are directly comparable with the control P2-RANTES.

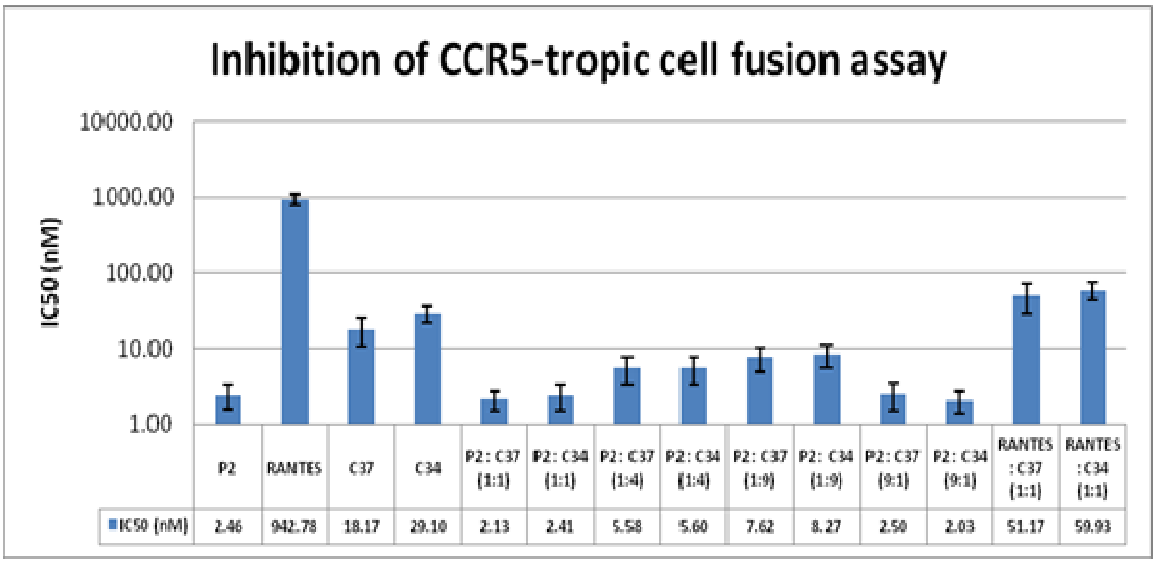

Figure III-2: CCR5-tropic cell fusion assay.

It has been used to evaluate the anti-HIV potency of different compounds and combination of them at different ratio. The IC_{50} of all the ratios describe total drug concentrations. P2: P2-RANTES

Table III-2: Varying molar ratios of P2-RANTES with C37/C34 inhibit HIV-1 (ADA) env mediated cell–cell fusion.

Inhibition of R5-tropic cell-cell fusion (10^4 HeLa-P5L cells and 10^4 HeLa-ADA cells per well) by various molar ratios of P2-RANTES and C37/C34. Inhibitory concentrations are for each individual component of the combination. Values are shown ± the standard deviation. CI is the combination index; DRI is dose reduction index, which is the ratio of the amount of that protein alone needed to obtain 50% inhibition divided by the amount needed in combination.

Ratio of P2-RANTES : C37/C34 at 50% Inhib.	P2-RANTES concentration (nM)		C37 / C34 concentration (nM)		CI at 50% inhib.	Dose reduction for P2-RANTES	Dose reduction for C37/ C34
	alone	conc P2-RANTES in combo	alone	conc C37 / C34 in combo			
1:4 (C37)	2.46 ±0.90	0.49 ±0.18	18.17 ±7.46	14.54 ±5.97	0.81	2.15	4.63
1:4 (C34)	2.46 ±0.90	0.49 ±0.18	29.10 ±7.31	23.28 ±5.85	0.68	2.15	6.50
1:9 (C37)	2.46 ±0.90	0.25 ±0.09	18.17 ±7.46	16.35 ±6.71	0.80	3.15	3.02
1:9 (C34)	2.46 ±0.90	0.25± 0.09	29.10 ±7.31	26.19 ±8.12	0.68	2.90	3.91
9:1 (C37)	2.46 ±0.90	2.21 ±0.81	18.17 ±7.46	1.87 ±0.75	0.94	1.07	82.8
9:1 (C34)	2.46 ±0.90	2.21 ±0.81	29.10 ±7.31	2.91 ±2.1	0.76	1.31	143.1

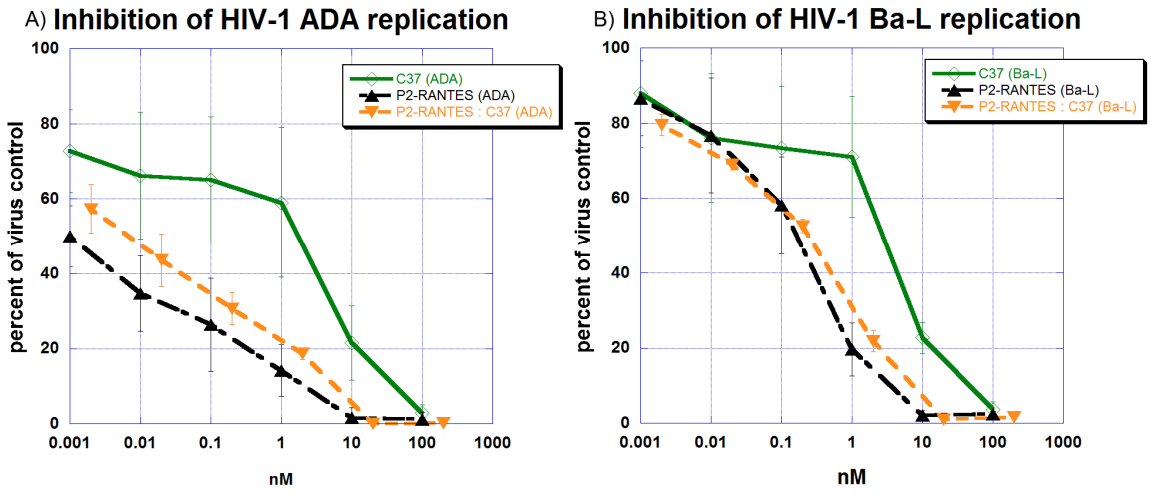

Figure III-3: HIV-1 infection assay.

ADA and Ba-L virus strains were used to infect MAGI cells. P2-RANTES : C37 (1:1) is plotted as a total concentration and the error bars represent the standard error of two independent experiments.

Table III-3: Inhibition of HIV-1 replication.

Inhibition in an HIV-1 infection assay in the presence of the inhibitors P2-RANTES and C37 in a 1:1 ratio. CI: combination index for a given percent inhibition. N.D.: Non determine

Compound	Ba-L (CCR5-tropic) in MAGI cells		ADA (CCR5-tropic) in MAGI cells		IIIB (CXCR4-tropic) in MAGI cells		Ba-L (CCR5-tropic) in PBMCs	
	IC_{50} nM	IC_{90} nM	IC_{50} nM	IC_{90} nM	IC_{50} nM	IC_{90} nM	IC_{50} nM	IC_{90} nM
P2-RANTES	0.27 ± 0.04	5.68 ± 1.13	0.10 ± 0.08	4.24 ± 0.02	>100	>100	4.21 ± 1.38	11.1 ± 4.0
C37	5.97 ± 0.42	85.0 ± 6.4	4.12 ± 0.52	73.7 ± 7.3	7.74 ± 0.54	> 100	4.77 ± 1.04	14.8 ± 2.0
P2-RANTES + C37 (1:1)	0.53 ± 0.23	7.15 ± 0.17	0.18 ± 0.15	5.67 ± 0.12	10.1 ± 7.9	>100	1.67 ± 0.07	4.76 ± 0.21
CI	**1.06**	**0.70**	**0.95**	**0.73**	**N.D.**	**N.D.**	**0.41**	**0.42**

FACS analysis

In order to study the mechanism of this moderate synergy between P2-RANTES and gp41 binding peptides, we hypothesized that the internalization of CCR5 to remove it from the cell surface by P2-RANTES may play an important role. As published by Hartley et al. (33), P2-RANTES not only tightly binds to CCR5 as other chemokines do, but also strongly internalizes the cell surface CCR5, while having negligible signaling effects on receptors CCR3 and CCR1 (33). RANTES also induces CCR5 initialization but inefficient compare to the AOP-RANTES (124). We used steady-state CCR5 down-modulation FACS experiments to study the internalization of CCR5 on HeLa-TZM cells by treatment with individual or a combination of drugs in 30 min of incubation at 37 ºC. As shown in Figure III-4, free C37 did not induce CCR5 internalization as expected, wild type RANTES caused minimal CCR5 internalization with the highest concentration (100 nM), but free P2-RANTES or P2-RANTES combined with C37 (1:1 ratio) showed significant internalization of CCR5 in a concentration dependent manner. This significant difference between wild type RANTES and P2-RANTES may play a role in the moderate synergy observed by P2-RANTES:C37 compared to wild type RANTES:C37, which shows no synergy. As a control, we also carried out a FACS analysis of CD4 levels on the surface of PBMC in the presence and absence of P2-RANTES and C37. Since neither P2-RANTES nor C37 has been shown to interact with or modulate CD4 levels at the cell surface, it was predicted that these molecules would not affect CD4 levels. As expected, neither P2-RANTES nor C37 nor their 1:1 or 10:1 combination had an effect on surface CD4 levels in PBMC (data not shown).

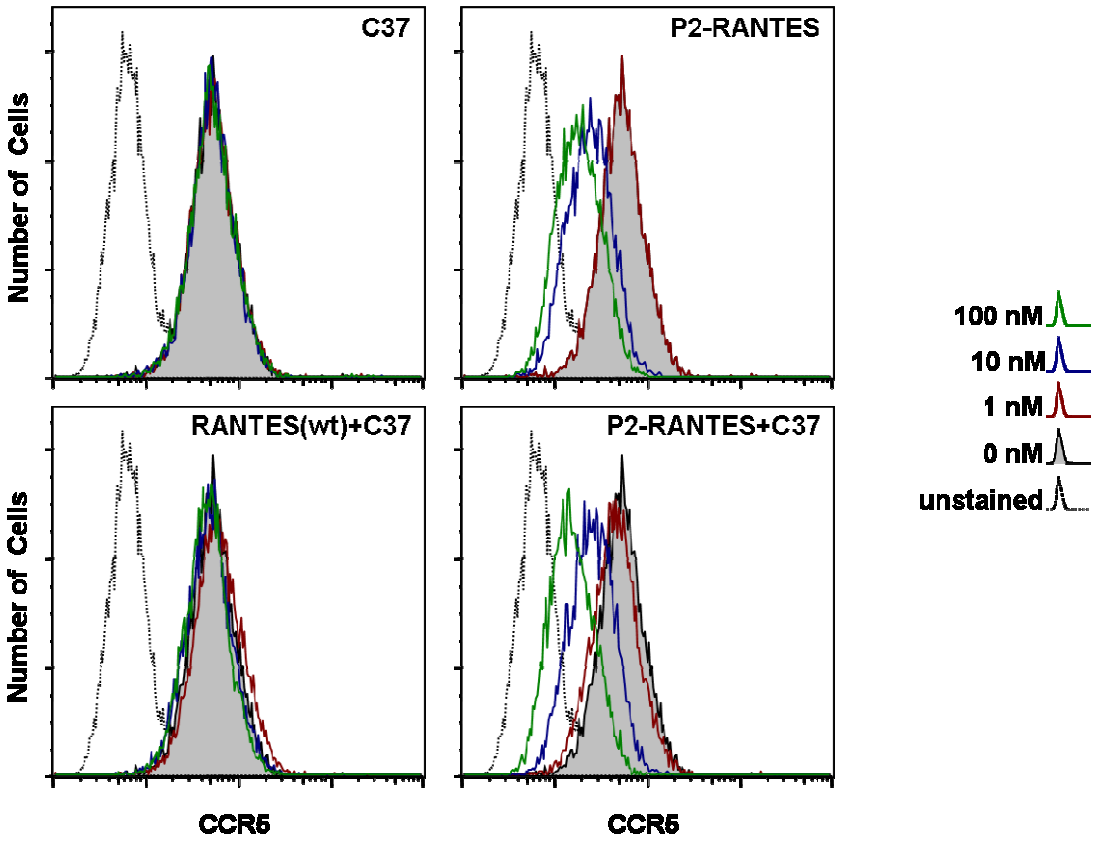

Figure III-4: CCR5 internalization, as measured by FACS.

The effect of free C37, P2-RANTES and the combination of wild type RANTES:C37 (1:1 ratio) and P2-RANTES:C37 (1:1 ratio) on the cell surface CCR5 population of HeLa-TZM cells was measured. Data are plotted as histograms of fluorescence intensity (cell surface CCR5), with the cell number normalized for each sample. The level of CCR5 expression is represented for cells treated with: 0 nM drug (black, shaded), 1 nM (brown), 10 nM (blue) and 100 nM (green). The cells stained with the secondary antibody but in the absence of CCR5 antibodies are shaded in light gray. Cell viability was determined by staining with propidium iodide (PI) at 1µg/ml final concentration 1 minute prior to analysis. Each histogram represents between 9000 and 9400 viable cells. Viability of the cells varied from 95% to 97%.

Discussion

HIV-1 entry into cells requires cell surface protein CD4 and coreceptor CCR5 or CXCR4 (119,121,122,125-127). CCR5 serves as the main coreceptor for transmitting HIV-1 infection (128), and CCR5 density level (molecules/cell) on CD4 T cells have been shown to be the driving force of cell-cell fusion (63,129). Reeves *et al.* (35,130) showed that "low" CCR5 density levels in cell lines lead to slower fusion kinetics and increased susceptibility to the C-peptide T-20. In addition, CCR5 levels were shown to affect the sensitivity of primary cells to T-20 (34). Rapamycin, which reduces CCR5 density on cells, was recently shown to moderately synergize with T-20, giving a dose reduction in T-20 of about 33-fold (22,131).

Synergy between drug therapies is an important strategy to allow effective disease control at low doses of drug (103,106-109,132,133). Several combinations of anti-HIV compounds have been reported that involve fusion inhibitors, including CCR5 antibodies, CCR5 antagonists and fusion inhibitors (103,105,108,109). Among the best of these, PRO 542 (a fusion of multiple CD4 subunits with immunoglobulin) and T-20 were shown to have strong synergy, with a combination index value of 0.34 at 50% inhibition in a cell-cell fusion assay (106). Even better synergy was reported by Safarian et al. who observed a CI_{50} of 0.06 for the combination of anti-CCR5 antibody PA14 and small molecule SCH-C; however, these authors do not report a dose reduction (107).

We report here a putative effective combination of anti-HIV agents, namely the combination of P2-RANTES and the gp41-binding peptides C37 and C34. This combination shows potent anti-HIV activity mainly in fusion assays and in some cases against viral infection. P2-RANTES and C37/C34 show synergy in fusion assays using

HeLa-P5L and HeLa-ADA cells. In the same assays RANTES and C37/C34 only show additivity.

One possible explanation for these results is that P2-RANTES internalizes CCR5 receptors better than RANTES, which FACS analysis supports in TZM cells. According to this analysis, RANTES causes minimal CCR5 receptor internalization at 100 nM. On the other hand, P2-RANTES significantly internalizes the CCR5 receptor at the same concentration.

Nevertheless, it is unclear whether or how these proteins will induce CCR5 internalization in different cell types. Mack et al showed that 100nM RANTES caused ~20% CCR5 internalization in CHO/CCR5 cells, but at the same concentration, RANTES caused ~70% CCR5 internalization in PBMC (124). This phenomenon may explain the observation that the combination of P2-RANTES and C37 acts synergistically in inhibiting HIV infection in PBMC cells but not in MAGI cells on the same viral strain Ba-L (Table III-3).

In Figure III-4 it becomes obvious that CCR5 internalization is heavily dependent on the concentration of P2-RANTES. At 1 nM concentration, P2-RANTES only slightly internalizes CCR5. This may explain why in MAGI cells we observe synergy in the IC_{90} but not in the IC_{50}, since in IC_{90} higher concentration of P2-RANTES was used, so at this concentration P2-RANTES may be better able to internalize CCR5. Very low concentrations of P2-RANTES may not cause significant CCR5 internalization and virus-cell fusion kinetics remain the same (35,130).

We also tested the hypothesis that different ratios of P2-RANTES : C37/C34 may affect the synergistic relationship of these two compounds in the fusion assay. None of

the different ratios of P2-RANTES : C37/C34 tested gave better synergy than the 1:1 ratio (Table III-2). It is unclear why a 1:1 ratio is best, but it seems again that low amounts of P2-RANTES may not cause significant CCR5 internalization. It also appears that low amounts of C37 in the case of P2-RANTES:C37 (9:1) does not help synergy.

In all of the above experiments, it is inconclusive how general of a phenomenon the synergy we observed between P2-RANTES and C37/C34 in cell fusion assays is. It is clear that the cell type, the amount of CCR5 receptors on the cell surface, CCR5 receptor internalization and recycling are important parameters that affect the outcome of P2-RANTES and c-peptide combination. Because the overall synergetic effect of the two compounds that we measured in the fusion assay was not that great (P2-RANTES:C37 (1:1) gives CI: 0.52) (Table III-1), our focus shifted to other HIV inhibitors that were more promising (see Chapter II).

On the next chapter, I am moving from the area of virology to the area of bioinformatics and I am working on finding unfavorable sequence motifs using phylogenetic and structural information.

CHAPTER IV

CONSERVATION OF UNFAVORABLE SEQUENCE MOTIFS THAT CONTRIBUTE TO THE CHEMOKINE QUATERNARY STATE*

Introduction

The second chapter of this dissertation uses CXCL8 to study the intriguing issue of the ability of proteins to dimerize. Although protein interactions can act both favorably and unfavorably, they are usually thought to be favorable and act in specific ways to help bring about a certain outcome in protein structure. Interactions can also be unfavorable, but by their very nature, they are not often thought to actively contribute to protein structure. In addition, discrete motifs producing unfavorable interactions have not been widely studied, because they are predominantly nonspecific and produce negative results that cannot be interpreted. However, specific unfavorable interactions have been used in protein design to prevent certain outcomes from occurring (134,135) and have been characterized in the termination of β-sheet structures (136). These unfavorable interactions should not be confused with the results from negative selection, where positive interactions are directly removed (137), or general negative design (138), where certain interactions are disfavored (139). Although general negative design strategies produce unfavorable interactions, specific motifs are not used to achieve their goal. In this work, we want to identify evolutionarily conserved motifs that confer unfavorable

* Reprinted with permission from "Conservation of unfavorable sequence motifs that contribute to the chemokine quaternary state." from (143) Kagiampakis I, Jin H, Kim S, Vannucci M, LiWang PJ, Tsai J, 2008. Biochemistry. 2008 Oct 7;47(40):10637-48 Copyright © 2008 American Chemical Society

interactions and characterize their role in determining protein quaternary structure. To accomplish this, we developed a predictive method combining structural with phylogenetic analysis that is validated using Bayesian variable selection (140). This approach was used in an investigation of how unfavorable interactions contribute to the chemokine dimerization state.

Chemokines are extracellular signaling proteins that play a general role in the innate and adaptive immune response, angiogenesis, cancer, and wound healing (32,141-143). In mammals, chemokines are separated into four main groups on the basis of the number of amino acids between the conserved cysteines (C) at the N-terminus of the protein (CXC, CC, CX3C, and C, where X is any amino acid). The largest group of chemokines consists of the CXC chemokines (21 human members) and the CC chemokines (29 human members) (Cytokine Family Database, http://cytokine.medic.kumamoto-u.ac.jp/). With the exception of some transmembrane domains containing chemokines, these proteins are generally small molecules (8 kDa). While the overall level of amino acid sequence conservation of the family is low, they all share the same tertiary fold of a single α-helix across a three-stranded antiparallel β-sheet (Figure IV-1) suggesting that they most likely originated from a common ancestor. At the quaternary level, chemokines can form dimers, tetramers, or even heterodimers (144,145). Possible roles of this oligomerization have been linked to chemokine function (146), such as suppression of specific surface-dependent neutrophil responses (147,148) and increasing in vitro antiproliferative effects (149). For homodimers, the quaternary structures of chemokines from different groups dimerize in different ways. As shown in Figure IV-1, CXCL8 chemokines interact across their β1 strands to form a globular

dimer, and in contrast, CCL4 dimerizes with its uncoiled N-terminus in a more extended conformation. While seemingly straightforward, attempts to disrupt the CXCL8 homodimer and retain the chemokine fold have required a set of mutations (144,145,147,150,151) from simultaneous changes in both the β1 strand and α-helix to a chemical modification of L25 (Table IV-1). In this work, we used a directed, computational approach to discover evolutionarily conserved motifs that produce a correctly folded CXCL8 monomer.

Because all chemokines share a common tertiary structure yet the CXC and CC subfamilies generally interact with different quaternary forms (Figure IV-1), we hypothesized that there must be motifs in the CC subfamily (dimerizing between their N-termini) that disfavor CXCL8 dimer formation across the β1 strand but still conserve the chemokine fold. To discover these sequence elements, our approach to sequence analysis focused on increasing the magnitude of the signal of conserved differences and decreasing the noise from differences caused by random mutations. Therefore, we limited our sequence analysis structurally to only the CXCL8 dimerization region (Figure IV-2) and evolutionarily to two CC clades (the one including CCL4 and another including CCL2; see Figure IV-3). The results underwent rigorous statistical validation to separate true negative motifs from all the other noise produced in an alignment (140). On the basis of this work, we created three variants of CXCL8: two mutants that should induce a stable monomer and one control mutant that should not. Surprisingly, one of the predicted monomeric mutations involves a very drastic two-residue deletion within the dimerization interface. For the two evolutionarily conserved motifs from the CC family placed into a CXCL8 background, we experimentally prove they inhibit β1 strand

dimerization, while retaining the chemokine fold. The control exhibited only a moderate decrease in the level of dimerization. These results demonstrate that sequences conferring unfavorable interactions are evolutionarily conserved, and the implications of these findings related to chemokine quaternary structure are discussed.

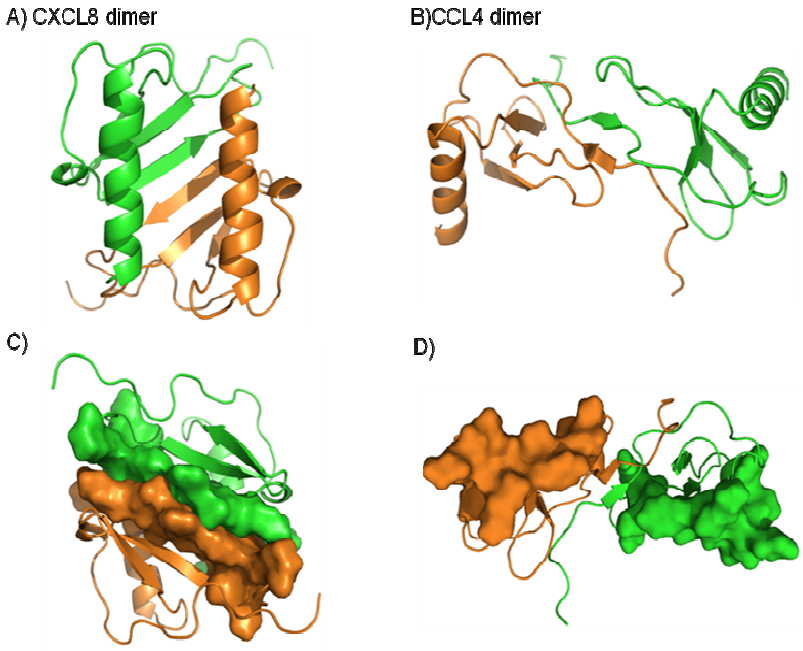

Figure IV-1: Comparing the quaternary structure of the CXCL8 and CCL4 homodimers.

All images were created using PyMOL. (A) Showing PDB entry 3il8 (152), CXCL8 dimerizes using the *β*1 strand and the *α*-helix. (B) Showing PDB entry 1hum (153), CCL4 dimerizes using the largely unstructured N-terminal region and the loops between strands *β*2 and *β*3. This interface forms eight interdomain hydrogen bonds: four from the small section of the antiparallel *β*-sheet formed by the *β*0 strands and four more backbone−backbone hydrogen bonds with the *β*3 strand. Apart from interactions with the *β*0 and *β*3 strands, CCL4's homodimer interacts primarily through hydrophobic interactions between residues that do not form canonical secondary structure elements. (C) CXCL8's *β*1 strand residues involved in the antiparallel *β*-sheet quaternary interaction are shown in space filling models. Overall, the CXCL8 interface forms eight hydrogen bonds and the molecular area of interaction is 361 Å^2, where 303 Å^2 comes from side chain interactions and only 58 Å^2 comes from backbone interactions. Specific details are illustrated in Figure IV-2. (D) Space filling models of the corresponding residues shown on CCL4 that are involved in CXCL8's *β*1 strand antiparallel *β*-sheet quaternary interaction.

Table IV-1: CXCL8 and its variants.

a In section A are listed the wild-type CXCL8 amino acid composition and the number and secondary structure of residues involved in the dimer interface shown in Figure IV-7 A,C, and 16. Secondary structure is given by sheet (E), helix (H), and coil (C) as defined by DSSP (154). The periods between residue numbers represent breaks in the sequence. The statistical analysis is given in section B. BVS stands for Bayesian variable selection. Amino acid substitutions shown in black and underlined represent strongly identified sites, whereas those shown in black are weakly identified sites (see Experimental Procedures). Sites not predicted are shown in gray with the wild-type amino acid. The deltas (Δ) are deleted residues in sections B−D. While analysis across all the residues was shown for completeness, this study focuses on only the analysis across the *β*1 strand (residues 24−28) and only those unique to the CC subfamily clade. For instance, we did not include the L25Y substitution, since it is seen in analysis with both clades. Section C lists CXCL8 variants used in this study. Mutations are shown in black, while the unchanged native sequence is shown in gray. Again, the complete wild-type sequence is shown along with the three variants used in this study: ΔRV, V27R, and R26A/V27A. In addition, we show the dimerization constant Kd (micromolar) and indicate monomer/dimer state, where M refers to monomer, D to dimer, and wD to weak dimer. Section D gives the same information for published mutations from previous experiments in the CXCL8 interface ordered by year the study was published. Following the same conventions, we show the amino acids to which residues are mutated in black and the native unchanged sequence in gray. L′ represents an N-methylleucine.

A) Sequence of CXCL8																			
Amino Acid	E	L	R	V	I	T	E	L	V	F	L	K	R	A	E	N	S		
Residue Number	24	25	26	27	28	. 37	38	. 43	. 62	. 65	66	67	68	69	70	71	72		
Secondary Structure	E	E	E	E	E	C	E	E	H	H	H	H	H	H	H	H	C		
B) BVS Prediction																			
Comparison with CCL4 clade	E	**Y**	Δ	Δ	I	T	**A**	**T**	Δ	F	L	K	**L**	A	E	N	S		
Comparison with CCL2 clade	E	**Y**	R	**R**	I	T	**A**	L	V	F	**D**	K	R	A	E	N	S		
C) CXCL8 Variants used in this study																		K_d (μM)	M/D
Wild Type	E	L	R	V	I	T	E	L	V	F	L	K	R	A	E	N	S	~0.1	D
ΔRV	E	L	Δ	Δ	I	T	E	L	V	F	L	K	R	A	E	N	S	--	M
V27R	E	L	R	**R**	I	T	E	L	V	F	L	K	R	A	E	N	S	--	M
R26A/V27A	E	L	**A**	**A**	I	T	E	L	V	F	L	K	R	A	E	N	S	18.2 ± 3.1	wD
D) Previous Experiments																			
(a) Lusti-Narasimhan et al., 1996	E	L′	R	V	I	T	E	L	V	F	L	K	R	A	E	N	S	--	M
(b) Lowman et al., 1997	**R**	L	R	V	**R**	T	E	L	V	F	L	K	R	A	E	N	S	7.6 ± 4.2	D
	E	L	R	V	I	**E**	E	L	V	F	L	K	R	**E**	E	N	**E**	--	M
	R	L	R	V	**R**	**E**	E	L	V	F	L	K	R	**E**	E	N	**E**	1800 ± 550	wD
	R	L	R	V	**R**	**E**	E	L	V	**H**	**E**	K	R	**E**	E	N	**E**	1800 ± 500	wD
(c) Jin et al., 2005	E	L	R	V	I	T	E	L	V	F	Δ	Δ	Δ	Δ	Δ	Δ	Δ	--	M
	E	**A**	R	**E**	I	T	E	L	V	F	L	K	R	A	E	N	S	151.5	wD
(d) Williams et al., 2005	E	**Y**	R	**R**	I	T	E	L	V	F	L	K	R	A	E	N	S	--	M
	L	**E**	R	V	I	T	E	L	V	F	L	K	R	A	E	N	S	--	M

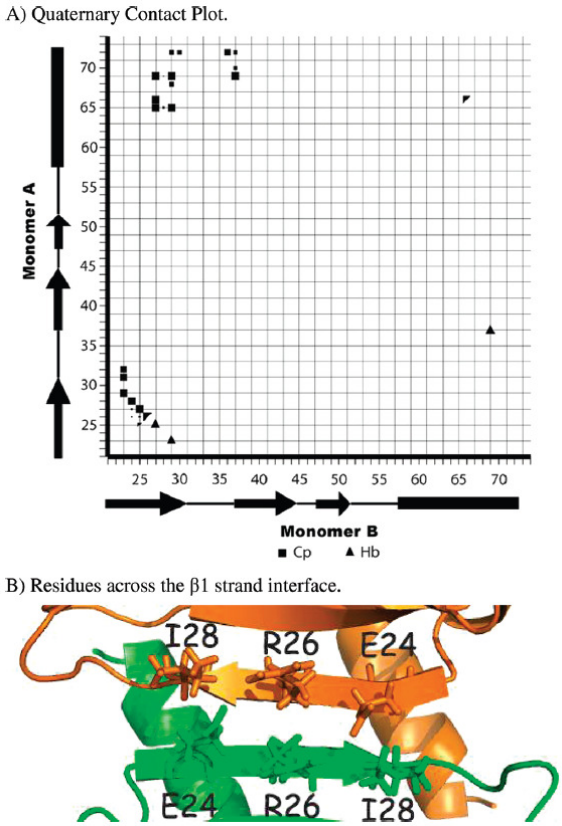

Figure IV-2: CXCL8 homodimer interaction interface.

(A) Quaternary contact plot. (B) Residues across the *β*1 strand interface. For panel A, contacts were calculated using Qcontacts (155) and are listed in Table IV-2. Because the dimer interface is symmetric across the diagonal, we can plot the hydrophobic carbon−carbon contacts as filled squares (■) above the diagonal and the hydrogen bonds as filled triangles (▲) below the diagonal. The plot clearly shows the three areas of interaction across the dimer interface. The *α*-helices from each CXCL8 monomer form a loose hydrophobic network, and this interaction between helices is centered on the interaction between the two L66 residues. The next part of the CXCL8 interface involves the C-terminal, *α*-helical residues 65−72 interacting with residues 27−37 running from the *β*1 strand into and through the turn between the *β*1 and *β*2 strands. In addition to the many hydrophobic contacts, two hydrogen bonds are formed (one from each monomer) between the side chain oxygen of T37 and the backbone carbonyl of A69. The last area across the two *β*1 strands of the CXCL8 homodimer contributes >50% of the interaction surface area as well as hydrogen bonds to the interface. Each monomer's edge *β*1 strand from residue 23 to 28 forms a regular antiparallel *β*-sheet interaction that unites a single six-stranded *β*-sheet with six backbone hydrogen bonds and a large, continuous area of interaction. For the whole interface, residue R26 sits on the axis of symmetry (interacts with the same residue on the opposing monomer) and coincidentally buries the most surface area. This is clearly shown in panel B, where residues E24, R26, and I28 are shown in the antiparallel sheet between the two *β*1 strands.

Table IV-2: Quaternary analysis of CXCL8.

These quaternary interactions were calculated using the Qcontacts (155), where interaction type is defined. In the table, the designations are H for hydrogen bond and V for hydrophobic van der Waals contact

	Chain A		Chain B		
Type of Interaction	AA number	AA name	AA number	AA name	Area Å^2
H	23	LYS	29	GLU	1.84
H	25	LEU	27	VAL	3.65
H	27	VAL	25	LEU	3.65
H	29	GLU	23	LYS	1.84
H	37	THR	69	ALA	0.91
H	69	ALA	37	THR	0.89
V	23	LYS	29	GLU	9.32
V	23	LYS	31	GLY	2.98
V	23	LYS	32	PRO	2.48
V	24	GLU	26	ARG	0.22
V	24	GLU	27	VAL	0.64
V	24	GLU	28	ILE	4.54
V	25	LEU	25	LEU	2.81
V	25	LEU	26	ARG	0.38
V	25	LEU	27	VAL	7.32
V	26	ARG	24	GLU	0.23
V	26	ARG	25	LEU	0.38
V	26	ARG	26	ARG	15.01
V	27	VAL	24	GLU	0.65
V	27	VAL	25	LEU	8.50
V	27	VAL	65	PHE	7.90
V	27	VAL	66	LEU	5.09
V	27	VAL	69	ALA	8.93
V	28	ILE	24	GLU	16.76
V	28	ILE	65	PHE	0.59
V	28	ILE	69	ALA	0.22
V	29	GLU	23	LYS	1.89
V	29	GLU	65	PHE	3.22
V	29	GLU	68	ARG	3.48
V	29	GLU	69	ALA	3.55
V	29	GLU	72	SER	3.41
V	30	SER	72	SER	2.87
V	31	GLY	23	LYS	7.49
V	32	PRO	23	LYS	6.19
V	36	ASN	72	SER	6.53
V	37	THR	69	ALA	9.34
V	37	THR	70	GLU	2.55
V	37	THR	72	SER	2.99
V	65	PHE	27	VAL	12.16
V	65	PHE	28	ILE	0.87
V	65	PHE	29	GLU	4.01
V	66	LEU	27	VAL	11.95
V	66	LEU	39	ILE	4.42
V	66	LEU	66	LEU	4.18
V	68	ARG	29	GLU	3.47
V	69	ALA	27	VAL	8.93
V	69	ALA	28	ILE	0.22
V	69	ALA	29	GLU	7.99
V	69	ALA	37	THR	6.91
V	70	GLU	37	THR	2.56
V	72	SER	29	GLU	5.21
V	72	SER	30	SER	2.88
V	72	SER	36	ASN	4.34
V	72	SER	37	THR	2.97

.

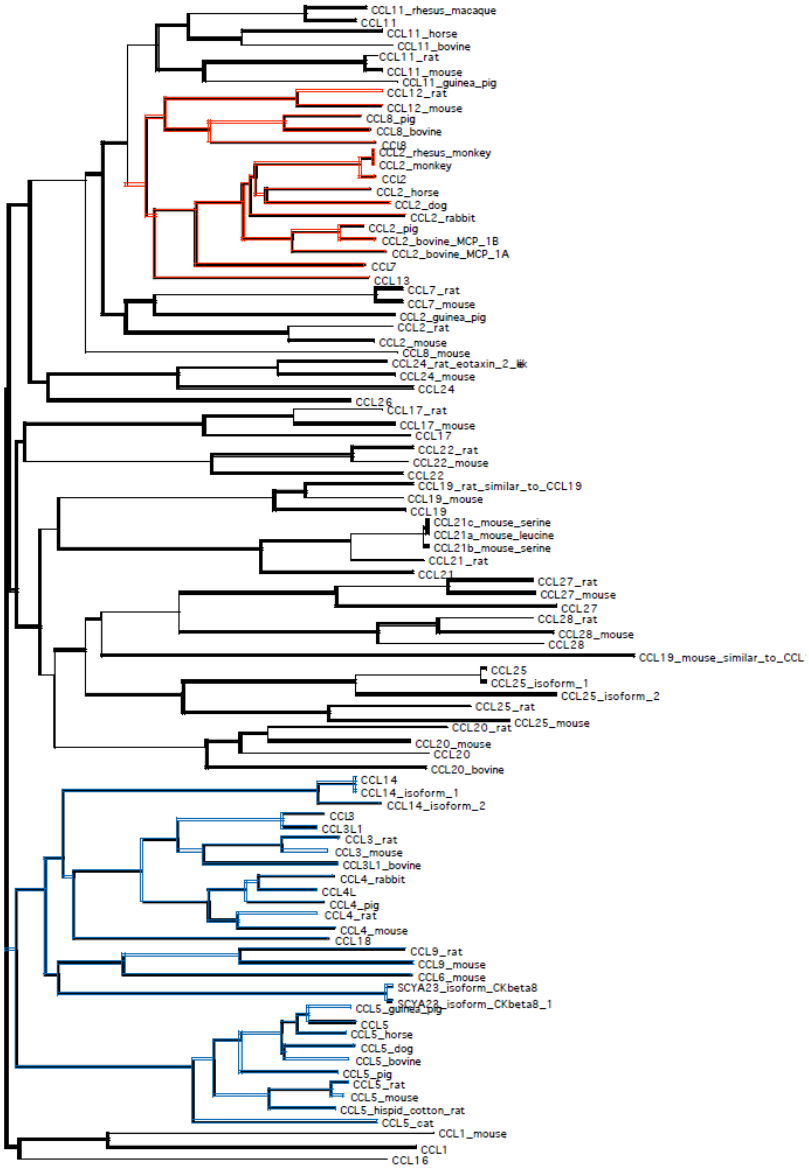

Figure IV-3: Phylogenetic tree of the vertebrate CCL chemokine family.

With the red color we underline the CCL2 clade and with the blue the CCL4 clade. The Neighbor Joining Tree was calculated using a Blosum 62 matrix from ClustalW program and the graphical representation of the tree was done using the Pfaat program.

Experimental Procedures

CXCL8 dimer and monomer surface area calculation

CXCL8's molecular surface area across its dimer interface was calculated using a Voronoi polyhedron-based procedure (155). The residue interactions are provided in Table IV-2. We used all 30 NMR1 structures of the CXCL8 dimer in PDB entry 2IL8 (156) for our calculations to allow for and sample the possible fluctuations across the dimer interface. Only contacts occurring in more than 15 of 30 structures were considered as an interaction and are shown in Figure IV-2. Values reported in Table IV-2 are averages.

Sequence alignment

All the protein sequences of the vertebrate CC chemokines that were highly similar to CXCL8 were downloaded from the Cytokine Family cDNA Database (http://cytokine.medic.kumamoto-u.ac.jp/). Sequences from signal peptides were not included. Using the phylogenetic tree shown in Figure IV-3, a ClustalW (157,158) or DiAlign (159) (depending upon the circumstances) multiple-sequence alignment was created using all the sequences of CC chemokines for every single node and starting from the bottom of the tree. The alignment in the initial node was found to be significant in cases where the multiple-sequence alignments in the area of CXCL8's dimerization remained partially unchanged in the smaller subtrees. Using this procedure, two major subtrees with constant differences in the area of CXCL8's β1 strand were constructed and named clade CCL4 (29 sequences in the blue subtree, Figure IV-3) and clade CCL2 (16 sequences in the red subtree, Figure IV-3). The sequences in these two clades were used to create the logo figures. To ensure the accuracy of the gap discovered at positions R26

and V27 of CXCL8 (Table IV-1), the alignment was repeated using DiAlign, which does not use gap penalties but the best diagonal without gaps in the alignment matrix (160). This alignment also predicted the two-residue deletion (data not shown). While the phylogenetic tree in Figure IV-3 suggests that these two mutations diverged from a common ancestor, it could equally be the case that a monomeric ancestor existed. This analysis considers only the differences between sequences and does not include bias about how they originated.

Validation by Bayesian variable selection

The method itself was discussed in more detail previously (140). We compared sequences only within the area of interaction defined above based on a simple hydropathy profile (161). To identify structural dissimilarities in protein alignments, we have applied the well-known variable selection method for classification with probit models proposed by Sha et al. (162). Bayesian variable selection is done via a binary vector with p entries that identifies the different sets of variables. The marginal posterior distribution of this binary vector is derived, and Markov chain Monte Carlo algorithms are used to sample from its posterior distribution. The method allows the identification of sets of discriminating variables and the classification of future samples (via least-squares or Bayesian model averaging). A site is identified as significant when there is a high posterior probability that the site is dissimilar (has had a mutation). Conversely, those sites that are not identified are those that have a small probability of being dissimilar. Classification of strong and weak was determined on the basis of a comparison from two runs using different input parameters: strong sites were those identified by both runs and weak ones those identified by only one. The sensitivity of the method to the input

parameters has been discussed previously (162). Because we are working from only one CXCL8 sequence, we needed to cross-validate our results. Once we identified the sites with a high posterior probability of being dissimilar, we tested how well we could discriminate between the groups (for example, CXCL8 from CCL2) on the basis of these sites. Taking one CCL2 sequence out, we try to "predict" whether this sequence is more similar to CXCL8 or to the other CCL2. If the answer should be the latter, it was considered a zero error.

Construction and purification of mutants

All the CXCL8 mutants were created in the pET-32a+ (Novagen) vector using Quikchange mutagenesis (Stratagene) and were confirmed via sequencing. Protein purification for all mutants and the wild type (WT) used a standard chemokine refolding protocol as described previously (112).

Size exclusion chromatography

The purified protein was first dissolved into 20 mM sodium phosphate buffer (pH 2.5) containing 150 mM NaCl, and then the pH of the solution was adjusted to 6.7 with 4 M NaOH. The solution was centrifuged at 12000 rpm for 20 min to remove any possible precipitation. The dissolved refolded protein (0.5 mL) was loaded onto a Superdex G75 (HR 10/30) gel filtration column (GE Healthcare) equilibrated with 20 mM sodium phosphate buffer (pH 6.7) containing 150 mM NaCl. The protein was eluted with this buffer and run using the Pharmacia Akta system. The gel filtration column was calibrated with several standard marker proteins (Bio-Rad) in the same running buffer, and the molecular masses of chemokine variants were estimated using the calibrated

standard curve. All sample elutions were performed at a rate of 0.4 mL/min; 1 mL fractions were collected, and the protein content was analyzed by 12% SDS−PAGE.

Analytical ultracentrifugation (AUC)

Sedimentation equilibrium data were collected on a Beckmann XL-A analytical ultracentrifuge using the An-60 Ti rotor at 25 °C. The following sets of speeds were used for each mutant: 26500 and 36500 rpm for R26A/V26A, 26500, 37500, and 48000 rpm for ΔRV, and 25000, 27500, 30000, 32000, 34000, 36000, and 38000 rpm for V27R. The absorbance for all three mutants was measured at 280 nm to determine the concentration of the protein during the sedimentation equilibrium. For V27R, the absorbance was measured at two additional wavelengths (235 and 245 nm). For each run, protein was dissolved in sodium phosphate buffer with 150 mM NaCl at pH 6.2. Initial protein concentrations were 110 μM for R26A/V26A and 25, 50, and 111 μM for ΔRV. For V27R, eight different concentrations between 50 and 500 μM were used. The data were processed using the Ultra Scan Data analysis software (http://www.ultrascan.uthscsa.edu/). The calculated molecular masses and dissociation constants as well as their respective standard deviations were calculated on the basis of a Monte Carlo simulation of the initial global fitting over all the data collected.

NMR spectroscopy

NMR samples of 1 mM protein for all the variants were prepared in 150 mM NaCl, 20 mM sodium phosphate (pH 6.7), 0.01% NaN3, 0.1 mM DSS, and a 95% H2O/5% D2O solvent mixture. The spectra were collected on a Varian Inova 600 MHz spectrometer at 25 °C. ^{1}H, ^{13}C, and ^{15}N chemical shifts were referenced to internal DSS (163). Sequence specific backbone assignments of $^{13}C\alpha$, $^{13}C\beta$, and ^{15}N were obtained

from CBCA(CO)NH and CBCANH experiments (164). For structure comparison, $^{1}H–^{15}N$ HSQC spectra were acquired with 512* points in the ^{1}H (direct) dimension and 64* points in the ^{15}N (indirect) dimension, where n* represents n complex points. The spectral width for 1H was 8000 Hz and for ^{15}N was 1700.68 Hz. Total acquisition times were 64 ms for the 1H and 37.6 ms for the ^{15}N dimension. The relaxation experiments were performed according to the following. The spin-lattice (T1) and spin-spin (T2) values were determined for 1mM ^{15}N labeled CXCL8_ΔRV, from ^{15}N-^{1}H-HSQC spectra collected using pulse sequences described above. Intensities of cross-peaks were obtained from peak-picking routines provided in the software PIPP package. Data from each amino acid residue was extracted in a straightforward fashion by measuring the intensities of cross-peaks in ^{15}N-^{1}H-HSQC spectra as a function of a relaxation delay. The ^{15}N T1 data was collected with ^{15}N delays of 0.02, 0.1, 0.12, 0.18, 0.25, 0.36, 0.52, 0.76, 1.00, and 1.25 s. T2 data was collected using ^{15}N delays of 32, 48, 64, 80, 96, 128, 144, 160, 192, and 240 ms. The T1, T2 data sets were processed using software nmrPipe (165). Data was excluded from the correlation time calculation if either T1 or T2 differed from the average value by >1 SD.

Results

Structural analysis of the dimer interfaces

We go into only as much detail comparing the CXCL8 and CCL4 interfaces as necessary to provide background to our analysis, since this comparison has been made previously (153) and in greater evolutionary and molecular detail (166). For the sake of consistency, we follow the same nomenclature. The monomers are 18% identical with each other in sequence, yet both exhibit the same fold (Cα rmsd between CXCL8 and CCL4 of 1.6 Å) as shown in Figure IV-1: a single α-helix over a β-sheet arranged in a Greek key motif (all the β-strands are antiparallel to each other and are numbered from the N-terminus β0, β1, β2, and β3). Even though they are so similar, each possesses certain unique features. CCL4 exhibits a small, extra section of β-sheet structure near the N-terminus, while CXCL8's α-helix is one turn longer at its C-terminal end. As Figure IV-1 clearly shows, CCL4 and CXCL8 dimerize quite differently. The CCL4 homodimer is elongated and interacts primarily through N-terminal β0 strand residues 2−16 with two areas on the opposing monomer: the same residues as well as residues 46−51 of the β3 strand (Figure IV-1B). In contrast, the CXCL8 dimer is more globular, and the dimerization interface appears more uniform (Figure IV-1A and highlighted in Figure IV-1C). From an analysis of quaternary interactions (155), the CXCL8 dimer interface combines interactions across three areas (Figure IV-3 and Table IV-1). Of the three, the interaction area that has drawn the most focus is the β1 strand, since it contributes the most surface area and hydrogen bonds to the homodimer interface (166). In contrast, the β1 strand does not contribute at all to the CCL4 homodimer, and as emphasized in Figure

IV-1D, CCL4's β1 strands do not contact each other in its dimer state. For these reasons, we have focused our sequence analysis on the β1 strand to identify the inhibitory sequence elements in the CC family of chemokines that disfavor the CXC homodimerization state.

Identifying conserved sequences conferring negative interactions

Structurally limiting our comparison to only a fragment of the CXCL8 sequence and evolutionarily to only CC chemokine subfamilies is unlike previous work that has tried to mutate the conserved residues found from an alignment over the entire chemokine sequence (144,145,147,150,151,166). As shown in Figure IV-4A, the breadth of such an alignment diminishes the conservation signal of all residues and the global alignment misaligns this region by a single-residue shift toward the C-terminus. As a result, many attempts to create a stable monomer have been performed, and each has used multiple point mutations (Table IV-1). Instead, we performed a more focused and statistically rigorous analysis that considered only those residues involved in the β1 strand of the CXCL8 dimer interface and also limited the comparison of the CXCL8 sequence to only an evolutionarily related subset or clade of the CC chemokine family. Although the approach is more thoroughly discussed in Experimental Procedures, we briefly summarize the steps and reasoning behind it. The clade analysis is based on the hypothesis that proteins with the same tertiary fold but different quaternary structure must have taken separate evolutionary paths from a common ancestral sequence and may have selected different mechanisms to achieve the same result. The choice of sequences to include in our clade analysis was defined by the branches in a phylogenetic tree of the CC chemokines (Figure IV-3). As the last step, the significance of our results was verified

using a rigorous statistical method based on Bayesian variable selection (140) to filter out any insignificant results due to the low complexity of the sequence space.

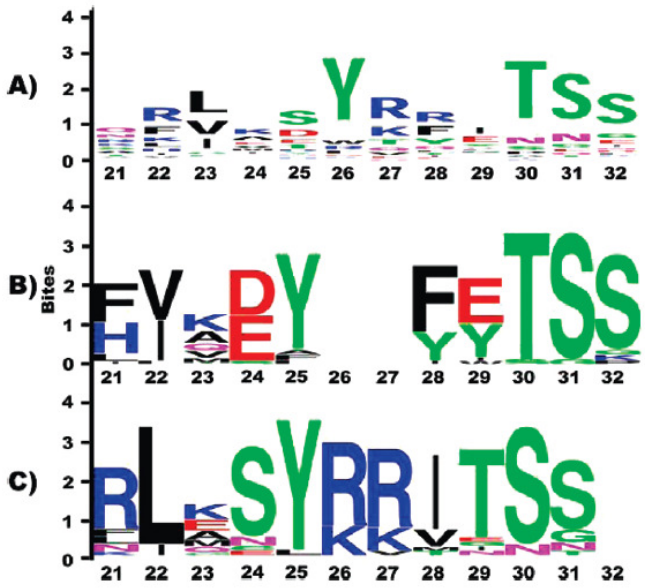

Figure IV-4: Logo plots of the *β*1 strand region.

Three multiple sequence alignments are represented using Weblogo (167). The overall height of the stack indicates the conservation at that position in the multiple-sequence alignment, and the height of the individual single-letter codes within the stack indicates the relative frequency of the corresponding amino acid at that position. The x-axis values refer to the residue position of the mature human CXCL8. Color coding for the class of amino acids: green and purple for polar, blue for basic, red for acidic, and black for hydrophobic. (A) Problems of a global multiple-sequence alignment over the entire CC chemokine family with the CXCL8 sequence. One is the reduction of the magnitude of the signal (see the smaller letters of the Arg residues at positions 27 and 28), and another is the apparent +1 residue shift in the middle of the alignment as compared to the two following alignments (see the shift in the Tyr residue at position 26 and the Arg residues at positions 27 and 28). (B) Results of the multiple-sequence alignment comparing the CXCL8 sequence with the sequences from the clade surrounding CCL4. The deletion in the center at positions 26 and 27 is quite evident. (C) Results of the multiple-sequence alignment comparing the CXCL8 sequence with the sequences from the clade surrounding CCL2. Again, the conservation of the Arg at positions 26 and 27 is very apparent.

On the basis of this procedure, we were able to identify a set of mutations that help us understand how the CC chemokine families negatively design against CXCL8 dimerization (summarized in Table IV-1). Because CCL4 possesses the same fold as CXCL8 yet dimerizes differently [as explained above (166)], our first comparison uses the clade surrounding CCL4. The sequence alignment shown in Figure IV-4B clearly indicates a two-residue deletion of R26 and V27 in the β1 strand. While a number of other residues exhibit strong conservation, only the two-residue deletion and the L25Y mutation exhibited statistical significance (Table IV-1). To further test this approach, we also made the same limited sequence comparison of CXCL8 with the CCL2 sequence clade. Sharing the same chemokine fold, CCL2 dimerizes in a fashion similar to that of CCL4 (168) but also shares a low level of sequence identity with CXCL8. As corroborated by our statistical analysis, Figure IV-4C highlights the existence of the two Arg residues in the center of the β1 strand created by a V27R mutation. Because we wanted to understand the sequence elements conferring negative interactions specific to each evolutionary branch, the L24Y mutation was disregarded since it was conserved across both the CCL4 and CCL2 clades. Therefore, our analysis produced two sets of negative interaction elements that break up a CXCL8 dimer yet retain the chemokine fold: a deletion of residues 26 and 27 (ΔRV) and a mutant creating a charge repulsion (V27R). As a control to test whether removal of the side chains or the rearrangement caused by the deletion is more important, the R26A/V27A double mutation was also introduced.

Monomeric state of the mutants

The two variants of CXCL8 (ΔRV and V27R) along with R26A/V27A and the WT control were constructed and purified as described in Experimental Procedures. It is predicted that making these mutations in CXCL8 will abrogate the dimer. For the sake of clarity, we will further refer to these mutations using their abbreviated names indicated in the previous sentence and noted in Table IV-1. Size exclusion chromatography (SEC) and analytical ultracentrifugation (AUC) were used to investigate the quaternary state. In the SEC analysis, we compared the elution profiles of WT CXCL8 to those of the ΔRV and R26A/V27A mutants of CXCL8 (Figure IV-5). The major peak in the ΔRV profile eluted at a volume later than that of the WT that is quite similar to known CXCL8 monomeric mutants (112). In contrast, the R26A/V27A control variant of CXCL8 elutes only slightly later than wild-type CXCL8, but significantly before known monomeric variants. This similarity in elution profile to the WT suggests that the R26A/V27A variant forms a dimer in solution. To further verify the dimerization status of these variants, the more rigorous AUC experiment was carried out. A single run for each mutant is shown in Figure IV-6; however, for the sake of accuracy, the oligomerization state was modeled from an extensive set of AUC experiments (see Experimental Procedures) performed for each variant at different speeds, wavelengths, and concentrations (Data not shown). The result of the AUC analysis is that both the ΔRV and V27R mutants fit a monomeric model with predicted molecular masses of 8.25 ± 0.52 and 8.74 ± 0.21 kDa, respectively. These values are close to the theoretical monomer molecular masses of these mutants. These fits of ΔRV and V27R mutants were run at concentrations of up to 111 and 500 μM (see Experimental Procedures),

respectively, which is far greater than the WT value of 0.194 μM (112) run under the same conditions. In comparison to other values of the WT, the Kd values of CXCL8 run under slightly different conditions ranging from 4 to 10 μM (150,169-171), these mutants are monomeric. Therefore, they show that the mutations strongly inhibit dimerization across the β1 strand. The R26A/V27A control fits best to a monomer−dimer equilibrium model with an estimated molecular mass of the monomer of 8.8 ± 0.6 kDa and a Kd of 18.2 ± 3.1 μM, which is a weaker dimer than WT CXCL8 [Kd = 0.1 μM (112)]. Comparison to other values of WT CXCL8 Kd noted above substantiates that R26A/V27A still dimerizes in a manner comparable to that of WT CXCL8. These results show that the mutation disrupts but does not abolish dimerization. These SEC and AUC results clearly demonstrate that the two types of evolutionarily conserved sequence motifs confer negative interactions to inhibit CXCL8 dimerization across the β1 strand.

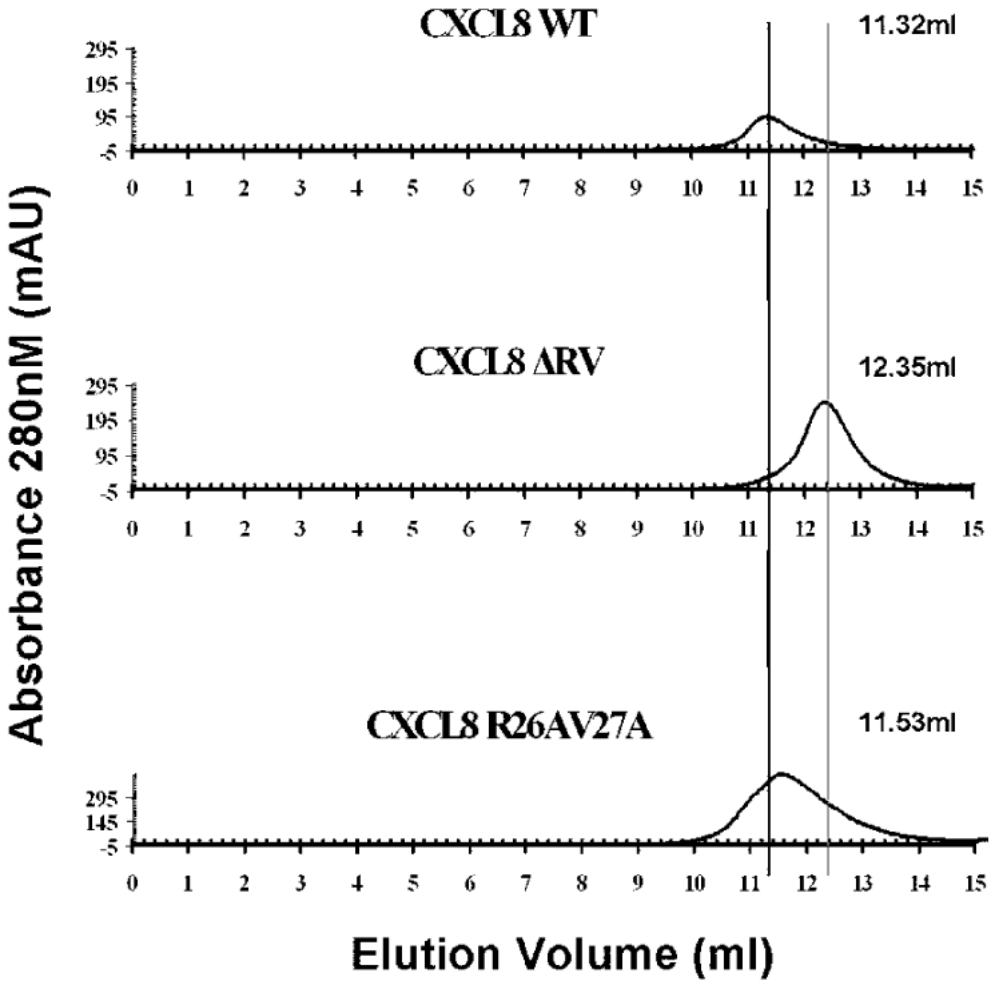

Figure IV-5: Size exclusion chromatography.

SEC is shown for WT CXCL8, the ΔRV variant, and the R26A/V27A mutant. The black line shows the expected earlier position for the dimer, and the gray line represents the expected later position for the monomer. Elution volumes of the peak are shown on the x-axis.

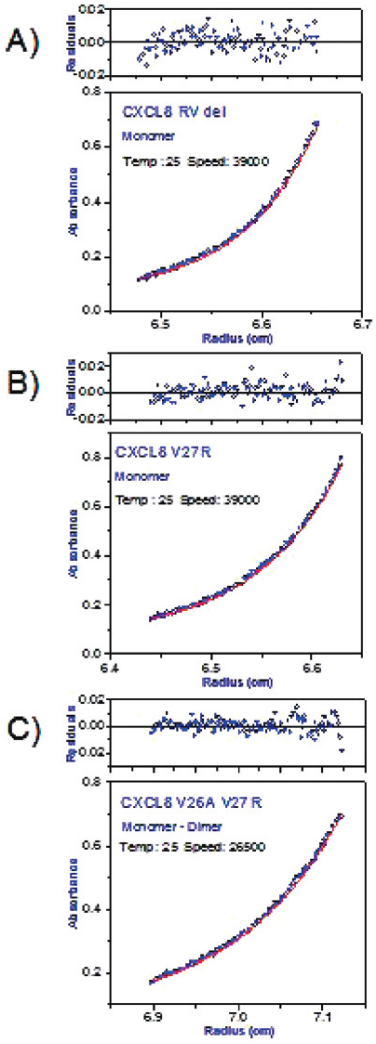

Figure IV-6: Individual analytical ultracentrifugation runs.

Single AUC residuals (top) and fits (bottom) are shown for (A) ΔRV, (B) the V27R variant, and (C) the R26A/V27A mutant. Speed and temperature are shown on each plot. The wavelength is 280 nm for ΔRV, 281 nm for V27R, and 280 nm for R26A/V27A. As explained in Experimental Procedures, although a single run is shown here, the oligomerization data were fit for each variant over several runs. Both the ΔRV and V27R mutants fit a monomeric model with predicted molecular masses of 8.25 ± 0.52 and 8.74 ± 0.21 kDa, respectively. These values are close to the theoretical monomer molecular mass of these mutants. The R26A/V27A control fits best to a monomer-dimer equilibrium model with an estimated molecular mass of the monomer of 8.8 ± 0.6 kDa and a Kd of 18.2 ± 3.1 μM, which is a weaker dimer than the WT (Kd ~ 0.1 μM). The randomness of residuals shown above each plot indicates a good fit.

NMR evidence indicating chemokine tertiary structure

Because the quaternary state is sensitive to the tertiary state, we used NMR to determine whether the CXCL8 mutants formed a chemokine fold. First, HSQC $^{15}N-^{1}H$ correlation spectra were compared. Figure IV-7 shows an overlay of the spectra of ΔRV, V27R, and WT CXCL8. The differences between these monomeric variants and WT CXCL8 are most likely due to the loss of intermolecular contacts across the dimer interface. We will first discuss the comparison of the HSQC spectra between the V27R mutant and WT, since it is only a single side chain mutation. We are confident that at NMR concentrations of 1 mM (see Experimental Procedures), the V27R mutant is a monomer since the AUC data were recorded at 0.5 mM, close to the NMR concentration. In Figure IV-7, this monomeric V27R mutant exhibits good peak dispersion and displays a spectrum similar to those of other known CXCL8 monomers (112), so we conclude that the V27R mutant exhibits a chemokine fold.

Because AUC for the ΔRV mutant was maximally run at 1/10 of the NMR concentration, we ran a ^{15}N relaxation experiment to verify that this mutant was a monomer. The ratio of ^{15}N relaxation parameters T1 and T2 can be used to estimate the size of a protein. For example, the wild-type CXCL8 dimer has been shown to have a T1/T2 ratio of 8.59 (172), and that of the CCL4 dimer is 8.3 (173). In contrast, monomeric variants of CCL4 have measured T1/T2 ratios of 3.9 and 4.0 (174). For this work, the CXCL8 mutant ΔRV was shown to have a T1/T2 ratio of 3.6, fully consistent with a monomeric chemokine. In Figure IV-7, the well-defined dispersion in the $^{15}N-^{1}H$ correlation spectra is also representative of a folded protein. Unlike the simple point mutation in V27R, the deletion of two residues in the case of the ΔRV mutant causes an

expected but significant change in the HSQC spectrum when compared to that of the WT. The deletion leads to loss of interactions across the protein−protein interface, and R26 and V27 also make several intramonomer contacts in the wild-type protein. When an analysis of tertiary contacts was performed (175), R26 and V27 make internal contacts with I28, T37, E38, I39, I40, V41, and K42 (data not shown). An assignment of ^{15}N, ^{1}HN, ^{13}Cα, and ^{13}Cβ resonances was carried out and confirmed that the residues contacting R26 and V27 in WT CXCL8 change environment in the ΔRV mutant (Figure IV-8). Although suggestive, the HSQC spectrum of the ΔRV variant does not provide conclusive evidence that this mutant retains the chemokine fold. Therefore, we turned to an NMR-based analysis of secondary structure (176) and oxidative state of cysteines (177) to prove that the ΔRV mutant folds into the chemokine structure shown in Figure IV-7. For secondary structure, we measured the ^{13}Cα and ^{13}Cβ deviation from random coil values (Figure IV-9), which has been established as a strong predictor of secondary structure (178,179). While the β3 strand is approximately the same length in ΔRV as in the WT, the β1 and β2 strands appear to be shorter. This potential fraying of the β1 strand would contribute to inhibition of dimer formation. In addition, the deviations in Figure IV-9 show that the helix in ΔRV is not structured toward the C-terminus. Our T1/T2 ratios corroborate this result since they cannot be calculated past residue 65 in the ^{15}N relaxation experiment (data not shown). The unstructured C-terminal residues are consistent with the loss of intersubunit contacts made by the helix as previously suggested (144) and explicitly described in a CXCL8 monomer (180). However, despite these small variations, the two proteins overall appear to exhibit very similar secondary structures. Analysis of the chemical shift assignments with TALOS (181) predicts and ψ

backbone torsion angles that corroborate our secondary structure analysis (data not shown). Furthermore, the ^{13}C NMR chemical shifts can distinguish between reduced, free cysteine and oxidized, disulfide-bonded cysteine (182). Since the chemical shift assignments for the backbone atoms of WT and ΔRV have been obtained using a series of three-dimensional experiments, we can easily compare the participation of cysteines in disulfide bonds between the two variants. As shown in Table IV-3, all of the $^{13}C\beta$ chemical shift values for the four cysteines in ΔRV are similar to those of WT CXCL8 in that they are greater than the cutoff value of 32 ppm for the reduced cysteine (182), which indicates that all cysteines in the ΔRV mutant are in the oxidized disulfide form, like the wild-type protein. In addition, the ΔRV's cysteine $^{13}C\beta$ and $^{13}C\alpha$ chemical shift values deviate only slightly from the WT CXCL8 values. Not only do these results show that the ΔRV mutant's cysteines are disulfide-bonded, but they also indicate that the ΔRV disulfides inhabit an environment similar to that of the wild-type protein. Therefore, ΔRV very likely shares the same disulfide pattern as WT CXCL8. Previous studies on the formation of these disulfide bonds have shown that they are integral to chemokine structure (183,184). In much the same spirit that Anfinsen's experiments used disulfide bonding patterns to prove correct refolding (185), the fact that ΔRV makes the same two disulfide bonds as WT CXCL8 (from β0 to β3 strands and from β0 to β2 strands) indicates that the β-sheet structure is like the WT. This evidence of correct chemokine β-sheet structure in conjunction with good dispersion in the $^{15}N-^{1}H$ correlation spectra and correct secondary structure formation strongly argues that, like the V27R mutant, the drastic ΔRV mutant retains a chemokine fold.

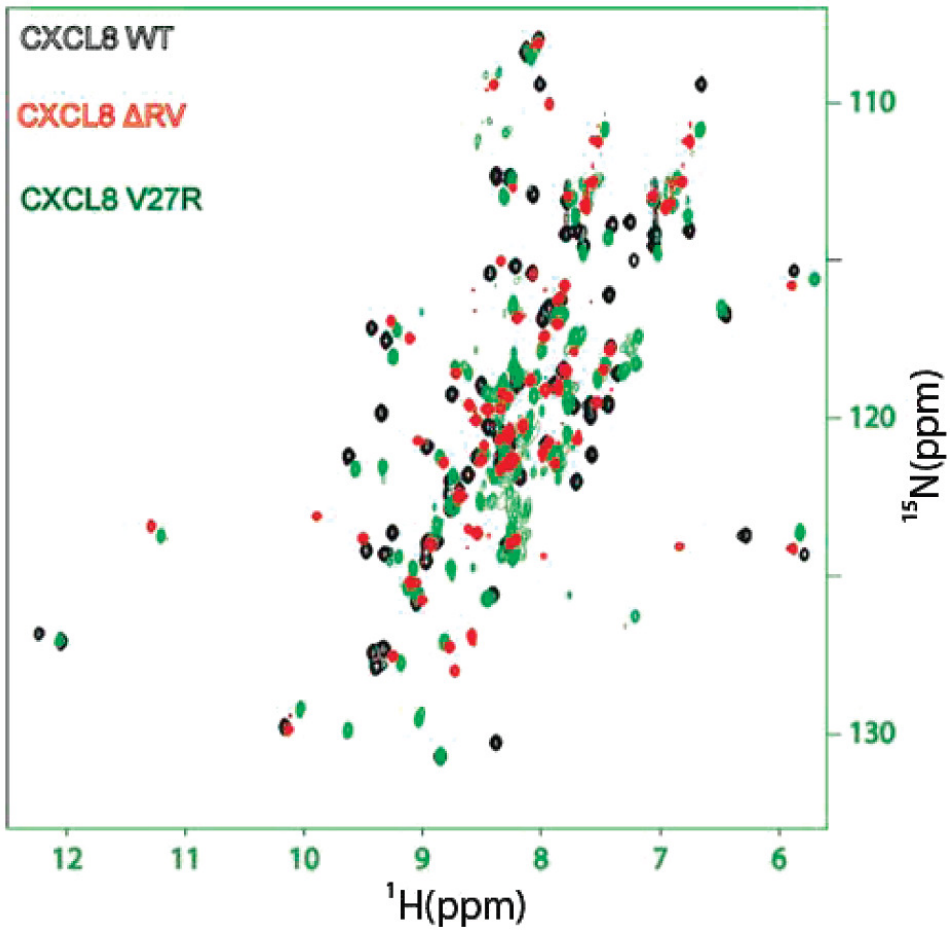

Figure IV-7: HSQC spectra.

Comparison of ^{15}N-^{1}H correlation spectra of wild-type CXCL8 to those of ΔRV and V27R. As labeled, data for wild-type CXCL8 are colored black. For contrast, peaks for ΔRV and V27R are colored red and green, respectively. Both of the mutant proteins display good dispersion of peaks, which implies that they are well-folded.

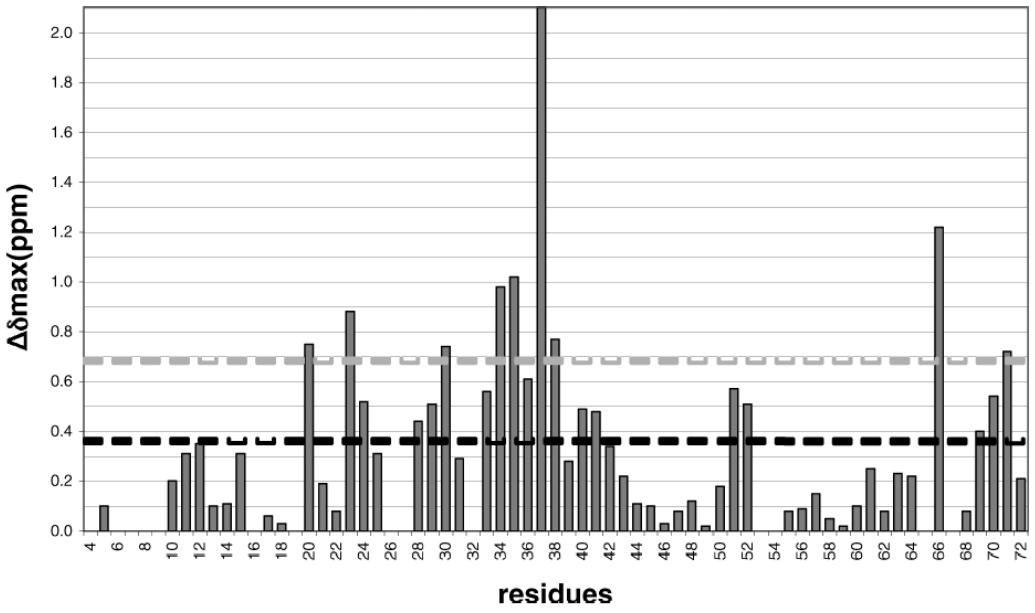

Figure IV-8: Chemical shift differences.

The ^{15}N- and ^{1}HN-weighted average chemical shift differences between WT CXCL8 and ΔRV are shown. The dashed black line represents the average chemical shift differences and the dashed gray line the standard deviation from the average. The weighted chemical shift differences (186) were calculated using the equation $\Delta\delta_{obs} = \{[(\Delta\delta_{HN})^2 + (\Delta\delta_N/5)^2]/2\}^{1/2}$. In this analysis of peak movement, the assignment of ^{15}N and ^{1}HN resonances showed that many residues' resonances in the *β*1 strand and the C-terminal portion of the R-helix change in the ΔRV mutant. All these peaks move in comparison to those of the WT, except I39. As discussed above, these expected changes in peak position indicate that the chemical environment around these amino acids has changed due to a lack of interface contacts and the two-residue deletion. In addition, the peaks corresponding to H33, C34, A35, and N36 have shifted in ΔRV, so the turn between the *β*1 and *β*2 strands has been affected, possibly because of the changes in the registry of the amino acid at the turn. The peaks corresponding to L51 and D52, in the turn between the *β*1 strand and *α*-helix, have also moved. Lastly, the peaks from L66, A69, E70, and N71, which belong to the top part of the *α*-helix, all have shifted.

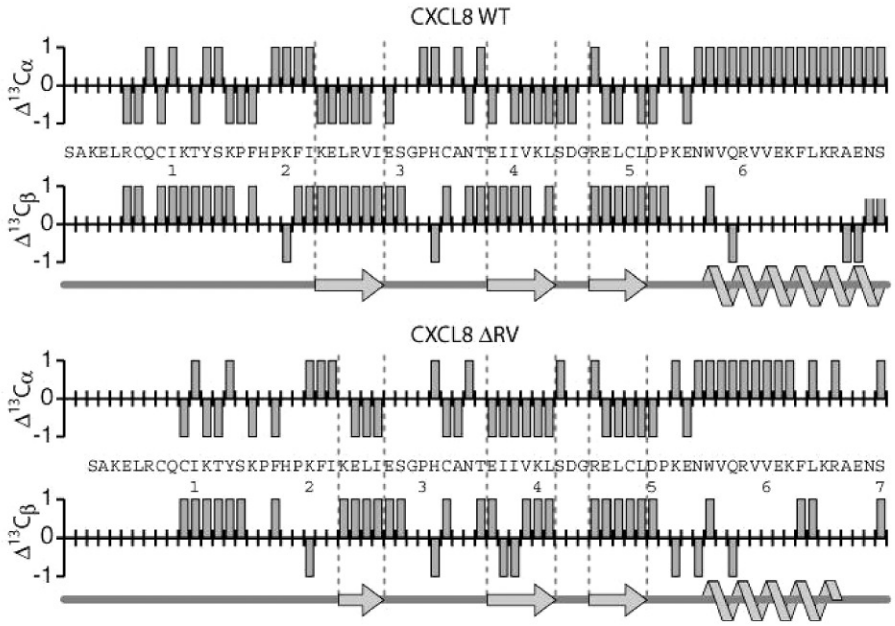

Figure IV-9: Chemical shift index values of $^{13}C\alpha$ and $^{13}C\beta$ deviations from random coil chemical shift values relative to DSS (2,2-dimethyl-2-silapentane-5-sulfonate sodium salt) (163).

Data for WT CXCL8 are shown on top and those for the ΔRV variant on the bottom. The vertical scale for the index is either -1, 0, or 1. For each, the sequence is shown with the residue number underneath marked by tens. Also, the secondary structures of sheets are helices and are noted, and dashed lines are provided for reference. For better comparison, the ΔRV sequence is shifted over by two residues at the start. Note for the ΔRV variant, the β1 strand is shorter and α-helix is four residues shorter than that of the wild type, as found for monomeric CXCL8 (144,180).

Table IV-3: Cysteine ^{13}C chemical shifts.

^{13}C	CXCL8	C7	C9	C34[a]	C50[a]
Cα	WT[b]	55.69	55.38	56.93	56.45
	^{2}RV[b]	55.57	55.95	55.20	55.62
Cβ	WT[b]	39.49	44.23	42.15	48.29
	^{2}RV[b]	39.27	42.49	41.77	46.06

[a] These two residues are references to the WT CXCL8 sequence. Because of the two-residue deletion in ΔRV, these residues are actually residues 32 and 48 in the ΔRV sequence, respectively. [b] Chemical shift values are in parts per million.

Discussion

In this investigation of differential chemokine quaternary structure, we applied a hybrid sequence analysis to identify conserved motifs within one chemokine protein interface and have experimentally shown that these motifs inhibit dimerization across the β1 strand. In an effort to maximize the signal over noise, the sequence analysis considered structure (localization of comparison to a particular portion involving the CXCL8 dimer interface) and phylogeny (limiting the comparison to clades consisting of proteins closely related in evolution). In comparing CXCL8's sequence with the CCL4 and CCL2 sequence clades, this analysis reveals that these two chemokine families conserved different motifs over their β1 strands (Figure IV-4). For the CCL4 sequence clade, a surprising two-residue deletion is found in the middle of the β1 strand, while for the CCL2 sequence clade, a simple V27R point mutation is found. As shown in Figure IV-4, limiting the sequence analysis is important. Crystallographic evidence shows that certain CC chemokine families can dimerize like CXCL8 (187,188). Including these sequences in our analysis would certainly cause ambiguity in the results, and as shown in Figure IV-4A, mutations suggested by a straightforward sequence alignment would not have found these sequence elements. In addition, because the double deletion was located in the middle of a strand, a structural alignment would have certainly assigned the missing residues to either side of the strand in loop regions and missed the importance of the deletions' position.

Placing the ΔRV and V27R negative interaction motifs in the CXCL8 background, we experimentally confirmed that these sequences affect CXCL8's ability to dimerize across the β1 strand without changing the chemokine fold. AUC and SEC

experiments indicate that the two CXCL8 variants form monomers and no longer dimerize (Figures 19 and 20, respectively). NMR HSQC analysis shows good peak dispersion for both of the CXCL8 variants (Figure IV-7), where the V27R variant displays a pattern similar to that of folded monomers found in previous work (112). Because the ΔRV mutation is more drastic and its HSQC spectrum is so different, it could be argued that the ΔRV mutation causes some rearrangement in chemokine structure in either the β-sheet, β1 strand, or helix. The NMR evidence showing the correct disulfide pattern (Table IV-3) verifies that the ΔRV variant forms a chemokine β-sheet, at least among the β0, β2, and β3 strands, while the ΔRV mutant's good dispersion in the $^{15}N-^{1}H$ correlation spectra results from a folded structure (Figure IV-8). In Figure IV-9, the $^{13}C\alpha$ and $^{13}C\beta$ deviation from random coil analysis (176) indicates that the β1 strand is formed and shows C-terminal fraying of the α-helix, which is indicative of a folded monomer in solution (180). In comparison with previous work on creating CXCL8 monomers (144,145,147,150,166,169), these results demonstrate that our hybrid sequence analysis provides a straightforward and successful approach to identifying sequence motifs that inhibit dimer formation. Overall, our results show that the two conserved sequence motifs introduce unfavorable interactions into the CXCL8 interface and inhibit CXCL8 homodimer formation.

The ΔRV and V27R motifs both disrupt CXCL8-type dimerization by more than just affecting the β1 strand interface. Ostensibly, ΔRV is a gross modification in the middle of a β-strand, yet it retains a chemokine fold. Because the R26A/V27A variant only weakens dimer formation by a ΔΔG of 12.9 kJ/mol, the ΔRV's effects include the removal of the side chain interactions across the β1 strand and the double deletion alters

interactions of the downstream turn and α-helix (Figure IV-2 and Figure IV-4). Both of these are involved in the dimer interface. As the double deletion derives from the CCL4 clade, this supposition is corroborated by the shortened β1 strand and downstream loop shown by CCL4. Figure IV-8 provides a clearer, better explanation. The β1 strand is shorter and the α-helix frayed toward the C-terminus in comparison to those of WT CXCL8, although the frayed α-helix is characteristic of a chemokine monomer (180). Such structural changes do not favor dimer formation. By contrast, as a modest, single-point mutation, the V27R substitution introduces a long positively capped side chain into the center of the CXCL8 interface that most likely creates an electrostatic repulsion with the adjoining R26 residue and a steric obstruction to the correct placement of the α-helices during dimer formation. A similar negative interaction has been found in a survey of protein β-sheet structures (136) and was used to inhibit dimerization in protein design (135). While this mutation has been shown in conjunction with the L25Y mutation to cause a chemokine monomer (147), our work is the first reported, single-natural amino acid substitution shown to disrupt the CXCL8 homodimer and retain the chemokine fold, where the other single-amino acid substitution was a non-natural l-methylleucine at residue 25 (145) (Table IV-1). These results for both the ΔRV and V27R negative interaction elements agree with previous work showing that mutations in both the β1 strand and α-helix are necessary to disrupt the CXCL8 dimer (144).

The finding of conserved sequence motifs that disfavor a certain type of homodimerization has several implications. First, these results suggest that at least one role of these motifs in the CCL4 and CCL2 sequence clades is to inhibit the more regular protein−protein interaction involving the β1 strand. As displayed in Figure IV-4, these

motifs are strongly conserved. ΔRV is found in all 29 sequences in the CCL4 clade (blue subtree of Figure IV-3), while V27R is found in the majority of the 16 sequences in the CCL2 clade (red subtree of Figure IV-3). For the other instances in the CCL2 clade, the residue is another positively charged lysine residue. This conservation strongly suggests that there is some evolutionary pressure to retain these motifs. One such pressure could be to favor N-terminal homodimerization. Since crystallographic structures have shown that it is possible to see chemokine tetramers with both types of interfaces (189,190), we can think of the various homodimerization states being in equilibrium. By disfavoring the β1 strand interface, the ΔRV and V27R sequence motifs indirectly favor homodimerization at the N-terminal interface. Because the exact function of homodimerization with chemokines is still being debated (38,146,150,174,191-197), we cannot say for certain that the primary role of these motifs is to indirectly favor CC-type homodimerization. However, with new evidence of chemokine heterodimerization (198), the inhibitory motifs could take on new significance by hindering cross reactivity with other chemokines in a CXC-like dimer. Because of the striking evolutionary persistence and the clear experimental findings, our results do support the conclusion that the ΔRV and V27R sequence elements are examples of conserved motifs conferring unfavorable interactions against CXC-type dimerization.

After the completion of this project, lab interest moved from chemokine dimerization studies to development of anti-HIV compounds since one of the most promising property of some chemokines, like for example RANTES, is to block HIV fusion to the target cell as it descript in details in Chapter I.

CHAPTER V

SUMMARY, CONCLUSIONS AND FUTURE WORK

Chapter II focuses on improving the properties of Griffithsin, a lectin that binds viral envelope glycoprotein gp120. The hypothesis is that a covalently linked Griffithsin and C37 (Griff37) would allow both of these compounds to bind at the same viral spike. This simultaneous binding could be beneficial for the anti-HIV activity of Griffithsin. As proof of concept, I used CD4M33, a peptide that also binds to gp120 at an area similar to Griffithsin, covalently linked to C37 ($C37CD4M33_{C1F23}$). Indeed, Griff37 showed better viral inhibition than Griffithsin alone both in fusion assays and viral assays in MAGI and PBMCs cells in R5 and X4 viral strains. In the case of $C37CD4M33_{C1F23}$, the lack of proper controls ($CD4M33_{C1F23}$) made it difficult to appreciate the success of this chimeric protein.

We consider Griff37 a good candidate for improvement, but before we do that, it is crucial to understand the mechanism of action of this chimeric protein. Some of the experiments proposed here are currently under way. The models proposed in Chapter III (Figure II-4) suggest that linker length is crucial in simultaneous binding of Griffithsin and C37. Shorter linker length is expected to reduce the anti-HIV potency of Griff37. If Griff37 with a shorter linker length has the same or higher anti-HIV activity, then the most probable model of action is shown in Figure II-4A, where Griffithsin and C37 do not bind simultaneously, but rather with one or the other. In order to test the role of C37 in Griff37, mutations will be introduced to C37 that cause a reduction in the binding affinity of C37 with viral protein gp41 (199). The drawback of this experiment is that a

linked C37 may act differently from a free C37 and significantly affect the k_{on} of C37, and the overall reduction of anti-HIV activity of Griff37 may be minimal.

Before Griff37 experiments progress, it is crucial to verify that the improvement in potency that we observed compared to Griffithsin is general enough to make Griff37 a good candidate for practical application. Griff37 needs to be tested in many more R5, R4 and dual tropic HIV strains from subtype B and C. Attention needs to be given to strains that show C37 resistance and Griffithsin resistance (some subtype C strains shows resistance to griffithsin (200)) since we expect the chimeric protein to show significant improvement in these viral strains (200). It is also desirable to test the potency of Griff37 in dendritic cells since, as I described in Chapter I, these are the cells that the virus encounters first as it travels deeper in the epithelium. Finally, if we receive satisfactory results from the experiments above, Griff37 should be tested in HIV-1 cervical explant assays and microbicide toxicity assays (67).

In Chapter III, I test the hypothesis that there is a synergistic effect in HIV inhibition between P2-RANTES, a modified version of the chemokine RANTES, and C-peptides C34 and C37. These peptides block the formation of the six-helix bundle of gp41 (see Chapter I). Although I observed synergy in a fusion assay between P2-RANTES and C37/C34, these effects seemed to be minimal when the compounds were tested in a viral assay in MAGI cells. When the compounds where tested in PBMCs in viral assays, we observed synergy. From these results, it was clear that the synergetic effect between P2-RANTES and C37/C34 was heavily dependent on the cell type, the amount of CCR5 receptor on the surface of the cell, and on the capability of the cells to internalize and recycle the CCR5 receptor. Because of the lack of generality, and taking

into account the complexity of the virus-human interaction described in Chapter I, it is expected that the practical applications of the synergetic effects of these drug combinations will be limited. Resources would be better spent on more attractive HIV fusion inhibitors.

Chapter IV moves from the field of virology to bioinformatics. In this chapter, I used a chemokine family to test the hypothesis that unfavorable sequence motifs can be evolutionarily conserved and can be detected using structural alignment combined with phylogeny. This chemokine family exhibited the same tertiary fold, but members of certain subfamilies, including CXCL8, formed a homodimer across the β1 strand, while members of other subfamilies, including CCL4 and CCL2, formed a homodimer on the opposite side of the chemokine fold. These results suggest that, at least in this protein family, we detected conserved unfavorable sequence motifs. The usefulness of this method can be summarized as a way to reduce the "noise" in structural alignment that is accumulated through random mutations in a protein sequence. This is critical when we are searching for unfavorable sequence motifs that do not need to be evolutionarily highly conserved.

Further tests are needed in different protein families with similar properties to verify the generality of this phenomenon. The possibility of developing a user friendly structural alignment program that would take into account phylogeny information and would allow the user to determine the area of interest would be a breakthrough in detecting unfavorable sequence motifs and allow better understanding of the evolution of protein families.

NOMENCLATURE

AIDS	Acquired Immune Deficiency Syndrome
AOP	Aminooxypentane
AUC	Analytical Ultracentrifugation
BSA	Bovine Serum Albumin
BME	β-Mercaptoethanol
CCR	CC Chemokine Receptor
CXCR	CXC Chemokine Receptor
CHO	Chinese Hamster Ovary
CRPG	Chlorphenol Red-β-D-Galactopyranoside
EDTA	EthyleneDiamineTetraacetic Acid
NOE	Nuclear Overhauser Effect
PSC	[L-ThiaPro2, L-α-cyclohexyl-Gly3]-NNY
Da	Dalton
DSS	4, 4-Dimethyl-4-Silapentane-1-Sulfonate
DMEM	Dulbecco's Modified Eagle's Medium
env	HIV-1 Envelope Protein
FACS	Fluorescence Activated Cell Sorting
FCS	Fetal Calf Serum
FDA	Food and Drug Administration
FBC	Fetal Bovine Serum
GAG	Glycosaminoglycan

HPLC	High Performance Chromatography
HIV	Human Immunodeficiency Virus
HSQC	Heteronuclear Single-Quantum Coherence
IC50	Concentration of 50% Inhibition
IL-8	Interleukin-8 (CXC Chemokine Ligand 8 or CXCL8)
IPTG	Isopropyl-β-D-Thiogalactopyranoside
Kd	Dissociation Constant
MIP	Macrophage Inflammatory Protein (MIP-1α, CCL4; MIP-1β, CCL3)
MW	Molecular Weight
NMR	Nuclear Magnetic Resonance
PBS	Phosphate Buffered Saline
PBMC	Peripheral Blood mononuclear Cells
PCR	Polymerase Chain Reaction
PEEA	Polyethyleneamine
PEG	Polyethylene Glycol
PF-4	Platelet Factor 4 (CXCL4)
PI	Propidium Iodide
RANTES	Regulated on Activation of Normal T-Cell Expressed and Secreted (CCL5)
RMSD	Root Mean Square Deviation
RPMI	Roswell Park Memorial Institute
SD	Standard Deviation
SDS-PAGE	Sodium Dodecyl Sulfate Polyacrylamide Gel Electrophoresis

TFA Trifluroacetic Acid

WT Wild Type

REFERENCES

1. **Adachi, A., H. E. Gendelman, S. Koenig, T. Folks, R. Willey, A. Rabson, and M. A. Martin.** 1986. Production of acquired immunodeficiency syndrome-associated retrovirus in human and nonhuman cells transfected with an infectious molecular clone. J Virol **59:**284-91.

2. **Alexandre, K. B., E. S. Gray, B. E. Lambson, P. L. Moore, I. A. Choge, K. Mlisana, S. S. Karim, J. McMahon, B. O'Keefe, R. Chikwamba, and L. Morris.** 2010. Mannose-rich glycosylation patterns on HIV-1 subtype C gp120 and sensitivity to the lectins, Griffithsin, Cyanovirin-N and Scytovirin. Virology **402:**187-96.

3. **Alkhatib, G., C. Combadiere, C. C. Broder, Y. Feng, P. E. Kennedy, P. M. Murphy, and E. A. Berger.** 1996. CC CKR5: a RANTES, MIP-1alpha, MIP-1beta receptor as a fusion cofactor for macrophage-tropic HIV-1. Science **272:**1955-8.

4. **Anfinsen, C. B.** 1973. Principles that govern the folding of protein chains. Science **181:**223-30.

5. **Baldwin, E. T., I. T. Weber, R. St Charles, J. C. Xuan, E. Appella, M. Yamada, K. Matsushima, B. F. Edwards, G. M. Clore, A. M. Gronenborn, and et al.** 1991. Crystal structure of interleukin 8: symbiosis of NMR and crystallography. Proc Natl Acad Sci U S A **88:**502-6.

6. **Berger, E. A., P. M. Murphy, and J. M. Farber.** 1999. Chemokine receptors as HIV-1 coreceptors: roles in viral entry, tropism, and disease. Annu Rev Immunol **17:**657-700.

7. **Bleul, C. C., M. Farzan, H. Choe, C. Parolin, I. Clark-Lewis, J. Sodroski, and T. A. Springer.** 1996. The lymphocyte chemoattractant SDF-1 is a ligand for LESTR/fusin and blocks HIV-1 entry. Nature **382:**829-833.

8. **Burrows, S. D., M. L. Doyle, K. P. Murphy, S. G. Franklin, J. R. White, I. Brooks, D. E. McNulty, M. O. Scott, J. R. Knutson, D. Porter, and et al.** 1994. Determination of the monomer-dimer equilibrium of interleukin-8 reveals it is a monomer at physiological concentrations. Biochemistry **33:**12741-5.

9. **Cane, P. A.** 2009. New developments in HIV drug resistance. J Antimicrob Chemother **64 Suppl 1:**i37-40.

10. **Chackerian, B., E. M. Long, P. A. Luciw, and J. Overbaugh.** 1997. Human immunodeficiency virus type 1 coreceptors participate in postentry stages in the virus replication cycle and function in simian immunodeficiency virus infection. J Virol **71:**3932-9.

11. **Champagne, K., A. Shishido, and M. J. Root.** 2009. Interactions of HIV-1 inhibitory peptide T20 with the gp41 N-HR coiled coil. J Biol Chem **284:**3619-27.

12. **Chan, D. C., C. T. Chutkowski, and P. S. Kim.** 1998. Evidence that a prominent cavity in the coiled coil of HIV type 1 gp41 is an attractive drug target. Proceedings of the National Academy of Sciences of the United States of America **95:**15613-7.

13. **Chan, D. C., D. Fass, J. M. Berger, and P. S. Kim.** 1997. Core structure of gp41 from the HIV envelope glycoprotein. Cell **89:**263-73.

14. **Chan, D. C., and P. S. Kim.** 1998. HIV entry and its inhibition. Cell **93:**681-4.

15. **Chen, B., E. M. Vogan, H. Gong, J. J. Skehel, D. C. Wiley, and S. C. Harrison.** 2005. Structure of an unliganded simian immunodeficiency virus gp120 core. Nature **433:**834-41.

16. **Chou, T. C., and P. Talalay.** 1984. Quantitative analysis of dose-effect relationships: the combined effects of multiple drugs or enzyme inhibitors. Adv Enzyme Regul **22:**27-55.

17. **Ciminale, V., B. K. Felber, M. Campbell, and G. N. Pavlakis.** 1990. A bioassay for HIV-1 based on Env-CD4 interaction. AIDS Res Hum Retroviruses **6:**1281-7.

18. **Clark-Lewis, I., K. S. Kim, K. Rajarathnam, J. H. Gong, B. Dewald, B. Moser, M. Baggiolini, and B. D. Sykes.** 1995. Structure-activity relationships of chemokines. J Leukoc Biol **57:**703-11.

19. **Clore, G. M., Appella, E., Yamada, M., Matsushima, K., Gronenborn, A.M.** 1990. Three dimensional structure of Interleukin-8 in solution. Biochemistry **29:**1689-1696.

20. **Clore, G. M., and A. M. Gronenborn.** 1997. NMR structures of proteins and protein complexes beyond 20,000 M(r). Nat Struct Biol **4 Suppl:**849-53.

21. **Cocchi, F., A. Devico, A. Garzinodemo, P. Lusso, and R. C. Gallo.** 1995. Role of beta chemokines in suppressing HIV replication. Science **270:**1811.

22. **Connor, R. I., B. K. Chen, S. Choe, and N. R. Landau.** 1995. Vpr is required for efficient replication of human immunodeficiency virus type-1 in mononuclear phagocytes. Virology **206:**935-44.

23. **Cornilescu, G., F. Delaglio, and A. Bax.** 1999. Protein backbone angle restraints from searching a database for chemical shift and sequence homology. J Biomol NMR **13:**289-302.

24. **Covell, D. G., G. W. Smythers, A. M. Gronenborn, and G. M. Clore.** 1994. Analysis of hydrophobicity in the alpha and beta chemokine families and its relevance to dimerization. Protein Sci **3:**2064-72.

25. **Crooks, G. E., G. Hon, J. M. Chandonia, and S. E. Brenner.** 2004. WebLogo: a sequence logo generator. Genome Res **14:**1188-90.

26. **Crown, S. E., Y. Yu, M. D. Sweeney, J. A. Leary, and T. M. Handel.** 2006. Heterodimerization of CCR2 chemokines and regulation by glycosaminoglycan binding. J Biol Chem **281:**25438-46.

27. **Da, L. T., J. M. Quan, and Y. D. Wu.** 2009. Understanding of the bridging sheet formation of HIV-1 glycoprotein gp120. J Phys Chem B **113:**14536-43.

28. **Delaglio, F., S. Grzesiek, G. W. Vuister, G. Hu, J. Pfeifer, and A. Bax.** 1995. NMRPipe: A multidimensional spectral processing system based on UNIX pipes. J. Biomol. NMR **6:**277-293.

29. **Delaglio, F., S. Grzesiek, G. W. Vuister, G. Zhu, J. Pfeifer, and A. Bax.** 1995. NMRPipe: a multidimensional spectral processing system based on UNIX pipes. J Biomol NMR **6:**277-93.

30. **DeLean, A., P. J. Munson, and D. Rodbard.** 1978. Simultaneous analysis of families of sigmoidal curves: application to bioassay, radioligand assay, and physiological dose-response curves.[see comment]. American Journal of Physiology **235:**E97-102.

31. **Deng, H., R. Liu, W. Ellmeier, S. Choe, D. Unutmaz, M. Burkhart, P. Di Marzio, S. Marmon, R. E. Sutton, C. M. Hill, C. B. Davis, S. C. Peiper, T. J. Schall, D. R. Littman, and N. R. Landau.** 1996. Identification of a major co-receptor for primary isolates of HIV-1. Nature **381:**661-6.

32. **Deng, Y., Q. Zheng, T. J. Ketas, J. P. Moore, and M. Lu.** 2007. Protein design of a bacterially expressed HIV-1 gp41 fusion inhibitor. Biochemistry **46:**4360-9.

33. **Derdeyn, C. A., J. M. Decker, J. N. Sfakianos, X. Wu, W. A. O'Brien, L. Ratner, J. C. Kappes, G. M. Shaw, and E. Hunter.** 2000. Sensitivity of human immunodeficiency virus type 1 to the fusion inhibitor T-20 is modulated by coreceptor specificity defined by the V3 loop of gp120. J Virol **74:**8358-67.

34. **Desjarlais, J. R., and G. A. Lazar.** 2003. Negative design for improved therapeutic proteins. Trends Biotechnol **21:**425-7.

35. **Dey, B., C. S. Del Castillo, and E. A. Berger.** 2003. Neutralization of human immunodeficiency virus type 1 by sCD4-17b, a single-chain chimeric protein, based on sequential interaction of gp120 with CD4 and coreceptor. J Virol **77:**2859-65.

36. **Dragic, T., V. Litwin, G. P. Allaway, S. R. Martin, Y. Huang, K. A. Nagashima, C. Cayanan, P. J. Maddon, R. A. Koup, J. P. Moore, and W. A.**

Paxton. 1996. HIV-1 entry into CD4+ cells is mediated by the chemokine receptor CC-CKR-5. Nature **381:**667-73.

37. **Eckert, D. M., and P. S. Kim.** 2001. Mechanisms of viral membrane fusion and its inhibition. Annu Rev Biochem **70:**777-810.

38. **Emau, P., B. Tian, R. O'Keefe B, T. Mori, J. B. McMahon, K. E. Palmer, Y. Jiang, G. Bekele, and C. C. Tsai.** 2007. Griffithsin, a potent HIV entry inhibitor, is an excellent candidate for anti-HIV microbicide. J Med Primatol **36:**244-53.

39. **Fackler, O. T., and H. G. Krausslich.** 2006. Interactions of human retroviruses with the host cell cytoskeleton. Curr Opin Microbiol **9:**409-15.

40. **Feng, Y., C. C. Broder, P. E. Kennedy, and E. A. Berger.** 1996. HIV-1 entry cofactor: functional cDNA cloning of a seven-transmembrane, G protein-coupled receptor. Science **272:**872-7.

41. **Fernando, H., C. Chin, J. Rosgen, and K. Rajarathnam.** 2004. Dimer dissociation is essential for interleukin-8 (IL-8) binding to CXCR1 receptor. J Biol Chem **279:**36175-8.

42. **Fischer, T. B., J. B. Holmes, I. R. Miller, J. R. Parsons, L. Tung, J. C. Hu, and J. Tsai.** 2006. Assessing methods for identifying pair-wise atomic contacts across binding interfaces. J Struct Biol **153:**103-12.

43. **Frank, M. K., Clore., G.M., and Gronenborn, A.M.** 1995. Structural and dynamic characterization of the urea denatured state of the immunoglobulin binding domain of streptpcoccal protein G by multidimensional heteronuclear NMR spectroscopy. Protein Sci. **4:**2605-2615.

44. **Gartner, S., P. Markovits, D. M. Markovitz, M. H. Kaplan, R. C. Gallo, and M. Popovic.** 1986. The role of mononuclear phagocytes in HTLV-III/LAV infection. Science **233:**215-9.

45. **Gendelman, H. E., L. M. Baca, C. A. Kubrak, P. Genis, S. Burrous, R. M. Friedman, D. Jacobs, and M. S. Meltzer.** 1992. Induction of IFN-alpha in peripheral blood mononuclear cells by HIV-infected monocytes. Restricted antiviral activity of the HIV-induced IFN. J Immunol **148:**422-9.

46. **Gendelman, H. E., J. M. Orenstein, L. M. Baca, B. Weiser, H. Burger, D. C. Kalter, and M. S. Meltzer.** 1989. The macrophage in the persistence and pathogenesis of HIV infection. AIDS **3:**475-95.

47. **Gendelman, H. E., J. M. Orenstein, M. A. Martin, C. Ferrua, R. Mitra, T. Phipps, L. A. Wahl, H. C. Lane, A. S. Fauci, D. S. Burke, and et al.** 1988. Efficient isolation and propagation of human immunodeficiency virus on recombinant colony-stimulating factor 1-treated monocytes. J Exp Med **167:**1428-41.

48. **Gerard, C., and B. J. Rollins.** 2001. Chemokines and disease. Nat Immunol **2:**108-15.

49. **Giomarelli, B., K. M. Schumacher, T. E. Taylor, R. C. Sowder, 2nd, J. L. Hartley, J. B. McMahon, and T. Mori.** 2006. Recombinant production of anti-HIV protein, griffithsin, by auto-induction in a fermentor culture. Protein Expr Purif **47:**194-202.

50. **Gouwy, M., S. Struyf, J. Catusse, P. Proost, and J. Van Damme.** 2004. Synergy between proinflammatory ligands of G protein-coupled receptors in neutrophil activation and migration. J Leukoc Biol **76:**185-94.

51. **Grasberger, B. L., A. M. Gronenborn, and G. M. Clore.** 1993. Analysis of the backbone dynamics of interleukin-8 by 15N relaxation measurements. J Mol Biol **230:**364-72.

52. **Grzesiek, S., H. Dobeli, R. Gentz, G. Garotta, A. M. Labhardt, and A. Bax.** 1992. 1H, 13C, and 15N NMR backbone assignments and secondary structure of human interferon-gamma. Biochemistry **31:**8180-90.

53. **Hamburger, A. E., S. Kim, B. D. Welch, and M. S. Kay.** 2005. Steric accessibility of the HIV-1 gp41 N-trimer region. J Biol Chem **280:**12567-72.

54. **Handel, T. M., and P. J. Domaille.** 1996. Heteronuclear (1H, 13C, 15N) NMR assignments and solution structure of the monocyte chemoattractant protein-1 (MCP-1) dimer. Biochemistry **35:**6569-84.

55. **Harmon, B., and L. Ratner.** 2008. Induction of the Galpha(q) signaling cascade by the human immunodeficiency virus envelope is required for virus entry. J Virol **82:**9191-205.

56. **Hart, C. E., and T. Evans-Strickfaden.** 2007. HIV-1 entry inhibitors as microbicides, p. 99-117. *In* J. D. Reeves and C. A. Derdeyn (ed.), Entry Inhibitors in HIV Therapy. Birkhauser Verlag, Switzerland.

57. **Hartley, O., K. Dorgham, D. Perez-Bercoff, F. Cerini, A. Heimann, H. Gaertner, R. E. Offord, G. Pancino, P. Debre, and G. Gorochov.** 2003.

Human immunodeficiency virus type 1 entry inhibitors selected on living cells from a library of phage chemokines. J Virol **77:**6637-44.

58. **Hartley, O., and R. E. Offord.** 2005. Engineering chemokines to develop optimized HIV inhibitors. Current Protein & Peptide Science **6:**207-19.

59. **Hartley, O., and R. E. Offord.** 2005. Engineering chemokines to develop optimized HIV inhibitors. Curr Protein Pept Sci **6:**207-19.

60. **Havranek, J. J., and P. B. Harbury.** 2003. Automated design of specificity in molecular recognition. Nat Struct Biol **10:**45-52.

61. **Hecht, M. H., J. S. Richardson, D. C. Richardson, and R. C. Ogden.** 1990. De novo design, expression, and characterization of Felix: a four-helix bundle protein of native-like sequence. Science **249:**884-91.

62. **Heredia, A., B. Gilliam, A. DeVico, N. Le, D. Bamba, R. Flinko, G. Lewis, R. C. Gallo, and R. R. Redfield.** 2007. CCR5 density levels on primary CD4 T cells impact the replication and Enfuvirtide susceptibility of R5 HIV-1. AIDS **21:**1317-22.

63. **Heredia, A., B. Gilliam, O. Latinovic, N. Le, D. Bamba, A. Devico, G. B. Melikyan, R. C. Gallo, and R. R. Redfield.** 2007. Rapamycin reduces CCR5 density levels on CD4 T cells and this effect results in potentiation of Enfuvirtide (T-20) against R5 HIV-1 in vitro. Antimicrob Agents Chemother **51:**2489-96.

64. **Higgins, D. G., J. D. Thompson, and T. J. Gibson.** 1996. Using CLUSTAL for multiple sequence alignments. Methods Enzymol **266:**383-402.

65. **Hladik, F., and T. J. Hope.** 2009. HIV infection of the genital mucosa in women. Curr HIV/AIDS Rep **6:**20-8.

66. **Hladik, F., and M. J. McElrath.** 2008. Setting the stage: host invasion by HIV. Nat Rev Immunol **8:**447-57.

67. **Hutter, G., D. Nowak, M. Mossner, S. Ganepola, A. Mussig, K. Allers, T. Schneider, J. Hofmann, C. Kucherer, O. Blau, I. W. Blau, W. K. Hofmann, and E. Thiel.** 2009. Long-term control of HIV by CCR5 Delta32/Delta32 stem-cell transplantation. N Engl J Med **360:**692-8.

68. **Jacobson, J. M., R. J. Israel, I. Lowy, N. A. Ostrow, L. S. Vassilatos, M. Barish, D. N. Tran, B. M. Sullivan, T. J. Ketas, T. J. O'Neill, K. A. Nagashima, W. Huang, C. J. Petropoulos, J. P. Moore, P. J. Maddon, and W. C. Olson.** 2004. Treatment of advanced human immunodeficiency virus type 1 disease with the viral entry inhibitor PRO 542. Antimicrob Agents Chemother **48:**423-9.

69. **Jekle, A., E. Chow, E. Kopetzki, C. Ji, M. J. Yan, R. Nguyen, S. Sankuratri, N. Cammack, and G. Heilek.** 2009. CD4-BFFI: a novel, bifunctional HIV-1 entry inhibitor with high and broad antiviral potency. Antiviral Res **83:**257-66.

70. **Ji, C., E. Kopetzki, A. Jekle, K. G. Stubenrauch, X. Liu, J. Zhang, E. Rao, T. Schlothauer, S. Fischer, N. Cammack, G. Heilek, S. Ries, and S. Sankuratri.** 2009. CD4-anchoring HIV-1 fusion inhibitor with enhanced potency and in vivo stability. J Biol Chem **284:**5175-85.

71. **Ji, C., J. Zhang, M. Dioszegi, S. Chiu, E. Rao, A. Derosier, N. Cammack, M. Brandt, and S. Sankuratri.** 2007. CCR5 small-molecule antagonists and monoclonal antibodies exert potent synergistic antiviral effects by cobinding to the receptor. Mol Pharmacol **72:**18-28.

72. **Jin, H., G. L. Hayes, N. S. Darbha, E. Meyer, and P. J. LiWang.** 2005. Investigation of CC and CXC chemokine quaternary state mutants. Biochem Biophys Res Commun **338:**987-99.

73. **Jin, H., I. Kagiampakis, P. Li, and P. J. Liwang.** 2010. Structural and functional studies of the potent anti-HIV chemokine variant P2-RANTES. Proteins **78:**295-308.

74. **Jin, H., I. Kagiampakis, P. Li, and P. J. Liwang.** 2009. Structural and functional studies of the potent anti-HIV chemokine variant P2-RANTES. Proteins **78:**295-308..

75. **Jin, H., X. Shen, B. R. Baggett, X. Kong, and P. J. LiWang.** 2007. The human CC chemokine MIP-1beta dimer is not competent to bind to the CCR5 receptor. J. Biol. Chem. **282:**27976-83.

76. **Jin, H., X. Shen, B. R. Baggett, X. Kong, and P. J. LiWang.** 2007. The human CC chemokine MIP-1beta dimer is not competent to bind to the CCR5 receptor. J Biol Chem **282:**27976-83.

77. **Kabsch, W., and C. Sander.** 1983. Dictionary of protein secondary structure: pattern recognition of hydrogen-bonded and geometrical features. Biopolymers **22:**2577-637.

78. **Kahle, K. M., H. K. Steger, and M. J. Root.** 2009. Asymmetric deactivation of HIV-1 gp41 following fusion inhibitor binding. PLoS Pathog **5:**e1000674.

79. **Ketas, T. J., P. J. Klasse, C. Spenlehauer, M. Nesin, I. Frank, M. Pope, J. M. Strizki, G. R. Reyes, B. M. Baroudy, and J. P. Moore.** 2003. Entry inhibitors

SCH-C, RANTES, and T-20 block HIV type 1 replication in multiple cell types. AIDS Res Hum Retroviruses **19:**177-86.

80. **Kim, S., J. Tsai, I. Kagiampakis, P. LiWang, and M. Vannucci.** 2007. Detecting protein dissimilarities in multiple alignments using Bayesian variable selection. Bioinformatics **23:**245-6.

81. **Klein, J. S., P. N. Gnanapragasam, R. P. Galimidi, C. P. Foglesong, A. P. West, Jr., and P. J. Bjorkman.** 2009. Examination of the contributions of size and avidity to the neutralization mechanisms of the anti-HIV antibodies b12 and 4E10. Proc Natl Acad Sci U S A **106:**7385-90.

82. **Kopetzki, E., A. Jekle, C. Ji, E. Rao, J. Zhang, S. Fischer, N. Cammack, S. Sankuratri, and G. Heilek.** 2008. Closing two doors of viral entry: intramolecular combination of a coreceptor- and fusion inhibitor of HIV-1. Virol J **5:**56.

83. **Kortemme, T., L. A. Joachimiak, A. N. Bullock, A. D. Schuler, B. L. Stoddard, and D. Baker.** 2004. Computational redesign of protein-protein interaction specificity. Nat Struct Mol Biol **11:**371-9.

84. **Kwong, P. D., R. Wyatt, J. Robinson, R. W. Sweet, J. Sodroski, and W. A. Hendrickson.** 1998. Structure of an HIV gp120 envelope glycoprotein in complex with the CD4 receptor and a neutralizing human antibody. Nature **393:**648-59.

85. **Kwong, P. D., R. Wyatt, J. Robinson, R. W. Sweet, J. Sodroski, and W. A. Hendrickson.** 1998. Structure of an HIV gp120 envelope glycoprotein in

complex with the CD4 receptor and a neutralizing human antibody. [see comments]. Nature **393:**648-59.

86. **Kyte, J., and R. F. Doolittle.** 1982. A simple method for displaying the hydropathic character of a protein. J Mol Biol **157:**105-32.

87. **Lackman-Smith, C., C. Osterling, K. Luckenbaugh, M. Mankowski, B. Snyder, G. Lewis, J. Paull, A. Profy, R. G. Ptak, R. W. Buckheit, Jr., K. M. Watson, J. E. Cummins, Jr., and B. E. Sanders-Beer.** 2008. Development of a comprehensive human immunodeficiency virus type 1 screening algorithm for discovery and preclinical testing of topical microbicides. Antimicrob Agents Chemother **52:**1768-81.

88. **Laurence, J. S., C. Blanpain, J. W. Burgner, M. Parmentier, and P. J. LiWang.** 2000. CC chemokine MIP-1 beta can function as a monomer and depends on Phe13 for receptor binding. Biochemistry **39:**3401-9.

89. **Laurence, J. S., C. Blanpain, A. De Leener, M. Parmentier, and P. J. LiWang.** 2001. The Importance of Basic Residues and Quaternary Structure in the Function of MIP-1b: CCR5 Binding and Cell Surface Sugar Interactions. Biochemistry **40:**4990-4999.

90. **Laurence, J. S., A. C. LiWang, and P. J. LiWang.** 1998. Effect of N-terminal truncation and solution conditions on chemokine dimer stability: nuclear magnetic resonance structural analysis of macrophage inflammatory protein 1 beta mutants. Biochemistry **37:**9346-54.

91. **Leonard, J. T., and K. Roy.** 2006. The HIV entry inhibitors revisited. Curr Med Chem **13:**911-34.

92. **Leong, S. R., H. B. Lowman, J. Liu, S. Shire, L. E. Deforge, B. L. Gillece-Castro, R. McDowell, and C. A. Hebert.** 1997. IL-8 single-chain homodimers and heterodimers: interactions with chemokine receptors CXCR1, CXCR2, and DARC. Protein Sci **6:**609-17.

93. **Leong, S. R., H. B. Lowman, J. Liu, S. Shire, L. E. Deforge, B. L. Gillece-Castro, R. McDowell, and C. A. Hébert.** 1997. IL-8 single-chain homodimers and heterodimers:Interactions with the chemokine receptors CXCR1, CXCR2, and DARC. Protein Science **6:**609-617.

94. **Letvin, N. L.** 2009. Virology. Moving forward in HIV vaccine development. Science **326:**1196-8.

95. **Liu, S., H. Lu, J. Niu, Y. Xu, S. Wu, and S. Jiang.** 2005. Different from the HIV fusion inhibitor C34, the anti-HIV drug Fuzeon (T-20) inhibits HIV-1 entry by targeting multiple sites in gp41 and gp120. J Biol Chem **280:**11259-73.

96. **Liu, S., S. Wu, and S. Jiang.** 2007. HIV entry inhibitors targeting gp41: from polypeptides to small-molecule compounds. Curr Pharm Des **13:**143-62.

97. **Liu, Y., N. V. Belkina, and S. Shaw.** 2009. HIV infection of T cells: actin-in and actin-out. Sci Signal **2:**pe23.

98. **LiWang, A. C., J. J. Cao, H. Zheng, Z. Lu, S. C. Peiper, and P. J. LiWang.** 1999. Dynamics Study on the anti-human immunodieficiency virus chemokine viral macrophage inflammatory protein-II (vMIP-II) reveals a fully monomeric protein. Biochemistry **38:**442-453.

99. **Lodi, P. J., D. S. Garrett, J. Kuszewski, M. L. Tsang, J. A. Weatherbee, W. J. Leonard, A. M. Gronenborn, and G. M. Clore.** 1994. High-resolution solution

structure of the beta chemokine hMIP-1 beta by multidimensional NMR. Science **263:**1762-7.

100. **Lowman, H. B., W. J. Fairbrother, P. H. Slagle, R. Kabakoff, J. Liu, S. Shire, and C. A. Hebert.** 1997. Monomeric variants of IL-8: effects of side chain substitutions and solution conditions upon dimer formation. Protein Sci **6:**598-608.

101. **Lu, M., S. C. Blacklow, and P. S. Kim.** 1995. A trimeric structural domain of the HIV-1 transmembrane glycoprotein. Nature Structural Biology **2:**1075-82.

102. **Lu, M., and P. S. Kim.** 1997. A trimeric structural subdomain of the HIV-1 transmembrane glycoprotein. J Biomol Struct Dyn **15:**465-71.

103. **Lubkowski, J., G. Bujacz, L. Boque, P. J. Domaille, T. M. Handel, and A. Wlodawer.** 1997. The structure of MCP-1 in two crystal forms provides a rare example of variable quaternary interactions. Nature Structural Biology **4:**64-69.

104. **Lusti-Narasimhan, M., A. Chollet, C. A. Power, B. Allet, A. E. Proudfoot, and T. N. Wells.** 1996. A molecular switch of chemokine receptor selectivity. Chemical modification of the interleukin-8 Leu25 --> Cys mutant. J Biol Chem **271:**3148-53.

105. **Mack, M., B. Luckow, J. Cihak, G. Simmons, P. R. Clapham, N. Signoret, M. Marsh, M. Strassinger, F. Borlat, T. Wells, D. Scholondorff, and A. E. I. Proudfoot.** 1998. AOP-RANTES induces CCR5 internalization but inhibits recycling: a novel inhibitory mechanism of HIV infectivity. J. Exp. Med. **187:**1215-1224.

106. **Malik, Z. A., and B. F. Tack.** 2006. Structure of human MIP-3alpha chemokine. Acta Crystallogr Sect F Struct Biol Cryst Commun **62:**631-4.

107. **Markosyan, R. M., F. S. Cohen, and G. B. Melikyan.** 2003. HIV-1 envelope proteins complete their folding into six-helix bundles immediately after fusion pore formation. Mol Biol Cell **14:**926-38.

108. **Martin, L., C. Blanpain, P. Garnier, V. Wittamer, M. Parmentier, and C. Vita.** 2001. Structural and functional analysis of the RANTES-glycosaminoglycans interactions. Biochemistry **40:**6303-18.

109. **Martin, L., F. Stricher, D. Misse, F. Sironi, M. Pugniere, P. Barthe, R. Prado-Gotor, I. Freulon, X. Magne, C. Roumestand, A. Menez, P. Lusso, F. Veas, and C. Vita.** 2003. Rational design of a CD4 mimic that inhibits HIV-1 entry and exposes cryptic neutralization epitopes. Nat Biotechnol **21:**71-6.

110. **McCornack, M. A., D. M. Boren, and P. J. LiWang.** 2004. Glycosaminoglycan disaccharide alters the dimer dissociation constant of the chemokine MIP-1 beta. Biochemistry **43:**10090-101.

111. **McCornack, M. A., C. K. Cassidy, and P. J. LiWang.** 2003. The binding surface and affinity of monomeric and dimeric chemokine macrophage inflammatory protein 1 beta for various glycosaminoglycan disaccharides. J Biol Chem **278:**1946-56.

112. **Meunier, S., J. M. Bernassau, J. C. Guillemot, P. Ferrara, and H. Darbon.** 1997. Determination of the three-dimensional structure of CC chemokine monocyte chemoattractant protein 3 by 1H two-dimensional NMR spectroscopy. Biochemistry **36:**4412-22.

113. **Miyauchi, K., Y. Kim, O. Latinovic, V. Morozov, and G. B. Melikyan.** 2009. HIV enters cells via endocytosis and dynamin-dependent fusion with endosomes. Cell **137:**433-44.

114. **Miyauchi, K., M. M. Kozlov, and G. B. Melikyan.** 2009. Early steps of HIV-1 fusion define the sensitivity to inhibitory peptides that block 6-helix bundle formation. PLoS Pathog **5:**e1000585.

115. **Mkrtchyan, S. R., R. M. Markosyan, M. T. Eadon, J. P. Moore, G. B. Melikyan, and F. S. Cohen.** 2005. Ternary complex formation of human immunodeficiency virus type 1 Env, CD4, and chemokine receptor captured as an intermediate of membrane fusion. J Virol **79:**11161-9.

116. **Morgenstern, B.** 2004. DIALIGN: multiple DNA and protein sequence alignment at BiBiServ. Nucleic Acids Res **32:**W33-6.

117. **Morgenstern, B., K. Frech, A. Dress, and T. Werner.** 1998. DIALIGN: finding local similarities by multiple sequence alignment. Bioinformatics **14:**290-4.

118. **Mori, T., B. R. O'Keefe, R. C. Sowder, 2nd, S. Bringans, R. Gardella, S. Berg, P. Cochran, J. A. Turpin, R. W. Buckheit, Jr., J. B. McMahon, and M. R. Boyd.** 2005. Isolation and characterization of griffithsin, a novel HIV-inactivating protein, from the red alga Griffithsia sp. J Biol Chem **280:**9345-53.

119. **Murga, J. D., M. Franti, D. C. Pevear, P. J. Maddon, and W. C. Olson.** 2006. Potent antiviral synergy between monoclonal antibody and small-molecule CCR5 inhibitors of human immunodeficiency virus type 1. Antimicrob Agents Chemother **50:**3289-96.

120. **Murphy, P. M.** 1997. Neutrophil receptors for interleukin-8 and related CXC chemokines. Semin Hematol **34:**311-8.

121. **Nagashima, K. A., D. A. Thompson, S. I. Rosenfield, P. J. Maddon, T. Dragic, and W. C. Olson.** 2001. Human immunodeficiency virus type 1 entry inhibitors PRO 542 and T-20 are potently synergistic in blocking virus-cell and cell-cell fusion. J Infect Dis **183:**1121-5.

122. **Nesmelova, I. V., Y. Sham, A. Z. Dudek, L. I. van Eijk, G. Wu, A. Slungaard, F. Mortari, A. W. Griffioen, and K. H. Mayo.** 2005. Platelet factor 4 and interleukin-8 CXC chemokine heterodimer formation modulates function at the quaternary structural level. J Biol Chem **280:**4948-58.

123. **O'Keefe, B. R., F. Vojdani, V. Buffa, R. J. Shattock, D. C. Montefiori, J. Bakke, J. Mirsalis, A. L. d'Andrea, S. D. Hume, B. Bratcher, C. J. Saucedo, J. B. McMahon, G. P. Pogue, and K. E. Palmer.** 2009. Scaleable manufacture of HIV-1 entry inhibitor griffithsin and validation of its safety and efficacy as a topical microbicide component. Proc Natl Acad Sci U S A **106:**6099-104.

124. **Oberlin, E., Amara, A., Bachelerie, F., Bessia, C., Virelizier, J.-L., Arenzana-Seisdedos, Schwartz, O., Heard, J.-M., Clark-Lewis, I., Legler, D.F., Loetscher, M., Baggiolini, M., Moser, B.** 1996. The CXC chemokine SDF-1 is the ligand for LESTR/fusin and prevents infection by T-cell-line-adapted HIV-1. Nature **382:**833-835.

125. **Paavola, C. D., S. Hemmerich, D. Grunberger, I. Polsky, A. Bloom, R. Freedman, M. Mulkins, S. Bhakta, D. McCarley, L. Wiesent, B. Wong, K. Jarnagin, and T. M. Handel.** 1998. Monomeric monocyte chemoattractant

protein-1 (MCP-1) binds and activates the MCP-1 receptor CCR2B. J Biol Chem **273:**33157-65.

126. **Pace, C. N., F. Vajdos, L. Fee, G. Grimsley, and T. Gray.** 1995. How to measure and predict the molar absorption coefficient of a protein. Protein Science **4:**2411-23.

127. **Page, K. A., N. R. Landau, and D. R. Littman.** 1990. Construction and use of a human immunodeficiency virus vector for analysis of virus infectivity. J Virol **64:**5270-6.

128. **Paolini, J. F., D. Willard, T. Consler, M. Luther, and M. S. Krangel.** 1994. The chemokines IL-8, monocyte chemoattractant protein-1, and I-309 are monomers at physiologically relevant concentrations. J Immunol **153:**2704-17.

129. **Platt, E. J., K. Wehrly, S. E. Kuhmann, B. Chesebro, and D. Kabat.** 1998. Effects of CCR5 and CD4 cell surface concentrations on infections by macrophagetropic isolates of human immunodeficiency virus type 1. J Virol **72:**2855-64.

130. **Pleskoff, O., C. Treboute, A. Brelot, N. Heveker, M. Seman, and M. Alizon.** 1997. Identification of a chemokine receptor encoded by human cytomegalovirus as a cofactor for HIV-1 entry. Science **276:**1874-8.

131. **Popovic, M., S. Gartner, E. Read-Connole, B. Beaver, and M. Reitz.** 1989. Cell Tropism and Expression of HIV-1 isolated in natural targets, p. 65-112. *In* Girard and Valette (ed.), Retroviruses of Human AIDS and Related Animal Diseases. Elsevier, Marnes-La-Coquette, Paris.

132. **Popovic, M., E. Read-Connole, and R. C. Gallo.** 1984. T4 positive human neoplastic cell lines susceptible to and permissive for HTLV-III. Lancet **2:**1472-3.

133. **Popovic, M., M. G. Sarngadharan, E. Read, and R. C. Gallo.** 1984. Detection, isolation, and continuous production of cytopathic retroviruses (HTLV-III) from patients with AIDS and pre-AIDS. Science **224:**497-500.

134. **Poveda, E., V. Briz, and V. Soriano.** 2005. Enfuvirtide, the first fusion inhibitor to treat HIV infection. AIDS Reviews **7:**139-47.

135. **Prabakaran, P., A. S. Dimitrov, T. R. Fouts, and D. S. Dimitrov.** 2007. Structure and function of the HIV envelope glycoprotein as entry mediator, vaccine immunogen, and target for inhibitors. Adv Pharmacol **55:**33-97.

136. **Proudfoot, A. E., T. M. Handel, Z. Johnson, E. K. Lau, P. LiWang, I. Clark-Lewis, F. Borlat, T. N. Wells, and M. H. Kosco-Vilbois.** 2003. Glycosaminoglycan binding and oligomerization are essential for the in vivo activity of certain chemokines. Proc Natl Acad Sci U S A **100:**1885-90.

137. **Ptak, R. G., P. A. Gallay, D. Jochmans, A. P. Halestrap, U. T. Ruegg, L. A. Pallansch, M. D. Bobardt, M. P. de Bethune, J. Neyts, E. De Clercq, J. M. Dumont, P. Scalfaro, K. Besseghir, R. M. Wenger, and B. Rosenwirth.** 2008. Inhibition of human immunodeficiency virus type 1 replication in human cells by Debio-025, a novel cyclophilin binding agent. Antimicrob Agents Chemother **52:**1302-17.

138. **Rajagopalan, L., C. C. Chin, and K. Rajarathnam.** 2007. Role of intramolecular disulfides in stability and structure of a noncovalent homodimer. Biophys J **93:**2129-34.

139. **Rajarathnam, K., I. Clark-Lewis, and B. D. Sykes.** 1995. 1H NMR solution structure of an active monomeric interleukin-8. Biochemistry **34:**12983-90.

140. **Rajarathnam, K., G. N. Prado, H. Fernando, I. Clark-Lewis, and J. Navarro.** 2006. Probing receptor binding activity of interleukin-8 dimer using a disulfide trap. Biochemistry **45:**7882-8.

141. **Rajarathnam, K., B. D. Sykes, B. Dewald, M. Baggiolini, and I. Clark-Lewis.** 1999. Disulfide bridges in interleukin-8 probed using non-natural disulfide analogues: dissociation of roles in structure from function. Biochemistry **38:**7653-8.

142. **Rajarathnam, K., B. D. Sykes, C. M. Kay, B. Dewald, T. Geiser, M. Baggiolini, and I. Clark-Lewis.** 1994. Neutrophil activation by monomeric interleukin-8. Science **264:**90-2.

143. **Rajarathnam, K., Sykes, B.D., Kay, C.M., Dewald, B., Geiser, T., Baggiolini, M., and Clark-Lewis, I.** 1994. Neutrophil Activation by Monomeric Interleukin-8. Science **264:**90-92.

144. **Ratner, L., W. Haseltine, R. Patarca, K. J. Livak, B. Starcich, S. F. Josephs, E. R. Doran, J. A. Rafalski, E. A. Whitehorn, K. Baumeister, and et al.** 1985. Complete nucleotide sequence of the AIDS virus, HTLV-III. Nature **313:**277-84.

145. **Ravindran, A., P. R. Joseph, and K. Rajarathnam.** 2009. Structural basis for differential binding of the interleukin-8 monomer and dimer to the CXCR1 N-domain: role of coupled interactions and dynamics. Biochemistry **48:**8795-805.

146. **Rawat, S. S., J. Eaton, S. A. Gallo, T. D. Martin, S. Ablan, S. Ratnayake, M. Viard, V. N. KewalRamani, J. M. Wang, R. Blumenthal, and A. Puri.** 2004.

Functional expression of CD4, CXCR4, and CCR5 in glycosphingolipid-deficient mouse melanoma GM95 cells and susceptibility to HIV-1 envelope glycoprotein-triggered membrane fusion. Virology **318:**55-65.

147. **Reeves, J. D., S. A. Gallo, N. Ahmad, J. L. Miamidian, P. E. Harvey, M. Sharron, S. Pohlmann, J. N. Sfakianos, C. A. Derdeyn, R. Blumenthal, E. Hunter, and R. W. Doms.** 2002. Sensitivity of HIV-1 to entry inhibitors correlates with envelope/coreceptor affinity, receptor density, and fusion kinetics. Proc Natl Acad Sci U S A **99:**16249-54.

148. **Reeves, J. D., J. L. Miamidian, M. J. Biscone, F. H. Lee, N. Ahmad, T. C. Pierson, and R. W. Doms.** 2004. Impact of mutations in the coreceptor binding site on human immunodeficiency virus type 1 fusion, infection, and entry inhibitor sensitivity. J Virol **78:**5476-85.

149. **Richardson, J. S., and D. C. Richardson.** 2002. Natural beta-sheet proteins use negative design to avoid edge-to-edge aggregation. Proc Natl Acad Sci U S A **99:**2754-9.

150. **Root, M. J., M. S. Kay, and P. S. Kim.** 2001. Protein design of an HIV-1 entry inhibitor. Science **291:**884-8.

151. **Root, M. J., and H. K. Steger.** 2004. HIV-1 gp41 as a target for viral entry inhibition. Curr Pharm Des **10:**1805-25.

152. **Root, M. J., and H. K. Steger.** 2004. HIV-1 gp41 as a target for viral entry inhibition.1805-25.

153. **Rosenkilde, M. M., and T. W. Schwartz.** 2004. The chemokine system -- a major regulator of angiogenesis in health and disease. APMIS **112:**481-95.

154. **Roux, K. H., and K. A. Taylor.** 2007. AIDS virus envelope spike structure. Curr Opin Struct Biol **17:**244-52.

155. **Ryser, H. J., and R. Fluckiger.** 2005. Progress in targeting HIV-1 entry. Drug Discov Today **10:**1085-94.

156. **Sabbe, R., G. R. Picchio, C. Pastore, O. Chaloin, O. Hartley, R. Offord, and D. E. Mosier.** 2001. Donor- and ligand-dependent differences in C-C chemokine receptor 5 reexpression. J Virol **75:**661-71.

157. **Safarian, D., X. Carnec, F. Tsamis, F. Kajumo, and T. Dragic.** 2006. An anti-CCR5 monoclonal antibody and small molecule CCR5 antagonists synergize by inhibiting different stages of human immunodeficiency virus type 1 entry. Virology **352:**477-84.

158. **Sattentau, Q. J., J. P. Moore, F. Vignaux, F. Traincard, and P. Poignard.** 1993. Conformational changes induced in the envelope glycoproteins of the human and simian immunodeficiency viruses by soluble receptor binding. J Virol **67:**7383-93.

159. **Schwarz, M. K., and T. N. Wells.** 2002. New therapeutics that modulate chemokine networks. Nat Rev Drug Discov **1:**347-58.

160. **Sha, N., M. Vannucci, M. G. Tadesse, P. J. Brown, I. Dragoni, N. Davies, T. C. Roberts, A. Contestabile, M. Salmon, C. Buckley, and F. Falciani.** 2004. Bayesian variable selection in multinomial probit models to identify molecular signatures of disease stage. Biometrics **60:**812-9.

161. **Sharma, D., and K. Rajarathnam.** 2000. 13C NMR chemical shifts can predict disulfide bond formation. J Biomol NMR **18:**165-71.

162. **Sharma, D., and K. Rajarathnam.** 2000. 13C NMR chemical shifts can predict disulfide bond formation. J Biomol NMR **18:**165-71.

163. **Shu, W., J. Liu, H. Ji, L. Radigen, S. Jiang, and M. Lu.** 2000. Helical interactions in the HIV-1 gp41 core reveal structural basis for the inhibitory activity of gp41 peptides. Biochemistry **39:**1634-42.

164. **Sougrat, R., A. Bartesaghi, J. D. Lifson, A. E. Bennett, J. W. Bess, D. J. Zabransky, and S. Subramaniam.** 2007. Electron tomography of the contact between T cells and SIV/HIV-1: implications for viral entry. PLoS Pathog **3:**e63.

165. **Stoddart, C. A., G. Nault, S. A. Galkina, K. Thibaudeau, P. Bakis, N. Bousquet-Gagnon, M. Robitaille, M. Bellomo, V. Paradis, P. Liscourt, A. Lobach, M. E. Rivard, R. G. Ptak, M. K. Mankowski, D. Bridon, and O. Quraishi.** 2008. Albumin-conjugated C34 peptide HIV-1 fusion inhibitor: equipotent to C34 and T-20 in vitro with sustained activity in SCID-hu Thy/Liv mice. J Biol Chem **283:**34045-52.

166. **Sullivan, N., Y. Sun, Q. Sattentau, M. Thali, D. Wu, G. Denisova, J. Gershoni, J. Robinson, J. Moore, and J. Sodroski.** 1998. CD4-Induced conformational changes in the human immunodeficiency virus type 1 gp120 glycoprotein: consequences for virus entry and neutralization. J Virol **72:**4694-703.

167. **Swaminathan, G. J., D. E. Holloway, R. A. Colvin, G. K. Campanella, A. C. Papageorgiou, A. D. Luster, and K. R. Acharya.** 2003. Crystal structures of oligomeric forms of the IP-10/CXCL10 chemokine. Structure **11:**521-32.

168. **Takeuchi, Y., M. O. McClure, and M. Pizzato.** 2008. Identification of gammaretroviruses constitutively released from cell lines used for human immunodeficiency virus research. J Virol **82:**12585-8.

169. **Thompson, J. D., D. G. Higgins, and T. J. Gibson.** 1994. CLUSTAL W: improving the sensitivity of progressive multiple sequence alignment through sequence weighting, position-specific gap penalties and weight matrix choice. Nucleic Acids Res **22:**4673-80.

170. **Tremblay, C.** 2004. Effects of HIV-1 entry inhibitors in combination. Curr Pharm Des **10:**1861-5.

171. **Tremblay, C., D. P. Merrill, T. C. Chou, and M. S. Hirsch.** 1999. Interactions among combinations of two and three protease inhibitors against drug-susceptible and drug-resistant HIV-1 isolates. J Acquir Immune Defic Syndr **22:**430-6.

172. **Tremblay, C. L., F. Giguel, C. Kollmann, Y. Guan, T. C. Chou, B. M. Baroudy, and M. S. Hirsch.** 2002. Anti-human immunodeficiency virus interactions of SCH-C (SCH 351125), a CCR5 antagonist, with other antiretroviral agents in vitro. Antimicrob Agents Chemother **46:**1336-9.

173. **Tremblay, C. L., C. Kollmann, F. Giguel, T. C. Chou, and M. S. Hirsch.** 2000. Strong in vitro synergy between the fusion inhibitor T-20 and the CXCR4 blocker AMD-3100. J Acquir Immune Defic Syndr **25:**99-102.

174. **Tsai, J., M. Gerstein, and M. Levitt.** 1997. Simulating the minimum core for hydrophobic collapse in globular proteins. Protein Sci **6:**2606-16.

175. **UNAIDS.** 2008. 2008 Report on the Global AIDS epidemic. WHO/UNAIDS.

176. **Vita, C., E. Drakopoulou, J. Vizzavona, S. Rochette, L. Martin, A. Menez, C. Roumestand, Y. S. Yang, L. Ylisastigui, A. Benjouad, and J. C. Gluckman.** 1999. Rational engineering of a miniprotein that reproduces the core of the CD4 site interacting with HIV-1 envelope glycoprotein. Proc Natl Acad Sci U S A **96:**13091-6.

177. **Wang, H. G., R. E. Williams, and P. F. Lin.** 2004. A novel class of HIV-1 inhibitors that targets the viral envelope and inhibits CD4 receptor binding. Curr Pharm Des **10:**1785-93.

178. **Wang, W., and M. H. Hecht.** 2002. Rationally designed mutations convert de novo amyloid-like fibrils into monomeric beta-sheet proteins. Proc Natl Acad Sci U S A **99:**2760-5.

179. **Waugh, D. J., and C. Wilson.** 2008. The interleukin-8 pathway in cancer. Clin Cancer Res **14:**6735-41.

180. **Wei, X., J. M. Decker, H. Liu, Z. Zhang, R. B. Arani, J. M. Kilby, M. S. Saag, X. Wu, G. M. Shaw, and J. C. Kappes.** 2002. Emergence of resistant human immunodeficiency virus type 1 in patients receiving fusion inhibitor (T-20) monotherapy. Antimicrob Agents Chemother **46:**1896-905.

181. **Westervelt, P., H. E. Gendelman, and L. Ratner.** 1991. Identification of a determinant within the human immunodeficiency virus 1 surface envelope glycoprotein critical for productive infection of primary monocytes. Proc Natl Acad Sci U S A **88:**3097-101.

182. **Wild, C., T. Greenwell, and T. Matthews.** 1993. A synthetic peptide from HIV-1 gp41 is a potent inhibitor of virus-mediated cell-cell fusion. AIDS Res Hum Retroviruses **9:**1051-3.

183. **Wild, C. T., D. C. Shugars, T. K. Greenwell, C. B. McDanal, and T. J. Matthews.** 1994. Peptides corresponding to a predictive alpha-helical domain of human immunodeficiency virus type 1 gp41 are potent inhibitors of virus infection. Proc Natl Acad Sci U S A **91:**9770-4.

184. **Williams, G., N. Borkakoti, G. A. Bottomley, I. Cowan, A. G. Fallowfield, P. S. Jones, S. J. Kirtland, G. J. Price, and L. Price.** 1996. Mutagenesis studies of interleukin-8. Identification of a second epitope involved in receptor binding. J Biol Chem **271:**9579-86.

185. **Williams MA, Cave CM, Quaid G, Robinson C, Daly TJ, Witt D, Lentsch AB, and S. JS.** 2005. Interleukin 8 dimerization as a mechanism for regulation of neutrophil adherence-dependent oxidant production. Shock **23:**371-376.

186. **Williams, M. A., C. M. Cave, G. Quaid, C. Robinson, T. J. Daly, D. Witt, A. B. Lentsch, and J. S. Solomkin.** 2005. Interleukin 8 dimerization as a mechanism for regulation of neutrophil adherence-dependent oxidant production. Shock **23:**371-6.

187. **Williamson, D., I. J. McLennan, A. Bax, M. P. Gamcsik, and J. D. Glickson.** 1990. Two-dimensional nMR study of bleomycin and its zinc(II) complex: reassignment of 13C resonances. J Biomol Struct Dyn **8:**375-98.

188. **Wishart, D. S., C. G. Bigam, J. Yao, F. Abildgaard, H. J. Dyson, E. Oldfield, J. L. Markley, and B. D. Sykes.** 1995. 1H, 13C and 15N chemical shift referencing in biomolecular NMR. J Biomol NMR **6:**135-40.

189. **Wishart, D. S., C. G. Bigam, J. Yao, F. Abildgaard, H. J. Dyson, E. Oldfield, J. L. Markley, and B. D. Sykes.** 1995. ^{1}H, ^{13}C, ^{15}N chemical shift referencing in biomolecular NMR. J. Biomol. NMR **6:**135-140.

190. **Wishart, D. S., and B. D. Sykes.** 1994. Chemical shifts as a tool for structure determination. Methods Enzymol **239:**363-92.

191. **Wishart, D. S., B. D. Sykes, and F. M. Richards.** 1992. The chemical shift index: a fast and simple method for the assignment of protein secondary structure through NMR spectroscopy. Biochemistry **31:**1647-51.

192. **Wu, Y., and A. Yoder.** 2009. Chemokine coreceptor signaling in HIV-1 infection and pathogenesis. PLoS Pathog **5:**e1000520.

193. **Yi, L., J. Fang, N. Isik, J. Chim, and T. Jin.** 2006. HIV gp120-induced interaction between CD4 and CCR5 requires cholesterol-rich microenvironments revealed by live cell fluorescence resonance energy transfer imaging. J Biol Chem **281:**35446-53.

194. **Zeitlin, L., M. Pauly, and K. J. Whaley.** 2009. Second-generation HIV microbicides: continued development of griffithsin. Proc Natl Acad Sci U S A **106:**6029-30.

195. **Zhang, L., T. He, A. Talal, G. Wang, S. S. Frankel, and D. D. Ho.** 1998. In vivo distribution of the human immunodeficiency virus/simian immunodeficiency virus coreceptors: CXCR4, CCR3, and CCR5. J Virol **72:**5035-45.

196. **Zhang, Y., and B. J. Rollins.** 1995. A dominant negative inhibitor indicates that monocyte chemoattractant protein 1 functions as a dimer. Mol Cell Biol **15:**4851-5.

197. **Zhu, P., J. Liu, J. Bess, Jr., E. Chertova, J. D. Lifson, H. Grise, G. A. Ofek, K. A. Taylor, and K. H. Roux.** 2006. Distribution and three-dimensional structure of AIDS virus envelope spikes. Nature **441:**847-52.

198. **Ziolkowska, N. E., B. R. O'Keefe, T. Mori, C. Zhu, B. Giomarelli, F. Vojdani, K. E. Palmer, J. B. McMahon, and A. Wlodawer.** 2006. Domain-swapped structure of the potent antiviral protein griffithsin and its mode of carbohydrate binding. Structure **14:**1127-35.

199. **Ziolkowska, N. E., S. R. Shenoy, B. R. O'Keefe, J. B. McMahon, K. E. Palmer, R. A. Dwek, M. R. Wormald, and A. Wlodawer.** 2007. Crystallographic, thermodynamic, and molecular modeling studies of the mode of binding of oligosaccharides to the potent antiviral protein griffithsin. Proteins **67:**661-70.

200. **Ziolkowska, N. E., S. R. Shenoy, B. R. O'Keefe, and A. Wlodawer.** 2007. Crystallographic studies of the complexes of antiviral protein griffithsin with glucose and N-acetylglucosamine. Protein Sci **16:**1485-9.

VITA

Ioannis Kagiampakis received his Bachelor of Science degree in biology from the University of Crete at Iraklion, Greece in 2001. He entered the graduate program at the same university in September 2001 and received his Master of Science degree in molecular biology and biomedicine in May 2003. He started his doctoral studies at Texas A&M University in August 2003 and graduated in August 2010 with a Ph.D in Biochemistry. His research interest is currently focusing in virology.

Ioannis Kagiampakis can be reached at National Cancer Institute, NCI-Frederick, P.O. Box B, Building 535, Frederick, MD 21702-1201. His email is: bio620@gmail.com